

DISSERTATION

UNDERSTANDING AND LEVERAGING MECHANICAL FORCES IN HAEMOSTASIS

Submitted by

Iain Macleod Briongos

School of Biomedical Engineering

In partial fulfilment of the requirements

For the Degree of Doctor of Philosophy

Colorado State University

Fort Collins, Colorado

Fall 2023

Doctoral Committee:

Advisor: David Bark

Charles Henry
Christine Olver
Ketul Popat

Copyright by Iain Macleod Briongos 2023

All Rights Reserved

ABSTRACT

UNDERSTANDING AND LEVERAGING MECHANICAL FORCES IN HAEMOSTASIS

Cardiovascular disease accounts for one third of deaths worldwide, of which over 75% are in low- and middle-income countries. Platelets and von Willebrand Factor play a central role in haemostasis and in cardiovascular diseases, being involved in both excess clotting that causes heart attacks and strokes, and excess bleeding. Herein, we outline a method for leveraging paper microfluidics with the aim of developing a WHO ASSURED criteria compliant point-of-care device for the diagnosis of von Willebrand Disease, as well as work to increase the understanding of mechanical force generation by platelets through Traction Force Microscopy.

ACKNOWLEDGEMENTS

I would like to acknowledge my PI, David Bark, who has worked tirelessly to advance my project and those of everyone in his lab, and whose work ethic is admirable. Alex, Banafshe, Alireza and Peter from the lab as well as Harvinder, Tom and Chris for their help and companionship at CSU. Chuck Henry for allowing me to use his equipment extensively. Zach for his help and guidance early in the microfluidic work.

I would like to acknowledge Alan Schenkel and Mark Zabel who sparked my fascination with the immune system. While my research changed very early on, they were instrumental for it. Also, to Jen Cappa, the three of you are incredible teachers.

Finally, a tongue-in-cheek thank you to the one who generously gifted me a chip for my shoulder. I could have done it without you, but I don't know if I would have.

DEDICATION

As I close this chapter of my life, I dedicate this dissertation foremost to Jen, my love, confidant, and co-conspirator, who has accompanied, supported, and uplifted me throughout.

To my little monkeys, Santiago, and León, who bring joy to my life every day and have been counting down the days!

To my parents, Marta and Colin, and my sister, Alba. Your love and unequivocal support made me the man, husband, and father I am today. I'm here for you, like you are for me.

To Kenneth (d. 2018) and Hetty (d. 2023), both of whom inspired my love for science and leave me with beautiful memories.

To Chris (d. 2017).

To Mairi, with us in body and terribly missed in mind.

TABLE OF CONTENTS

ABSTRACT	ii
ACKNOWLEDGEMENTS	iii
DEDICATION	iv
LIST OF TABLES	vii
LIST OF FIGURES	viii
Chapter 1 – Literature Review	1
Overview of Haemostasis and Haemostatic Disease	1
Mechanotransduction	14
Traction Force Microscopy (TFM)	22
von Willebrand Factor (VWF) and von Willebrand Disease (VWD)	33
Microfluidics: An Emerging Diagnostic Tool for VWD	43
Chapter 2 – Specific Aims	52
Chapter 3 – Maximising Flow Rate in Single Paper Layer Microfluidic Devices	53
Introduction	53
Experimental	55
Results and Discussion	58
Conclusion	67
Additional Figures	68
Chapter 4 – Assessing the Viability of μ PADS in the Diagnosis of VWD	72
Introduction	72
Experimental	74

Results and Discussion	78
Conclusion	85
Chapter 5 – Investigating Platelet Response to Surface Stiffness	87
Introduction.....	87
Experimental.....	89
Results and Discussion	93
Conclusion	99
Chapter 6 – Conclusion and Future Directions.....	101
Conclusion	101
Future Directions	102
Bibliography	103

LIST OF TABLES

Table 1 – Platelet Activators, their effect, how they contribute, and drug targets	3
Table 2 – Coagulation Cascade with Reactants, Products, and Drug Targets.....	10
Table 3 – Structure and function of VWF Domains	34
Table 4 – von Willebrand Disease Types and Subtypes.....	36
Table 5 – von Willebrand Disease Diagnosis.....	39
Table 6 – Comparison of Microfluidic Systems	46

LIST OF FIGURES

Figure 1 – Overview of Haemostasis.....	1
Figure 2 – Overview of the coagulation cascade	8
Figure 3 – The Virchow Triad.....	12
Figure 4 – Overview of Signal Transduction	15
Figure 5 – Overview of Molecular Clutch Mechanism	20
Figure 6 – Overview of TFM.....	23
Figure 7 - Assured Criteria and Expertise/Accuracy Trade-off	50
Figure 8 - An Overview of Fast Flow Channel Construction	56
Figure 9 - Wetted Area for Different Paper Channel Widths	59
Figure 10 - Wetted Area for Different Laser Cut Widths.....	61
Figure 11 - Wetted Area for Branching Grooves	63
Figure 12 - Comparison of Best Result Flow Rates	64
Figure 13 - Representative Average Distance of the Leading Front of Water	66
Figure 14 - Timelapse Displaying How Liquid Flows in Channels (S1)	69
Figure 15 - Laser Cut Strength Comparison (S2)	69
Figure 16 - Width of Laser Cut Grooves (S3)	70
Figure 17 - Flow Rate Within Grooves of Figure 15 (S4)	71
Figure 18 - An Overview of VWD Channel Construction	76
Figure 19 - An Overview of Channel Constrictions	76
Figure 20 - Dyed Water in VWD channels	79
Figure 21 - Volumetric Flow Rates for Water in VWD Channels.....	80

Figure 22 - Peak Flow Rates	81
Figure 23 - Erythrocytes in VWD Channels	82
Figure 24 - Whole Blood with Ristocetin in VWD Channels.....	84
Figure 25 - Shear Stress Values for Water and Haematocrit	85
Figure 26 - TFM Image Processing Workflow	92
Figure 27 – An Overview of the Force Generation and Bead Displacement	94
Figure 28 - Relationship Between Platelet Area and Force Generation	96
Figure 29 - Temporal Relationship of Platelets and Surface Stiffness.....	98
Figure 30 - Time Taken for Platelets to Release Surface Upon Death	99

CHAPTER 1: LITERATURE REVIEW

1. Overview of Haemostasis and Haemostatic Disease

1.1 Basics of Haemostasis

Haemostasis is the process through which the body stops bleeding. Following vascular injury, platelet adhesion, activation and aggregation occur (primary haemostasis). At the same time, the coagulation cascade is initiated (secondary haemostasis). The culmination of these steps is the formation of a blood clot that covers the damaged vessel wall, prevents further blood loss and entry of external material, and contributes to the repair process.

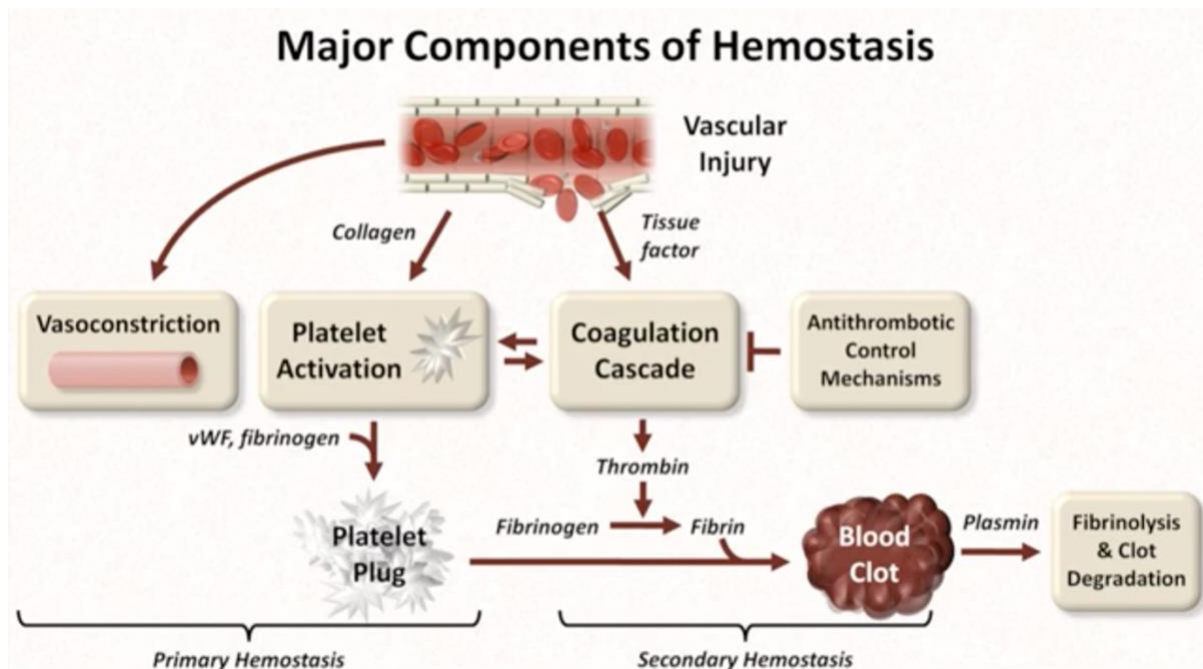


Figure 1 – Overview of Haemostasis¹

1.2 Primary Haemostasis – Platelet Adhesion, Activation and Aggregation

Adhesion: Upon vascular injury, damage to endothelial cells that line blood vessels exposes the subendothelial matrix, which is composed of a densely packed network of collagen fibres, glycoproteins such as von Willebrand Factor (VWF), fibronectin, laminins, and more^{2,3}.

Platelet adhesion in high shear conditions (conditions where there is a high force gradient parallel to the vessel wall), such as in arterial circulation, is mediated by VWF. VWF exists in circulation as a compact, globular protein⁴, as well as stored in endothelial cells in Weibel-Palade bodies⁵. Upon vascular injury and VWF binds exposed collagen, leading to a conformational change (in combination with high shear) that causes it to unfold from a globular bundle into an elongated string^{6,7}. Elongation exposes multiple protected domains on VWF, including the A1 domain which binds with the glycoprotein(GP) Ib-IX-V complex, specifically the alpha subunit, known as GP1b α ^{8,9}. The other subunits in the complex contribute to the VWF-platelet bond stability. VWF-GP1b α bonding can be transient and reversible, which allows for platelets sequestered from circulation to roll along the blood vessel wall, reducing velocity and triggering adhesion^{10,11}. The bond also triggers intracellular cascades that initiate platelet activation¹². GPIIb/IIIa (also known as integrin α Ib β 3) also contributes to platelet adhesion in primary haemostasis. While always present on the platelet surface, in inactive platelets it has low affinity for its ligand fibrinogen and proteins with RGD binding sites. Upon activation (such as through VWF, collagen, Adenosine Diphosphate (ADP), thrombin and many others), α Ib β 3 undergoes a conformational change that increases its affinity, leading to bonding with VWF and circulating fibrinogen. As mentioned before, adhesion in areas of high shear is mediated by VWF. In areas of low shear, however, platelet adhesion is mediated by multiple proteins, including collagen and

VWF¹³. Adhesion is influenced by binding site availability, which will influence the concentration and functionality of platelets, affecting the overall haemostatic process.

Activation: Following adhesion, platelet activation is critical for aggregation and subsequent thrombus formation. As with most biological processes, activation is regulated so that there is a balance between clotting and bleeding, otherwise disease states can occur¹⁴. Excess clotting can lead to blocked blood vessels, causing heart attacks and strokes. Insufficient clotting can lead to bleeding disorders such as von Willebrand Disease (VWD) and haemostasis. Platelets are activated by a range of agonists, including thrombin, ADP, collagen, thromboxane A2 and more (Table 1).

Table 1 – Platelet Activators, their effect, how they contribute, and drug targets.

Platelet Activator	Primary Interact ion Site(s)	Primary Intracellular Effect(s)	Details	Feedback Loop	Drug Targets
Thrombin	PAR1 PAR4 ¹⁵	Alters platelet shape ¹⁵ Secretion and activation of GPIIb/IIIa (α I II β 3) ¹⁶	Potent activator	Indirectly by platelet activation	Direct thrombin inhibitors ¹⁷

Collagen	GPVI, integrin $\alpha_2\beta_1$ ¹⁸	Activation of Src family kinases, PLC γ 2, PKC \uparrow cytoplasmic Ca ²⁺ 18,19	Initiates platelet activation	Indirectly by platelet activation	-
ADP	Initiated by P2Y1, Amplified by P2Y12 ²⁰	\uparrow cytoplasmic Ca ²⁺ Production of TXA2 Alters platelet shape ²¹	Released by injured cells and activated platelets	Yes	P2Y12 receptor antagonists ²²
TXA2	TP ²³	Amplifies activation and aggregation	Released by activated platelets	Yes	Aspirin ²⁴
Epinephrine	α_2 - adrenergic receptors ²⁵	\uparrow cytoplasmic Ca ²⁺ Activates PKC ^{26,27}	Acts by enhancing other activators (such as ADP	Enhancer	Multiple types ^{29,30}

			and thrombin) ²⁸		
Platelet Activating Factor (PAF)	PAF receptor ³¹	↑cytoplasmic Ca ²⁺ , enhances aggregation ³²	Potent phospholipid mediator ³³	Enhancer	PAF receptor antagonists
Serotonin (5-HT)	5-HT receptors	↑cytoplasmic Ca ²⁺ Amplifies aggregation	Enhances effects of ADP and others	Enhancer ³⁴	SSRIs (reduce platelet 5-HT storage) ³⁵
VWF	GPIIb-IX-V complex	Activation of intracellular signalling pathways	More recognized for adhesion than activation	Indirectly by platelet activation	Anti-VWF therapies in development ^{36,37}
Fibrinogen	GPIIb/IIIa receptors	Inside-out signalling	Involved in platelet aggregation	Indirectly by platelet activation	GPIIb/IIIa inhibitors ³⁸

Shear Stress	Mechanoreceptors ³⁹	Conformational changes ⁴⁰	Potent under high shear conditions	Indirectly by platelet activation	Cause dependent (intervention or drugs)
--------------	--------------------------------	--------------------------------------	------------------------------------	-----------------------------------	---

Contact with these agonists triggers a series of signalling cascades, leading to the activation of platelets resulting in – an increase in intracellular calcium levels, shape change, granule release, and integrin activation^{41,42}. Elevated calcium initiates the activity of contractile machinery in platelets, causing them to expand from a discoidal to a more spherical shape with pseudopodal extensions, increasing their surface area^{43,44}. Platelets secrete multiple types of granules. Alpha granules are the most abundant type and contain clotting factors V and VIII (discussed in Secondary Haemostasis), platelet adhesion molecules (including VWF, and fibronectin), growth factors and more⁴⁵⁻⁴⁷. Dense granules are less abundant, but contain ADP and ATP, which will contribute to the recruitment of more platelets, calcium, magnesium, and more⁴⁸⁻⁵⁰. They also contain lysosomal granules and T granules, which contain degrading enzymes and toll-like receptors respectively, indicating a role for platelets in immune system activities^{51,52}. Finally, platelet activation causes the conformational change of GPIIb/IIIa from a relaxed, low affinity state to an activated, high affinity state. This allows for platelets to bind to fibrinogen, leading to cross-linking, platelet aggregation, and clot formation^{53,54}.

Aggregation: The final stage of primary haemostasis is the aggregation of platelets where activated platelets adhere to each other through mediatory proteins and form a platelet plug, or thrombus, sealing the vessel to prevent the passage of blood. Shear is important in mediating aggregation. At low shear stresses, platelet aggregation occurs through fibrinogen as a bridging protein¹¹. As mentioned before conformational changes in GPIIb/IIIa upon platelet activation give it a high affinity for fibrinogen. Fibrinogen is bivalent and can bind two GPIIb/IIIa, usually on separate platelets, cross-linking them^{55,56}. This cascades, leading to aggregation. At high shear stresses, VWF mediates this aggregation¹¹. VWF exists as a globular multimer in circulation that can be extended when exposed to shear, with many monomers that make up the multimer, each with a platelet binding site. Thus, multiple platelets can bind to a single multimer, through which it can also self-associate to other VWF multimers⁵⁷⁻⁵⁹. ADP and TXA₂, both released from activated platelet dense granules, are potent platelet activators, and thus act in an autocrine and paracrine fashion, creating a powerful positive feedback loop. The result of this cascading aggregation is the formation of a platelet plug, a short-lived mass of platelets that works to cover the site of injury and prevent further blood loss. This form is not fully stable and requires secondary haemostasis to form a stable blood clot.

It is important to note that primary haemostasis has a range of control mechanisms to prevent runaway coagulation and to limit it to the site of injury. Loss of or malfunction of control mechanisms leads to disease states.

1.3 Secondary Haemostasis: Coagulation Cascade

The coagulation cascade is a complex series of procedural and feedback reactions that culminate in the formation of fibrin, which in combination with the platelet plug from primary haemostasis, leads to the formation of a stable blood clot. It is generally separated into the intrinsic and extrinsic pathways, two “separate” pathways that in reality interact frequently and combine later in the process into the common pathway (Figure 2).

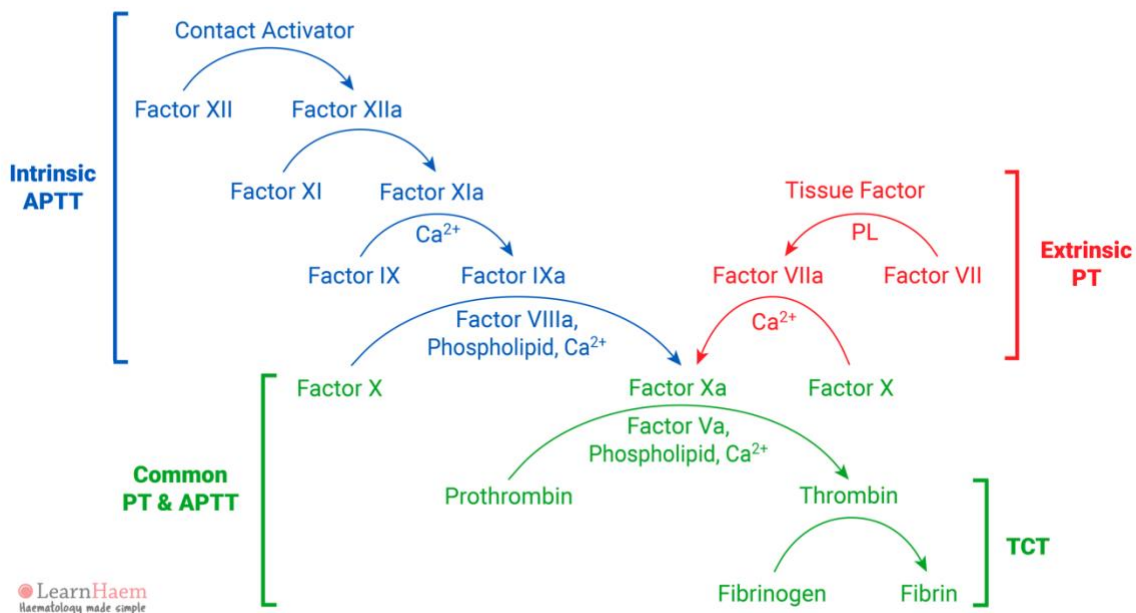


Figure 2 – Overview of the Coagulation Cascade⁶⁰.

Intrinsic Pathway: All the factors (clotting proteins) required for the intrinsic pathway are found within blood itself. Initiation occurs with the activation of Factor XII upon exposure to a negatively charged surface such as collagen - upon vascular injury, activated platelets, or many foreign substances that enter the bloodstream upon injury. Activated Factor XII (XIIa) converts pre-kallikrein to kallikrein. Kallikrein activates Factor XI (XIa), which activates Factor IX (IXa). Factor IXa, along with Factor VIIIa (which is activated by thrombin), calcium and activated platelets form an intrinsic Tenase complex, which acts as a catalyst to activate Factor X (Xa)⁶¹.

Extrinsic Pathway: The extrinsic pathway is so called because it requires the release of tissue factor (Factor III) from the subendothelium of damaged blood vessels and surrounding tissues (i.e., requires the presence of an extrinsic protein). Factor III binds and activates Factor VII (VIIa). Factor VIIa forms an extrinsic Tenase complex that can bind and activate Factor X (Xa), just like the last step of the intrinsic cascade⁶².

Common Pathway: Both pathways culminate in the production of a Tenase complex. The length of the pathway is temporally important – the shorter extrinsic pathway is faster and considered the primary initiator of coagulation. However, the intrinsic pathway has multiple positive feedback points, and thus contributes more Tenase⁶³. Activation of Factor X into Xa marks initiation of the common pathway. Factor Xa, combines with Factor Va, calcium, and activated platelets to form the prothrombinase complex, which converts prothrombin (Factor II) into thrombin (Factor IIa). From here, thrombin plays multiple roles. It feeds back into earlier parts of the cascade – activating Factor VIII (VIIIa) and Factor XI (XIa) in the intrinsic pathway and activating Factor V (Va) for the common pathway. It acts in the next two steps of the cascade – converting soluble fibrinogen into insoluble fibrin monomers, that spontaneously polymerise into strands. These fibrin strands aggregate, forming a network that incorporates activated platelets, blood cells, and other, stabilising the platelet plug into a blood clot. Fibrin also activates Factor XIII (XIIIa), which crosslinks fibrin, further strengthening and stabilising the blood clot⁶⁴⁻⁶⁶.

Table 2 – Coagulation Cascade with Reactants, Products, and Drug Targets⁶²⁻⁶⁵

Pathway	Reactant	Reactant	Product	Mechanism	Drug Targets
Extrinsic	TF	Factor VII	TF-VIIa complex	Secreted by damaged endothelial cells	Tissue factor pathway inhibitor (TFPI)
	TF-VIIa complex	Factor X	Factor Xa	-	Factor Xa inhibitors
Intrinsic	XIIa (contact activation)	Factor XI	Factor XIa	XII activated through contact with negative charges	High molecular weight kininogen, prekallikrein
	XIa	Factor IX	Factor IXa	-	-
	IXa + VIIIa	Factor X	Factor Xa	Activated by Ca ²⁺ and other	Factor IXa inhibitors, antithrombin (indirectly)
Common	Xa + Va	Factor II (Prothrombin)	Factor IIa (Thrombin)	Activated by Ca ²⁺ and other	Antithrombin (with heparin)
	IIa (Thrombin)	Fibrinogen	Fibrin monomers	-	Thrombin inhibitors

	IIa (Thrombin)	XIII	XIIIa	-	-
	XIIIa	Fibrin	Cross-linked fibrin	-	-

1.4 Thrombosis

As may be evident, malfunction of any step in the haemostasis process can lead to disease. In cases where this leads to the undesired formation of blood clots within a blood vessel, the blood clot is referred to as a thrombus. Thrombosis is a highly dangerous pathological event with often serious consequences including pulmonary embolisms, heart attacks and strokes. This is considered distinct from haemostasis, which is the normal and necessary response to damage to a blood vessel, leading to the formation of a healthy blood clot, subsequent repair of the vessel, and resolution of the clot. Thrombotic drivers are clinically categorised on the Virchow triad⁶⁷ (figure 3):

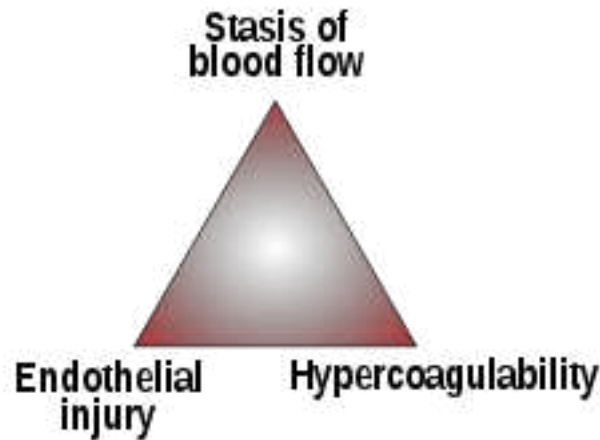


Figure 3 – The Virchow Triad⁶⁸

The Virchow triad indicates three distinct but interacting factors. Haemodynamic Stasis/Changes: Changes to the way in which blood flows can lead to clot formation, for example increase in blood viscosity, turbulent flow leading to increased shear stress and areas of recirculation, and blood stasis. Hypercoagulability/Thrombophilia: Factors that increases to the risk of coagulation such as medication, genetics, or disease. Endothelial Damage: Damage to the blood vessel, leading to exposure of the subendothelium and subsequent initiation of haemostasis.

These factors generally interact, each further increasing the risk of thrombosis (for example someone with altered blood flow that takes medication that increases platelet activity would be at significant risk of thrombosis. Thrombosis can occur anywhere in the vasculature. In periphery it can often be benign, however in certain areas can have lethal consequences. Occlusion of key suppliers to organs can lead to failure of the organ due to lack of oxygen and

subsequent damage from cell death and toxicity. Thrombosis in blood vessels that supply blood to the brain can lead to stroke and in coronary arteries can lead to heart attacks, and in deep veins in the body (commonly in legs) can lead to deep vein thrombosis (DVT)⁶⁹⁻⁷¹. DVT is of risk because these thrombi can break loose and be carried in the blood to the lungs, where their blockage can cause pulmonary embolism.

1.5 Bleeding Disorders

Inversely, if the haemostatic misfunction leads to a decrease in the ability to form blood clots, these are categorised as bleeding disorders. These are caused by medication, genetics, or disease. Clinically, these diseases are characterised by easy bruising, prolonged bleeding (even from minor injuries), excessive menstrual bleeding and bleeding into joints, GI, and urinary systems.

Some examples of bleeding disorders include von Willebrand Disease (VWD) – a group of diseases marked by dysfunction or deficiency of VWF, which will be discussed in section 4. Haemophilia, which is another group of genetic or drug induced diseases caused by dysfunction or deficiency of clotting factors from the coagulation cascade. Platelet diseases, which are a range of diseases caused by platelets. These can be thrombocytopenic (too many platelets), thrombocytopenic (too few), or due to dysfunction. Vitamin K Deficiency Disease caused by a lack of Vitamin K, a vitamer required to produce prothrombin, and hence vital for clotting.

2. Mechanotransduction

2.1 Overview of Mechanotransduction

Mechanotransduction refers to the process surrounding the cellular perception, interpretation, and response to mechanical stimuli from their environment, such as the extracellular matrix (ECM), or blood flow. These cues, and the subsequent response is essential in a vast range of biological processes, and malfunction leads to disease. The concept of mechanotransduction has been around for nearly a century, however it required much more recent advances in biophysical and molecular biology tools to study it successfully. Fundamentally, mechanotransduction requires three major components that act as an input-process-response system:

Mechanosensors – These are specialised structures found on cells, primarily receptors such as integrins, or stretch-sensitive channels^{72,73}. Under appropriate cues, such as a mechanical stimulus, these mechanosensors might undergo conformational changes, allow passage of molecules/ions, or bind a ligand.

Signal Transduction Pathway – once the mechanosensors have been activated, this stimulus is converted into a biochemical response. An intracellular cascade is triggered, where one molecule might activate or inactivate multiple others, leading to the activation of even more procedurally⁷⁴⁻⁷⁶.

Cellular Response – the increase in intracellular signalling molecules culminates in the cell’s change of behaviour. This is generally changes in gene expression leading to the production of different protein which on a cellular level might be responsible for adhesion, activation, migration, differentiation, or other.

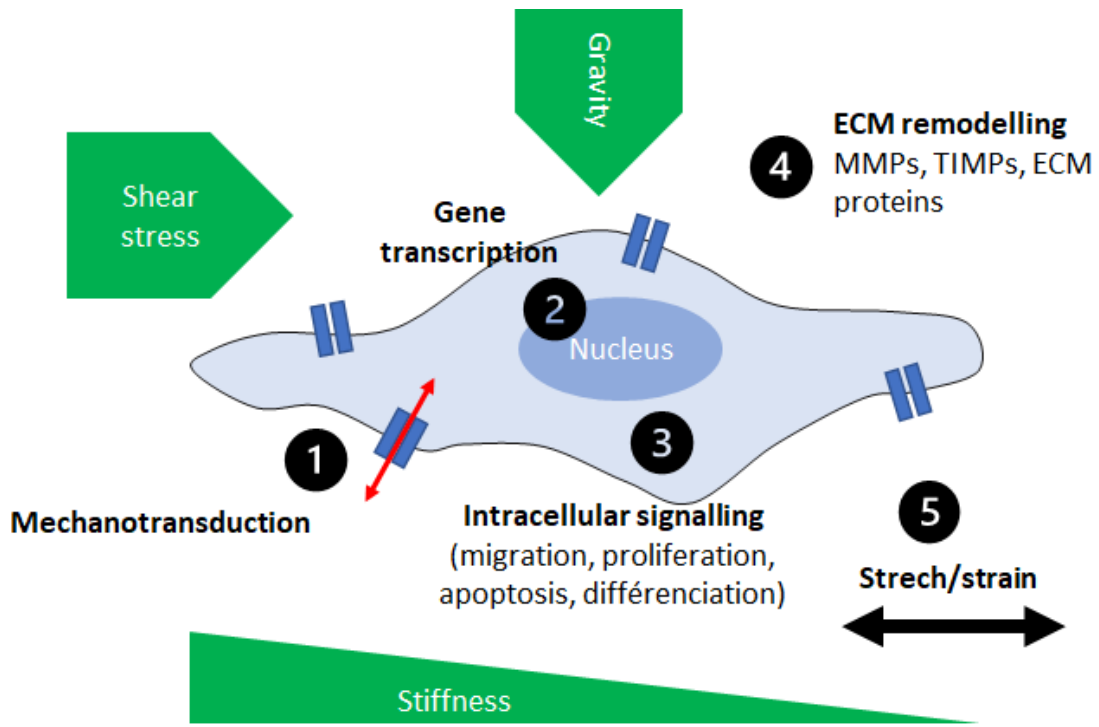


Figure 4 – Overview of Signal Transduction⁷⁷

On a systemic level, mechanotransduction is a crucial part of a range of physiological processes. Embryonic development is a combination of chemical and mechanical gradients, and specific combinations lead to the development of specific tissues, organs, and even protrusions that eventually turn into limbs⁷⁸. For example, in mammals, heart development starts as a straight tube that in response to circulatory pressure and myocardial contraction leads to looping and

eventual formation and separation of the chambers of the heart^{79,80}. In the musculature, muscle fibres stretch and contract in response to external mechanical cues, which are converted into bioelectrical information that the central nervous system and brain can then act upon⁸¹. Similarly, our auditory system relies on mechanical cues, where hair cells in the inner ear have protrusions that convert vibration into sound⁸², and our sensile system, where the mechanical interaction between our sensory receptors and any object are translated into actionable cues (such as the shape or texture of an object)⁸³.

In a pathologic context, incorrect mechanotransduction is associated with a range of diseases. In embryonic development, the wrong mechanical cues can lead to malformed body parts, systems, or death^{78,84}. Tumour cells often respond abnormally to mechanical cues, which may lead them to metastasise through excessive migration and proliferation^{85,86}. In the cardiovascular system, incorrect mechanical cues (or processing) can lead to blood vessel remodelling, causing hypertension or increasing thrombotic risk⁸⁴. Mechanotransduction is highly dynamic and because of the vast variety of cells is complex when looked at systemically. Understanding these processes leads to better understanding of pathology and in turn gives insight into therapeutic options.

2.2 Surface Stiffness in Cell Biology - Influence on Cell Morphology, Function and Migration

The stiffness of a surface is a measure of how resistant it is to deformation. In a biological environment, this can range from ultra-soft tissues such as fat, to ultra-hard such as bone. Through mechanoreceptors, cells sense these differences, which can lead to the activation

of different signal transduction cascades, and ultimately changes specific to their environment. Cell morphology and function are inextricably linked where changes in one will likely lead to changes in the other.

Cell structure, size and shape are dynamic characteristics that can be influenced by mechanical cues such as surface stiffness. Stiffer substrates can promote integrin clustering, which can lead to the formation of large focal adhesions⁸⁷ – transcellular proteins such as focal adhesion kinase and Src kinases that bundle together and are involved in binding a cell to its environment^{88,89}. These structures can act as anchors, causing stronger binding. This in turn allows for more actin bundles to polymerise through Rho GTPase family proteins such as Rac1 and RhoA, leading to bound cells spreading out more than they might^{90,91} on softer substances. It is worth noting that since different cells thrive on different surfaces, this is not necessarily a universal effect.

Localisation of these structures in response to stiffness, such as a stiffness gradient, can lead to migration by force transfer through the focal adhesions from high to low, or low to high stiffness^{92,93}. Cells filipodia (long, thin protrusions) and lamellipodia (wide protrusions) are associated with the leading edge of a cell (i.e., the side of the cell in the direction in which it is moving)⁹⁴. These structures contain many focal adhesions and binding is driven by mechanosensing from them). From the other side of the cell (i.e., opposite side from the direction the cell is moving), actomyosin contraction leads to rear-end retraction, where bonds between the cell and the substrate are broken to allow for cell movement⁹⁵. Here, RhoA mediation can lead to

a “mesenchymal” style of migration, as it increases cellular contractility and the formation of stress fibres. Meanwhile, Rac1 mediation leads to an “ameboid” style of migration. This influences directionality, as stable and regular focal adhesions in specific locations will promote movement in that direction (compared to the more “ameboid” style)⁹⁶. This can also happen without stiffness gradient, where chemokines and cytokines might lead to migration through mechanosensing (i.e., the mechanosensing machinery is still required even in response to biochemical cues). Changes in cell shape also affect cell structure. Migration speed is also influenced by stiffness and based on adhesion dynamics – intermediate stiffnesses will generally lead to highest speeds as it balances bond formation and stabilisation with bond breakage^{97,98}. From a metabolic perspective, surface stiffness also influences glycolysis and oxidative phosphorylation rates, as changes in structure and function need to be powered⁹⁹.

The changes in genetic expression due to surface stiffness can lead to dramatic effects. For example, stiffer substrates have been shown to cause the translocation of certain transcriptional co-activators (such as YAP and TAZ), which leads to the activation of genes involved in cellular proliferation and apoptotic downregulation¹⁰⁰. Inversely, extremely low stiffness surfaces can cause anoikis, a specific type of programmed cell death driven by lack of cell-matrix interactions¹⁰¹. Stiffness ranges, supported by other biomechanical cues, direct stem cell lineage specification. Hard substrates like bone can lead osteogenic differentiation¹⁰², soft substrates such as brain tissue can lead to neurogenic differentiation¹⁰³, and intermediate substrates can lead differentiation of cells that thrive at those stiffnesses¹⁰⁴.

Cell movement can also occur collectively, which adds complexity to mechanotransduction. In some situations, such as on softer substrates, cells can form strong bonds with each other, leading them to move cohesively. Meanwhile, on stiffer substrates, there can be a “leader-follower” phenomenon, where cells might “lead” others in a particular migratory pattern^{105,106}.

2.3. Molecular Clutch & The General Actomyosin Response

The molecular clutch is an analogy used to describe a way in which cells translate mechanical force into biochemical signals and then back into mechanical force. This is a dynamic process that is driven by components of mechanotransduction – the extracellular matrix (ECM), cell-surface mechanosensing receptors and their related proteins, and the intracellular actin skeleton. If all these components are bound and aligned, this allows force transmission¹⁰⁷. This can be thought of as a clutch, which can engage and disengage.

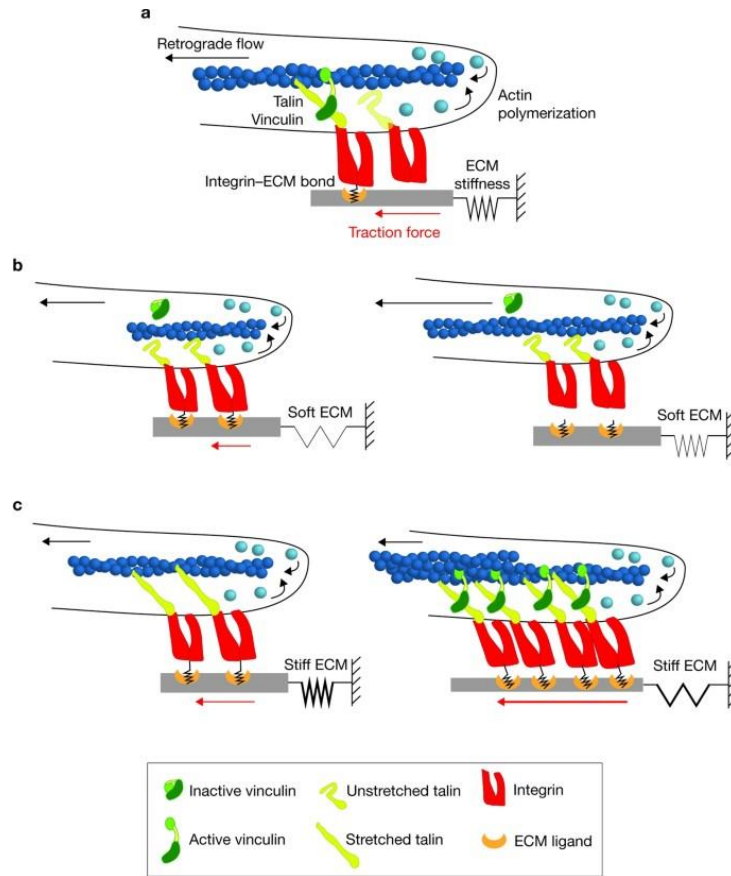


Figure 5 – Overview of Molecular Clutch Mechanism Showing Differential Roles and Responses to Substrate Stiffnesses. Actin/Actomyosin in Blue¹⁰⁸.

Actomyosin, a fundamental component of force generation, refers to the actomyosin complex that forms within the cytoskeleton and is composed of actin filaments and myosin motor proteins. Polymerised actin forms filaments that provide a scaffold along which myosin motor proteins can move, powered by ATP¹⁰⁹. The association of hundreds of myosin with actin filaments in a staggered array forms cross-bridges that when “powered” can generate significant traction force. These actomyosin structures push on the cytoskeleton, forming protrusions such as filopodia, lamellipodia and pseudopodia, depending on other factors^{110,111}. This dynamic is central to cell morphology and drives many of the processes discussed in previous sections such

as shape and motility. Translating these mechanical forces into activity requires focal adhesions, which are specialised structures that connect the actomyosin machinery through the cytoskeleton and to the exterior environment. Focal adhesions are composed of an integrin receptor with many support proteins such as vinculin, talin, and paxillin^{112,113}. The integrin receptor is transmembrane and binds to the ECM ligand, while the support proteins bind the integrin to actin. Rho GTPases modulate actin dynamics, leading to a process known as retrograde flow, where actin polymerises at the edge of the cell^{114,115}. This polymerisation pushes on the cell membrane, causing the actin filament to move retrograde (i.e., away from the membrane). This is where the molecular clutch acts. The focal adhesion proteins, when bound – or engaged – to actin, prevent retrograde flow. This causes actin polymerisation to push on the cell's cytoskeleton, essentially forcing a protrusion. It also leads to the transmission of force to the ECM. When unbound – or disengaged – retrograde flow can occur, and the protrusions do not form. This process is dynamic in nature – it assembles and disassembles in response to the environment (such as substrate stiffness) and cellular needs, it can result in a range of different processes (migration, spreading, or other)^{116,117}.

2.4. Platelet Actomyosin Response

Upon vascular injury, platelets activate through the process outlined in section 1. They go from discoidal cells to attachment and spreading with filopodia protrusions. As with other cells, this is an actomyosin driven process, where contractile forces contribute in large part to the attachment, adhesion, spreading and aggregation of platelets at the site of injury. It is unclear if platelets also display this molecular clutch to the same capacity that other cells do (for example, allowing for extensive migration). While much of the machinery is the same – focal adhesion-

like complexes that bridge actomyosin to the ECM - there are also some key differences that drive different behaviours. Platelets have been shown to migrate very short distances^{118,119}, however due to the nature of their role in coagulation, the platelet response needs to be immediate, as delay would lead to excess blood loss. They are also relatively short-lived cells and “single use”, so may lack long-term adaptive responses. Outside of their primary role, there is evidence that platelets, or maybe subpopulations of immunoresponsive platelets, do move more^{118,120}. Specific ligand-receptor interactions are also slightly different, meaning signal transduction is also different¹²¹. Platelets are sensitive to activation, which encourages them to strongly bind themselves to the substrate. A consequence of both their activation and their binding is the release of granules, which are unique to them^{45,49}. The chemokines within act to positively reinforce the activation pathways, leading to further, stronger activation, and therefore attachment to their surface. This works counter to much of the actomyosin role responsible for migration, as it limits the dynamicity that allows for attachment and detachment. The strong bonds formed between activated platelets and fibrinogen leads to aggregation, which also works against motility and detachment, as their role is to form a clot. The influence of substrate stiffness will be further discussed in the following section.

3. Traction Force Microscopy (TFM)

3.1. Principles of TFM

Traction Force Microscopy (TFM) is a method to leverage mechanical interactions and measure force exertion by cells upon their surroundings, by using an elastic substrate. When a cell mechanically interacts with a substrate, there is a transfer of force. By seeding a substrate of known mechanical properties with fluorescent nanobeads and imaging these cell-substrate interactions, minute movements in the beads can be tracked, measured, and traction forces can be measured (figure 6).

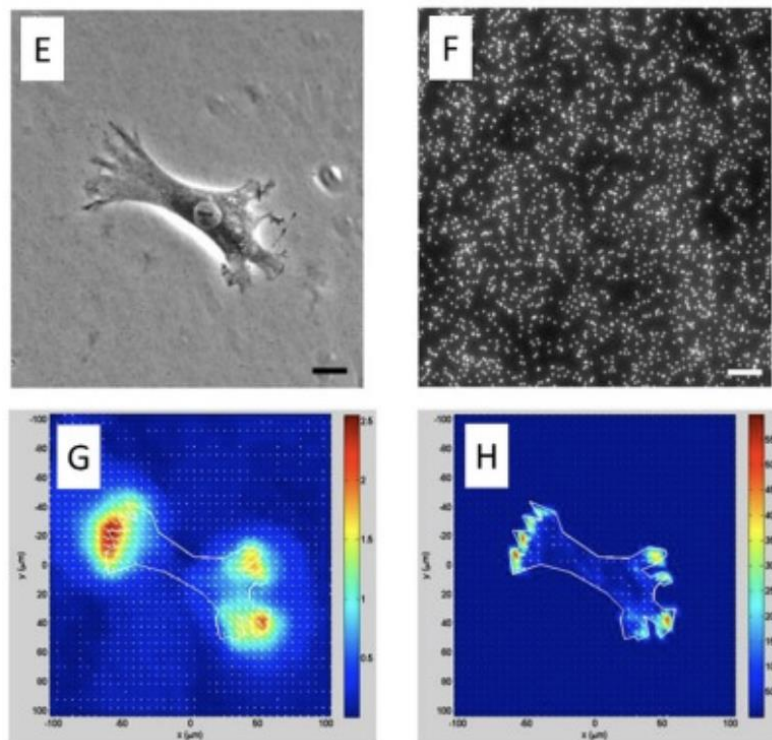


Figure 6 – Overview of TFM¹²²

3.2. Considerations and Techniques in TFM

Preparation of the Substrate: Substrates are chosen based on mechanical properties – they must be elastic to allow for deformation, but structurally strong to not be damaged. Additionally, the thickness and opacity of the gel must be considered, as imaging occurs through it¹²³.

Common choices include silicone polymers such as polydimethylsiloxane (PDMS) or hydrogels

such as polyacrylamide (PA), which are often used because of their easily tuneable stiffness^{124,125}.

Embedding of Fluorescent Beads: For visualisation of the deformations, fluorescent nanobeads are seeded into the substrate. These are typically a few hundred nanometres in diameter. Even distribution of the beads is important for good resolution¹²⁶. As the concentration of beads needs to be controlled to prevent image saturation (and therefore poor results), it is possible to increase resolution by seeding beads that fluoresce at different wavelengths^{127,128}.

Surface Functionalisation: To facilitate cell adhesion, the substrate surface is functionalised using proteins like fibronectin, collagen, or other integrin-binding proteins, as well as serum albumin to prevent non-specific binding^{124,125}. This ensures cells bond to the surface and promotes further interaction, while also stopping them from bonding so firmly that they cannot move or exert dynamic forces.

Imaging and Data Acquisition: While traditional fluorescence microscopes can be used, confocal microscopy is often preferred because it allows for optical sectioning, or the ability to image thin slices within a thicker specimen, which can remove background noise and in certain setups give 3D displacement data¹²⁹. Focus and directional drift of the image can be an issue, which can be limited using isolation tables and auto-focus attachments for microscopes. Other imaging setups can also be used, which are discussed in “advanced techniques”. Data acquisition has spatiotemporal considerations. Before putting cells onto the substrate, a reference image is

required showing the fluorescent beads in their relaxed state before deformation. The rate of imaging depends on cell dynamics and processes. Faster processes may require imaging every second.

Data Analysis: Before analysis can be run on images, drift, and focus issues must be accounted for. Drift correction software can be used on images to ensure that any movement of the beads is due to cell forces. Then, by comparing bead position after cell deformation with before, displacement vectors for each bead can be calculated, showing a map of substrate deformation. Paired with established elastic properties of the substrate (which can be found in the case of PA and PDMS or established using an atomic force microscope), mathematical models such as the Bayesian¹³⁰ or Fourier¹³¹ transform of the Boussinesq solution for elastic half-space combined with Finite Element Methods¹³¹ can be used to calculate forces. This can then be visualised using force vector arrows, showing direction and magnitude of the forces exerted, or by heat maps to represent regions of high and low force¹³².

Advanced Techniques: TFM has had some significant developments in recent years. **Higher dimension TFM:** While traditional TFM assumes 2 dimensions, (x and y on the surface of the gel), the reality is that gels are not 2D, and beads are not a uniform layer but rather dispersed within the gel. 2.5D TFM has been developed to account for some third-dimension depth without the need of full 3D environments¹³³⁻¹³⁵. This is sometimes called 3D TFM, although is distinct from analysing forces in fully 3D environments (also confusingly called 3D TFM), for example where a cell might be inside a matrix¹³⁶. This involves thicker gels and may require more

sophisticated microscopy, like multiphoton devices, to capture bead displacements throughout the gel¹³⁷. High-Throughput TFM: By micropatterning substrates¹³⁸, instead of seeding with nanobeads, the predictable patterns lead to higher-throughput, allowing for simultaneous imaging and analysis of many cells.

3.3. Limitations and Challenges of TFM

While TFM can be informative, it does come with a range of limitations that must be considered.

Technical: Spatial resolution is limited by the size and density of seeded beads. If beads are too large, densely clustered, or too few, your spatial resolution will be limited¹³⁹. This can be counteracted by using nanobeads with different fluorophores, however this also introduces challenges and will need more sophisticated equipment^{127,139}. Depth resolution is also limited and leads to assumptions during data processing. Further assumptions include uniform substrate elasticity and surface topology¹³¹. While 3D TFM can be used, it is more technically demanding, and carries its own limitations with regards to matrix size and depth. Finally, drift and noise can be a challenge. Positional drift can generally be corrected for using drift adjustment programs, however depending on the background noise and level of focal drift, it may provide additional challenge.

Biological: Cellular heterogeneity is a significant complication. Across and within cell types and subpopulations, cells do not exert the same forces^{138,140}. This natural variability can make it challenging to accurately distinguish between cellular differences and experimental noise. TFM experiments can often be long, so it is important to consider the durability and sensitivity of cells to external stimuli, particularly when using imaging setups that might require warm/bright lights. Regardless of the substrate used, it will not accurately mimic biological tissues. Structurally, the mechanical properties *in vivo* are complex and rarely uniform^{123,140,141}. Tissues are generally 3D and therefore cells will have forces acting on them in all directions. Many tissues have complex topologies that can't be mimicked and used in TFM. This could affect cell behaviour and not be representative of *in vivo*.

Data Interpretation: As previously mentioned, assumptions are made in the underlying mathematics that do not necessarily reflect reality. Substrates are assumed to be homogenous and have linear elasticity. Further, the surface is generally assumed to be flat, when in reality it will have peaks and troughs which will affect results. Complications caused by drift and focus can also cause issues during interpretation. Finally, without additional information, TFM will only give information on the forces generated by a cell, but not on which cytoskeletal structures are providing it. Inhibitor studies and other techniques need to be paired with TFM to give more clarity¹⁴². Complex environments also introduce challenges when interpreting data – for example deciphering individual contributions to cell-cell interactions, or accounting for cell-led remodelling of the local environment, and how this might affect substrate properties¹⁴³.

3.4 TFM in Practice

Cells are in a constant state of interaction with their environment, be it through chemotaxis (chemical gradients), thermotaxis (temperature gradients), phototaxis (light gradients), rheotaxis (fluid flow), mechanotransduction (response to mechanical/force stimulus), or other¹⁴⁴. Actin and myosin are significant drivers of intracellularly forces¹⁴⁵. Molecular motors, such as myosin, hydrolyse ATP, converting chemical energy into mechanical energy, which is used within the cell to generate force to push or pull on cytoskeletal filaments. Actin is a family of proteins that polymerise to form actin filaments. As these filaments assemble and disassemble, they change the intracellular structure. Together, actin-myosin interactions generate intracellular forces that are central to motility, spreading, and division¹¹¹.

When cells sense their environment, they make physical interactions and can form bonds with it, through focal adhesions. These specialised structures are composed of protein assemblies, usually including integrins¹⁴⁶ that bind to extracellular proteins, and talin and vinculin, which bind integrin to the actin cytoskeleton¹¹². These physical bonds allow for the transfer of force between the intracellular and extracellular environment, causing deformation in what it binds to, and it is through this that cells can attach, spread, and migrate. Hence, measuring these forces is integral for a better understanding of disease states processes where mechanotransduction is important, including arteriosclerosis, cancers, and bone, cartilage, and muscle defects¹⁴⁷. Beyond the forces that cells exert, they are also able to sense the stiffness of their substrates and adjust their behaviour accordingly, therefore TFM can also be a tool for analysing how they perceive and respond to the mechanical properties of their environments.

3.5 Cell-Substrate Interactions

Substrates have a range of properties, such as their topography, stiffness, and elasticity, which influence how cells interact with them. Surface features that make up the topography of a substrate, such as peaks, troughs, grooves, and ridges, can influence cell activity, leading to change in shape, activation state, and migration¹⁴⁸. On stiffer substrates, cells tend to spread out more and generate stronger traction forces¹⁴⁹, possibly due to an increased number of focal adhesions¹⁵⁰. Some cells experience increased motility and migration on these stiffer substrates, while others might experience inhibited movement. Further, stiffness gradients can influence cellular motility, with cells migrating towards areas of higher or lower stiffness¹⁵¹. Stiffness can also guide stem cell differentiation, following a neural or muscular fate if the surface stiffness mimics that of their respective environments¹⁵². In fact, surface stiffness paired with other tactile cues drives much of developmental biology, dictating the development and location of organs, limbs, and tissues¹⁵³. Likewise, the elastic properties of a surface can affect cell function, with cells taking pulling proteins off the surface with them¹¹⁸. Substrate coating can also play a significant role, with cells responding differently to different ligands, which might activate different intracellular cascades that alter gene expression, also influencing motility, activation, and shape^{142,154}.

3.6 TFM, Mechanotransduction, and Platelets

As established in previous sections, a significant part of platelet activity is mechanotransductive in nature – activation in response to high shear conditions. Therefore,

understanding when, where, how and how much force they produce is integral to understanding their role and developing therapeutic solutions that leverage it.

Substrate stiffness mediates platelet adhesion and spreading. When platelets were allowed to spread on polyacrylamide gels with different stiffnesses (ranging from 0.25-100kPa), it was found that as stiffness increases, so does both the number of platelets attaching to the surface and the average spread area of the platelets. This effect was independent of ligand density, as fibrinogen concentration was kept constant¹⁴⁹. Increased stiffness also increased platelet activation. Knockout studies in the same paper showed that Rac1, a Rho GTPase, was essential for mediating platelet adhesion to the substrate, and Rac1, myosin and actin polymerisation were all essential for spreading. Note that since platelets respond to multiple pathways, they still undergo thrombin-induced aggregation in the absence of Rac1¹⁵⁵. The suggested mechanism for these effects was that when a platelet “touches down” on softer, more easily deformable substrates, bond strength might be weaker, causing weaker platelet-substrate interactions. On stiffer surfaces, greater resistance leads to stronger bonds, increased outside-in signalling, and therefore an increase in cascade signals, leading to more activated platelets with more focal adhesions. A similar effect was found on different stiffness substrates with collagen as the ligand, albeit less marked than in the fibrinogen study¹⁵⁶.

Traction Force Microscopy work has advanced on these studies. Early studies suggest that platelets exert force on their substrate in geometric patterns such as circles, triangles, and lines, that line up with actin localisation in stained platelets, supporting the central role of actin in

force generation. Within their testing range, platelets were not shown to generate more force as substrate stiffness increased, although precise ranges were unclear (i.e., it may be that force generation differences are found in ranges as opposed to specific stiffnesses, and therefore outside of the range they studied, or that shape and size of platelets were not considered)¹⁵⁷.

Further, they suggest that platelets generate force in three distinct patterns – plateauing, where force generation quickly increases and maxes out; oscillating, where after an initial increase there is a period of force generation oscillating between high and low; and relaxing, where after the initial increase there is a gradual decrease. Finally, they support the idea of that the maximum total force generated by a cell is dependent on its spread area, which is also found in other cells^{158,159}.

The cause of force generation is something that can be elucidated using TFM. As there are a range of components involved in adhesion and spreading, they must all be investigated for their individual contributions. Ligand specificity influences platelet binding. At high shear rates, platelets preferentially bind von Willebrand Factor^{160,161}, whereas at low shear rates they bind fibrinogen¹⁶⁰. On-rate of VWF-GPIIb/IIIa bonds is high, meaning that at high shear stresses, when VWF elongates and binding sites are exposed, platelets can quickly bind it^{162,163}. Meanwhile, fibrinogen-platelet binding, which occurs through α IIb β 3 (an integrin which can also bind VWF), has lower on-rates¹⁶⁴, and are therefore bonds cannot form quickly enough at high shear rates. There is contradicting evidence for if surface ligand type and concentration is important for total force generation. Some work on fibrinogen suggests that so long as a platelet meets a threshold for thrombin activation^{165,166}, the amount of fibrinogen present is irrelevant - which supports previous work that suggests an “all or nothing” response from platelets, even in the

presence of activation inhibitors (i.e. if a platelet is activated, internal machinery leads it to produce maximum force, so long as that machinery isn't being inhibited)¹⁶⁷. However, it contradicts experiments using atomic force microscope cantilevers to measure contractile strength in platelets, where they found that a 2.5fold increase in cantilever stiffness resulted in a twofold increase in platelet force generation¹⁶⁸. It is also important to note that the cantilever work found lower overall forces, so a 2-fold increase was still below the force generation in the TFM work. The difference could be explained by the experimental methods – in TFM platelets spread and flatten on a surface, in the AFM work they were between two surfaces, which might be more representative of platelet activity *in vivo*. In future research, the same work with ADP as an agonist, and with fibronectin and collagen as substrates is yet to be carried out and would be of interest. Another study shows a difference in force generation and actomyosin localisation based on surface ligand – fibrinogen or VWF. VWF bound platelets generated more force, and f-actin was shown to radiate from the centre to the edges. Meanwhile, fibrinogen bound platelets generated less force and generally had a “hollow” actin structure (although morphology was more varied than in VWF), with actin localising around the platelet edge and not in the centre¹⁶⁹. Another recent work somewhat contradicts this, where they directly show on fibrinogen substrates that actomyosin as the driver of force generation through a combination of TFM and super resolution STED microscopy. Platelets in this paper did not display the “hollow” pattern to the same degree. Force generation was measured across time, and after 30 minutes, the same platelets were labelled for actin and vinculin. Vinculin is a focal adhesion protein responsible for linking integrins to actin¹⁷⁰. Peak forces on traction force maps lined up with the location of high concentrations of vinculin, as well as actin fibres orientated from the peak force zone towards the centre of the cell¹⁶⁵. It is worth noting that actin plays a dual role in platelets- initial

polymerisation forms filopodia and lamellipodia at the platelet edge to increase platelet area, allow for more binding opportunities, and help cover wound site, followed by the force generation which would be involved in clot contraction^{167,171,172}. That said, across the lifetime of a spread platelet, actin dispersion, as well as area and circularity (in spread shape) do strongly correlate with total force generation¹³⁸.

3.7 Potential Therapeutic Implications:

Ultimately, understanding how this range of factors – ligand, shape, size, cytoskeletal arrangement – and more are key to understanding the specifics of platelet activity, with the aim of translational solutions to platelet dysfunction. How platelets respond to substrates is of utmost importance when developing blood contacting devices – stents, valves, pumps, and more – as their thrombogenicity dictates the life of the device, which are often implanted through high-risk open surgeries^{173,174}. Enhancing platelet adhesion and force generation could be of potential therapeutic benefit in patients with haemophilia, certain subtypes of von Willebrand disease, and other bleeding disorders. Inversely decreasing adhesion and force generation would also be of benefit for patients with high clotting scores, reducing the risk of heart attack, strokes and DVTs.

4. von Willebrand Factor (VWF) and von Willebrand Disease (VWD)

4.1. VWF

VWF is a multimeric glycoprotein central to clotting that plays a role in both primary and secondary haemostasis. VWF is produced by both megakaryocytes that become platelets⁵⁷ and p

endothelial cells, where it is stored in specialised organelles called Weibel-Palade bodies⁵. Upon stimulation, such as during vascular injury, it is secreted. In primary haemostasis it bonds platelets to the site of injury¹². In circulation, it binds and stabilises Factor VIII, a key component in secondary haemostasis¹⁷⁵. Structurally, VWF is composed of 4 domains that combine to form a mature subunit, each domain contributing to its diverse role. These mature subunits can polymerise, forming large VWF structures¹⁷⁶. Genetic defect, disease (such as autoimmune) and drugs can affect VWF in a range of ways, leading to VWD, which will be discussed more later in this section.

Table 3 – Structure and function of VWF Domains.

Domain	Description	Function	Lack/Misfunction Causes
D1-D2	N-terminal	Site for VWF subunit multimerization	Biosynthetic defects ¹⁷⁷
D'	Factor VIII binding domain	Protects FVIII	Decreased FVIII levels
D3	Factor VIII binding domain	Stabilizes FVIII interaction	Decreased FVIII levels ¹⁷⁸
A1	Platelet binding domain	Binds to platelet GPIIb α under shear conditions ¹⁷⁹ Bind to collagen ¹⁸⁰	Type 2B and 2M VWD ¹⁸¹

A2	Central domain	ADAMTS13 cleavage site ¹⁸²	Type 2A VWD ¹⁸³
A3	Collagen binding domain	Binds to collagen ¹⁸⁴	Type 2M, presents as Type 1 VWD ¹⁸⁵
D4	Connecting domain	Connects A3 to the B domains	Qualitative and quantitative defects ¹⁸⁴
B1-B2-B3	Central domains	Structural	Necessary for VWF
C1-C2	Platelet/collagen binding	Platelet adhesion to fibrin and VWF ¹⁸⁶	Limit platelet adhesion/stabilisation
CK	C-terminal domain	VWF multimerization ¹⁸⁷	Limit VWF multimerization

4.2. Role of von Willebrand Factor in Haemostasis

As mentioned in Section 1, VWF is involved in the adhesion, activation, and aggregation of platelets. Under appropriate conditions, such as vascular injury, VWF binds to exposed subendothelial collagen through the A1 and A3 domains^{180,184}. Through glycoprotein GPIIb α , circulating platelets can bind to the A1 domain transiently and permanently. Transient binding slows the platelets, rolling them and allowing them to form stronger bonds¹⁸⁸. Adhesion of platelets through this bond leads to activation⁸, which triggers a range of intracellular cascades leading to more platelet adhesion, activation, and aggregation (as discussed in section 1). VWF is

a chaperone protein for Factor VIII, acting to stabilise and prevent degradation. Once secondary haemostasis has been triggered and thrombin is being made, thrombin cleaves Factor VIII from VWF, activating it into Factor VIIIa, which is then presented to Factor IXa, together activating Factor X (Xa), and forming the final step of the intrinsic pathway before it becomes part of the common pathway⁶³. VWF is regulated by ADAMTS13, a metalloproteinase that acts by cleaving large multimers into smaller, less reactive multimers⁴.

4.3 Types and Causes of von Willebrand Disease

Considering the importance of VWF, it is unsurprising that malfunction can lead to disease. Both a quantitative lack of and qualitative changes to VWF can cause excessive bleeding. These are generally categorised into types 1 and 3, which are caused by a mild to moderate and extreme/complete lack of VWF respectively; type 2 subtypes, which have VWF but certain aspects do not work properly; and acquired VWD (AVWD), which is deficiency or disfunction caused by other diseases or medications.

Table 4 – von Willebrand Disease Types and Subtypes¹⁸⁹⁻¹⁹¹.

Type/Subtype	Cause/Defect	Information
Type 1	Mild/moderate quantitative deficiency	Most common genetic type
Type 2	Qualitative defects	Four Subtypes:

		2A, 2B, 2M, and 2N
2A	Absence of high molecular weight (HMW) multimers	Loss/decrease of platelet-dependent function
2B	Increased binding to platelets	Risk of thrombocytopenia (low circulating platelets)
2M	Reduced binding to platelets not caused by 2A	Decreased platelet-dependent function
2N	Reduced binding of VWF to factor VIII	Can present as haemophilia A
Type 3	Extreme/complete quantitative deficiency	Rarest genetic type
Disease-induced AVWD	Acquired defect in VWF function/quantity	Myeloproliferative, Cardiovascular and Autoimmune Disorders
Drug-induced AVWD	Drug-related decrease in VWF activity or quantity	Common drugs include:

4.4 Diagnosis, Challenges in Diagnosis, and Treatment of VWD

Diagnosis: VWD diagnosis is a complex process, in part due to rarity, in part due to similarity to other diseases, and in part due to variability. Due to a significant genetic component,

clinical evaluation and family history is a common way of tracking this disease. If an issue with VWF is suspected, there are a series of blood tests that can be performed to assess for clotting factors and VWF. VWF multimer gels can be used to determine the distribution of multimer size for identifying the loss of high molecular weight multimers. This also usually coincides with functional changes in collagen and platelet binding. These binding interactions are usually normalized to the amount of VWF antigen. VWF:Ag test measures the amount of VWF in the blood through a VWF antigen. Decreased or non-existent levels could be indicative of all types of VWD but is important in showing that VWF levels are causal to excess bleeding¹⁹². VWF:RCo measures the functionality of VWF by exposing blood plasma to ristocetin¹⁹³. Ristocetin is a molecule that acts as a catalytic cofactor (possibly by causing a conformational change in VWF) that allows VWF-GPIb bonds to form, even outside of ideal conditions. This causes aggregation, which decreases the cloudiness of the plasma and allows more light to pass through a sample. This change in opacity can be measured and used as a proxy for the degree of platelet aggregation. This test measures the capacity that VWF has for platelet binding and is also reduced in all types. The ratio between the VWF:Ag and VWF:RCo tests is also important, as it can be indicative of the quality of bonding occurring¹⁹⁴.

Factor VIII Activity tests measure clotting time of blood mixed with specific reagents, which is also reduced in VWD¹⁹⁵. Once the diagnosis is confirmed, subtype testing may be required, which involves Ristocetin-Induced Platelet Agglutination (RIPA) and binding assays for factor VIII.

Table 5 – von Willebrand Disease Diagnosis^{189,196–200}.

Disease /Subtype	VWF:Ag	VWF:RCo	VWF Multimer Analysis	FVI II:C	FVIII:C Binding Assay	RIPA	APTT	FIX Activity	Comments
Type 1	↓	↓↓	=	↓	=	=	=	=	-
Type 2A	↓	↓↓↓	↓↓	↓	=	=	=	=	Often mistaken for Type 1
Type 2B	↓	↓↓	=/↓	↓	=	↑	=	=	RIPA is diagnostic
Type 2M	↓	↓↓↓	=	↓	=	=	=	=	Multimers Analysis distinguishes from Type 2A

Type 2N	=	=	=	=	↓↓	=	=	=	Mistaken with Haemophilia A. FVIII binding distinguishes
Type 3	↓↓↓/∅	∅	=	↓↓	=	=	=	=	-
Haemophilia A	=	=	=	↓↓	=	=	↑	=	VWF normal. FVIII:C assay is diagnostic.
Haemophilia B	=	=	=	=	=	=	↑	↓↓↓	VWF and FVIII:C normal. FIX

									diagnostic.
Platelet -type (pseudo) VWD	=	=	=	=	=	↑	=	=	Mimics Type 2B. Genetic testing differentiates.

Key:

↑: Increased

↓: Mildly decreased.

↓↓: Moderately decreased.

↓↓↓: Extremely decreased.

∅: Undetectable

=: Normal or no change

Challenges: Diagnosis of VWD continues to be complicated. Mild VWD may go undiagnosed until a severe injury occurs, with slightly prolonged bleeding being the only

symptom and hard to detect and having been normalised by patients. Within subtypes, VWF levels vary in response to a range of factors (medication, exercise, stress, infection and more), meaning multiple tests may be required before VWF levels are called into question. The requirement of retesting, specialised tests, and multiple types of tests adds complexity and can contribute to misdiagnosis. As VWD is a bleeding disorder, it might initially present similarly to other conditions in the same category, such as haemophilia, idiopathic thrombocytopenia purpura, drug-induced bleeding and other¹⁹⁸⁻²⁰⁰.

Treatment: With the primary cause of VWD being genetic and therefore presently without cure, the goal treatment is to control excessive bleeding. Treatment depends on diagnosis since different underlying for each type of WVD need to be addressed. Desmopressin is a synthetic hormone that stimulates endothelial cells to release VWF and FVIII into circulation. This is effective for Type 1, as it increases circulating VWF, however does not help most Type 2 or Type 3. For Type 1 patients who do not respond well to desmopressin, and for Type 2 and Type 3 patients, replacement therapies are effective, either through plasma transfusion or clotting factor concentrate transfusions^{197,198}. Recombinant VWF is a newer option also available²⁰¹. Some alternative methods to increasing VWF availability is to use antifibrinolytic agents, such as tranexamic acid and aminocaproic acid, that help to decrease clot breakdown; using fibrin sealants as topical agents that promote clotting at wound sites; the use of birth control pills to combat blood loss due to menstruation; and limiting the use of NSAIDS that interfere with clotting.²⁰²

5. Microfluidics: An Emerging Diagnostic Tool for VWD

5.1 Principles of Fluid Flow and Microfluidic Systems

Microfluidic systems allow for the manipulation of fluids on the micron scale. Due to the prevalence of fluids across disciplines, these systems are applicable in diverse settings from inkjet printers to healthcare²⁰³. Microfluidics leverage a few key concepts. Generally – although there are many exceptions²⁰⁴ - they operate at low Reynolds number (Re) – a dimensionless measure that describes the type of fluid flow or flow regime and determined by $Re = (\rho vL)/\mu$, where ρ is density, v is velocity, L is the length of the channel, and μ is the viscosity of the fluid. Many microfluidic systems operate at a low Re, resulting in laminar flow (where particles travel in parallel layers). This minimises turbulence and mixing and allows for predictable and precise fluid movement, particularly when paired with precise microfabrication techniques, such as photolithography²⁰⁵. No-slip conditions at the solid-fluid interface can promote surface interactions, useful in many biological and chemical systems. Despite low Re, techniques have been developed that allowing for rapid mixing and reaction times^{204,206}. They have high surface-to volume ratios, which can be important for chemical reactions and/or temperature transfer systems. They are generally low-volume systems, which can help control waste with respect to sample and reagent use, and speed up reactions. Often, these systems can also integrate multiple processes (for example preparation, mixing, reacting and subsequent detection of something using multiple reagents)^{207,208}. Many other principles can be leveraged, depending on application, such as electroosmotic flow, hydrodynamic focusing, and more. The field of microfluidics is one of active research and holds promise across many disciplines, including diagnostics of diseases of the blood.

Two key concepts of fluid flow for our research are those of shear stress and elongational flow. If you think of fluid as layers of particles, then the motion of each layer will carry with it a certain force. In situations where layers move at different speeds from their adjacent layers, the difference in motion creates a shear force, the gradient of which across multiple layers is the shear gradient. If you consider a straight tube with undisturbed fluid flowing through it, intermolecular forces between the layer closest to the wall and the wall, which is stationary and has a fixed molecular structure, create a “no slip” boundary, where molecules in the outermost fluid layer are stationary. The next layer in will experience a dragging effect from these stationary molecules also due to molecular interaction, albeit less strong than the no-slip due to the increased freedom of movement that liquids have compared to solids. This continues with each concentrically until you reach the innermost layer, which will have the greatest velocity. The velocity gradient (i.e., difference in velocity between layers) along with the viscosity of the liquid dictate the shear stress within a layer, the gradient of which is the shear gradient.

As an analogy, consider a block of gelatine made up of layers. If you push down on it with your hand and then move it laterally, the top layer will move the most since it's directly under your hand. Each layer under that will move a little bit less due to the resistance from the viscosity of the layer below it, and the bottom layer will not move at all as it is in contact with a solid. If your gelatine is more viscous, the gradient will be smaller. If it is less viscous, the gradient will be greater. When considering a stenosis, the space available for fluid to pass through becomes smaller than what was previously available. To maintain flow continuity (conservation of mass for a fluid in motion), fluid must increase in speed. This acceleration leads to higher concentric velocities and therefore a greater shear gradient.

While shear can be thought of as lateral sliding of fluid elements, elongational flow can be thought of as their stretching or compression (for example stretched lengthwise and narrowed widthwise) along the direction of flow. So, when flowing towards a stenosis, molecules are squeezed closer to each other as the space available for them decreases. As they pass through the stenotic region, they rapidly accelerate, again to maintain flow continuity (since the same volume must pass through this region as adjacent ones in any given time). Once they exit the stenosis, they move from high to lower velocity suddenly, causing deceleration and a local, transient increase in density caused by molecules bunching together.

As an analogy, consider a rubber band stretching. Pulling on both ends causes elongation and narrowing of the space between the top and bottom. This represents what happens in the stenosis. Letting go of one end will cause the rubber band to ping towards the other end. This represents what happens as the molecules exit the stenosis – deceleration and bunching.

5.2. Types of Microfluidic Systems

Design and functionality of microfluidic systems vary based on their required application. Because of this, there are a range of different types of systems in use and in research, each with their own advantages and disadvantages, as listed below.

Table 6 – Comparison of microfluidic systems^{209–215}. Ranking somewhat subjective.

Type of System	Complexity	Resolution	Volume	Throughput	Current Uses	Comments
Continuous Flow Microfluidics	Moderate	High	Micro to Milli	Medium	Chemical synthesis, cell sorting	
Droplet Microfluidics	Moderate to High	Very High	Nano to Micro	High	Single-cell analysis, high-throughput screening	Uses individual droplets
Paper-Based Microfluidics	Low	Moderate	Micro	Low to Medium	Point-of-care testing (POCT)	Capillary action-driven
Centrifugal Microfluidics	Moderate to High	High	Micro to Milli	High	Biomedical analyses	AKA lab-on-a-disk

Acoustic Microfluidics	High	High	Micro	Medium	Cell sorting, fluid mixing	Uses sound waves
Optofluidics	High	Very High	Nano to Micro	Medium	Biosensing, on-chip spectroscopy	Light manipulation
Thermal Microfluidics	Moderate	High	Micro	Medium	PCR amplification, enzymatic reactions	Uses temperature changes

5.3. Stenosis-Based Microfluidics for VWF

Microfluidic systems offer a simple, cost-effective platform for investigating the behaviours of blood components and their contribution to disease. By adding stenoses into microfluidic systems you can alter flow profiles, generating complex flow profiles with shear gradients and/or elongational flow, both of which affect VWF and its function^{7,188}.

In a resting state in circulation, VWF is structurally globular, this shape being maintained by a range of non-covalent bonds (hydrogen bonds, van der Waals forces and hydrophobic interactions). This structure hides many of the binding domains that VWF has, preventing activation. Under high enough mechanical force (i.e., high shear stress and elongational flow),

the non-covalent bonds break, and elongational forces cause VWF to extend. This exposes binding domains and allows for VWF-platelet bond formation¹². Elongational flow also allows for greater self-association through exposure of VWF-VWF bonding sites, and large multimers are generally even more reactive than shorter ones^{216,217}. As we've discussed, dysfunction in VWF causes VWD, and so being able to study VWF function in a simple microfluidic device could be a powerful diagnostic tool.

5.4. Paper Microfluidics and the World Health Organisation (WHO) ASSURED Criteria

Paper microfluidics is a developing field within microfluidics. By leveraging properties inherent to paper, the creation of microfluidic paper-based analytical devices (μ PADs) that act as chemical or biological tests is possible. Paper microfluidics are an attractive avenue of research for a variety of reasons. They are very cost-effective, with paper being a cheap material. Fabrication processes generally involve the use of wax and/or photolithography/laser printing and cutting, which are also cheap, relative to methods used in other microfluidic fields. They are compact, light, and designed to be single use and easily disposable. Fluid movement can be controlled using through wicking and capillary action, removing the need for electricity and external power sources. They are also generally designed for ease of use. They do, however, come with drawbacks. Due to the wicking nature of paper, there is a limit to the volume that can be used and therefore the range of tests that can be done. Due to variability in paper structure, accuracy and precision of paper is lower than microfluidic devices made from other materials. Their simplicity can mean that designing complex or multi-step assays is not possible. Paper can degrade over time, as well as be affected by a range of temperatures and humidity. The lack of a need for electricity can also be double-edged, as it limits ability to control aspects like flow rate,

which would be fully reliant on capillary action and modifications of it. Flow rates lower in μ PADs, which can limit reagent mixing and diffusion, can cause issues when considering sample evaporation and how that might affect reactions, and can lead to sample backflow and/or contamination acting against the desired effect^{205,218}.

While tools for the diagnosis of VWD already exist, they are not accessible to large parts of the world. With the aim of guiding the development of diagnostic tests for settings with limited resources (i.e., developing countries, rural regions, etc) the WHO introduced the ASSURED criteria (figure 7)²¹⁹. Tests must be:

Affordable- as low cost as possible to make them as accessible as possible.

Sensitive and Specific - with the aim of maximising accuracy and minimising false positives and negatives.

User-friendly - requiring as few complications in the process of using the POCT to minimise the risk of user-error influencing results.

Rapid & Robust – the tests need to be resistant to the elements to maximise useability worldwide.

Equipment free- not reliant on peripherals, electricity, etc.

Deliverable - to the end user, or as close to the end user as possible.

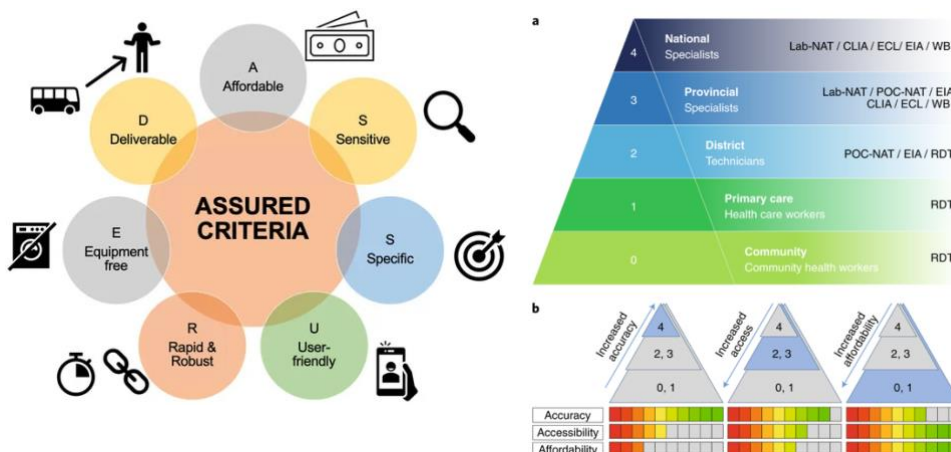


Figure 7: left Assured criteria, right Relationship between expertise level and accuracy trade-offs. High expertise offers the greatest accuracy of test, however, is expensive and not accessible. Tests that require low expertise, such as POCT, are much more accessible and affordable, however are less accurate.

Paper microfluidics offers significant potential when evaluated against the ASSURED criteria, however it has some limitations, as mentioned earlier.

5.5. Current and Future Applications of Paper Microfluidics

μ PADs have found application in a diverse range of fields. In environmental monitoring, they can be used for both water and air quality testing²²⁰, detecting heavy metals²²¹, pathogens²²², pollutants, and pollution levels²²³. In food safety, they can be used to detect pesticide levels and presence²²⁴. In agriculture, they can detect nutrient levels in soil to help guide fertiliser choice²²⁵. In the home, they are actively used to test for pregnancy and certain diseases such as COVID-19. There are early examples of other point-of-care tests (POCT) such as for the detection of HIV and malaria, as well as monitoring glucose levels^{226,227}. One of the earliest forms of microfluidic testing is the use of pH paper.

In a haematological setting, the potential of paper microfluidics is a field of active study. VWF levels and activity would help diagnose bleeding disorders quickly, cheaply, and accurately. Equally, platelet function tests evaluating adhesion and aggregation would help in haemophilia and others. On the other end of the bleeding spectrum, POCT for prothrombin time and international normaliser ratio tests for patients on anticoagulants. Complete Blood Count tests would eliminate the need for haematological analysers, with fewer reagents required and faster turnaround. Sickle cell disease could be screened for quickly and cheaply, especially in regions where it is commonly found, which coincide with developing countries. Finally, blood-borne diseases such as malaria parasite detection, HIV monitoring through CD4/CD8 ratios and others would be made much more accessible, affordable, and immediate through μ PADs.

CHAPTER 2: SPECIFIC AIMS

Aim 1: Determine Characteristics of Paper and Plastic Microfluidics in Relation to Stenoses and Flow Rates

Purpose: Can we make a framework to theoretically diagnose for von Willebrand Diseases?

Aim 2 – Determine the Viability of the System Developed in Aim 1 in the Diagnosis of von Willebrand Disease

Purpose: Does the framework work practically?

Aim 3 – Characterisation of Force Generation by Platelets on Deformable Substrates

Purpose: Better understand how platelets interact mechanically with surfaces they attach to.

CHAPTER 3: MAXIMISING FLOW RATE IN SINGLE PAPER LAYER, RAPID FLOW MICROFLUIDIC PAPER-BASED ANALYTICAL DEVICES

1. Introduction

Microfluidic paper-based analytical devices (μ PADs) offer many advantages for use in point-of-care assays. The low-cost of the components required, and the ease of larger scale production allows for extremely inexpensive devices^{228,229}. Multiple physical effects can be combined to manipulate fluid flow without the need of an external pump. The wicking nature of paper can be leveraged to promote flow through capillary action; hydrophilic plastics can be used to enclose the paper and help drive flow; hydrophobic wax barriers can effectively direct flow; as can surface tension effects from the formation of a droplet at the inlet²³⁰⁻²³⁵. Key to this is that it permits for the removal of the need of electricity as a constraint, making it an ideal tool in developing countries and emergency situations. These features are of particular benefit when considering the development of point-of-care microfluidic systems in a diverse range of biological and chemical applications, including infectious disease diagnostics²³⁶⁻²³⁸ and liquid quality testing²³⁹⁻²⁴¹ that are optimized for ease of usage, simplicity, and deliverability to the end user.

μ PADs have been limited to low-flow applications until recently, where cut-out channels have been shown to increase the speed of fluid traversing through a μ PAD^{230,242,243}. Other work creates partial²⁴⁴ and complete cut grooves within paper to increase and control flow rates up to 30 μ L/min²⁴⁵, which is otherwise not possible with traditional paper wicking. Controlling flow

rate enables the user to regulate transport relative to reaction kinetics when considering chemical or biological reactions^{246,247}. High flow rates can increase the speed of otherwise slow assays, which can be important in some point-of-care applications that require the transport of a liquid to multiple reagents or reaction sites. High speeds can help maintain polymers or cells in suspension²⁴⁸, as well as increase the rate of sample mixing²⁴⁹. Conversely, limiting the flow rate by using hydrophobic materials such as wax or paraffin, or through transverse cuts in paper can allow for separation of components, mixing, multiple assays on a single device, and more^{244,250}. Other microfluidic applications are reliant on control over wall shear rates or wall shear stress, e.g., when investigating cellular interactions that involve slip bonds or catch-slip bonds^{251–253}.

In fast flow μ PADs, the relative contribution of each flow driver: channel geometry, dimensions, bifurcations, and confluences, have not been fully elucidated²⁵⁴. Increasing the effect of interdependent features could have a net negative effect on the flow rate by counteracting the effect of others. Methods that have been studied to obtain higher speeds involve using different types of paper with different porosities^{254,255}, alterations to inlet size or volume of liquid provided or delivery method^{163,256}, hydrophilicity to maximise capillary flow, size and presence of laser cut grooves, and the overall channel dimensions, namely height, width, and length²⁵⁷.

This work describes a stepwise method of configuring cut channels to maximize the flow rate in single paper layer devices. Single paper layers can be advantageous over multiple layers, since the latter can introduce variability due to assembly challenges. Here we compare the relative role of several parameters, while evaluating modifications to the channels to determine

the most efficient ways of maximizing the flow rate within a self-driving paper-based pump, beyond increasing the number of channels, which was previously described²⁴⁵. Here, we obtain a flow rate that is 8x greater for single paper layers. This can increase the speed of an assay in some applications, while in others it may be necessary to maximize flow rates in a paper pump, e.g., to achieve high shear rates in a separate part of a channel to isolate specific shear-sensitive or flow-sensitive biological responses²⁵⁸. The resulting fast flow devices could be used independently or combined with other μ PAD design configurations for more complex applications.

2. Experimental

2.1 Materials and equipment

Whatman grade 4 qualitative filter paper (Maidstone, UK) was used as the central component. Xerox Printer Wax (Norwalk, CT, USA) was used to print device borders. All devices were printed with a Xerox Colorqube 8870 or 8850 wax printer (Norwalk, CT, USA). Paper was cut using a 30-Watt Epilog Zing Laser Cutter and Engraver (Golden, CO, USA). 3M Scotch laminator sheets (Saint Paul, MN, USA) were used to encase every device. All lamination was done using a Royal Sovereign IL-1346W (Rockleigh, NJ, USA). Inlet size was standardized using a Swingline hole punch (New York, NY, USA). Green coloured dye (KTDORNS, Amazon) was flown through channels to test them.

2.2 Device Fabrication

An overview of the device is shown in Figure 8. Devices were designed in CorelDRAW X4 (Corel, Ottawa, Canada). Whatman grade 4 qualitative paper was printed with coloured wax, forming hydrophobic regions that surround hydrophilic channels of various widths. The printed wax was melted on an Isotemp hot plate (Fisher Scientific, Hampton, NH, USA) at 150°C for 90 seconds, allowing it to perfuse through the paper, forming a hydrophobic barrier to contain and direct fluid flow. Device grooves, branches, and other features were designed in OnShape (Cambridge, MA, USA) which were then laser cut into the paper channels using a carbon dioxide laser engraver (Golden, CO, USA). As prior work has involved partially and completely cutting through the paper^{244,245}, laser strength was decided based on experiments involving evaluation cuts (Figure S1). Channels were put into 3mm laminator sheets where the top laminator layer and the channel layer had the inlet cut using a ¼ inch hole punch. The sheets were laminated using the 3mm setting. The far end from the inlet of each sheet was then cut-off to allow air to flow out and prevent the build-up of pressure that could otherwise limit flow. Post-fabrication, devices were excluded from the study if there were wax droplets in the channel area, if the laser cuts were not adequately centred in the channel, or if the inlet cut was not centred.

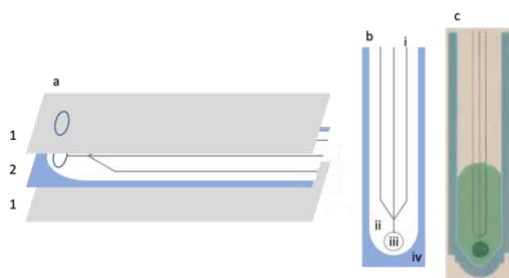


Figure 8 - An overview of the channel construction. a: layer composition and orientation; 1, the laminate sheet; 2, Whatman 4 cellulose filter paper. b: paper layer schematic; i, laser cut grooves; ii, the paper channel; iii, the inlet cut; iv, the wax perfused paper indicating the boundary of the channel. c: an example of a physical channel showing dyed water flowing through the channel.

2.3 Flow of liquid through channels

For easy visualization, 75 μ l of green, food-dye-infused deionized water was perfused through the devices. To avoid dependency on pipetting speed, the pipetted water was first allowed to form a droplet at the pipette tip and then gently placed onto the inlet of channels.

2.4 Image Analysis and Data Processing

All images were captured using an Apple iPhone 12 (Cupertino, CA, USA), converted on Windows using FFmpeg (ffmpeg.org). These were analysed in FIJI ImageJ²⁵⁹, where the total flown area was found at specific time intervals. The leading edge of liquid is not uniform, and the grooves do not contain paper, and therefore hold a greater volume of liquid. Therefore, the grooves were analysed by generating a kymograph in FIJI. The coordinates of the edge of the kymograph were used to generate lines in MATLAB (Mathworks, Natick, MA, USA) representative of the distance flown. From these combined, flow rates were calculated using the following modification of the standard volumetric flow rate equation to account for paper porosity:

$$Q = \frac{\Delta A}{\Delta t} h(1 + \zeta(P - 1)), \text{ where } \zeta = \frac{A_{\text{paper}}}{A}$$

, where Q is the volumetric flow rate, A is the total area, h is the channel height, ζ is the area fraction of wicking paper relative to the total area bounded by wax, P is the porosity of the paper, and t is the time. The modification was used to control for different groove cut numbers and compositions. Graphs and statistical analyses were generated in Graphpad Prism (San Diego, CA, USA).

3. Results and Discussion

3.1 Device Channel Width

The width of the wax-bounded paper channels can affect liquid wicking speeds²³⁵. Therefore, we investigated the specific effect on wax-bounded paper channels with a cut groove, with widths of 2.5-15mm at 2.5mm increments. Devices have a single, centred, straight-line laser cut channel from the inlet, extending 80mm, corresponding to the end of the paper.

As shown in Figure 9, increasing paper channel width results in an increased average travel area relative to time, leading to an average flow rate of 1.12 and 2.70 μ L/s in the 2.5mm and 15mm channels having, respectively, over the initial measured timeframe (5-10s).

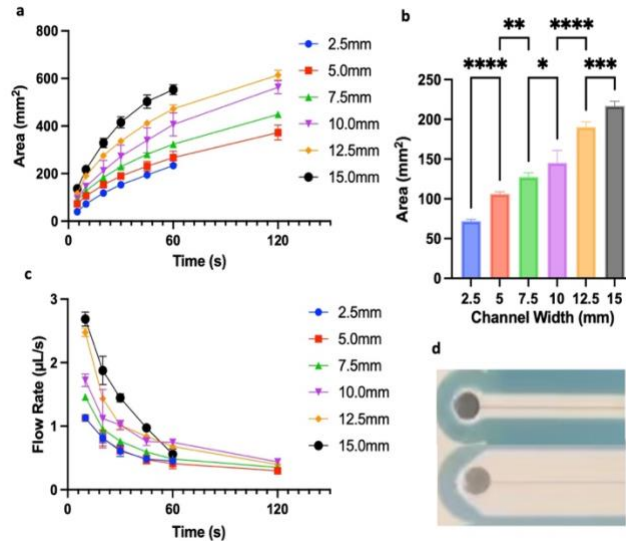


Figure 9 - (a) Wetted area at a given time for different paper channel widths with a single laser cut. At indicated times, the area of travel was measured. (b) Area change over first 10 seconds for each channel width, representing fastest measured flow rates. (c) Flow rates at given times, using the given volumetric flow rate equation. (d) Example channel widths for 5mm and 15mm. The absence of a data point at 120 seconds for the 2.5mm channel is due to the dye traveling to the end of the channel prior to 120 seconds. Absence for the 15mm channel is because all 75µL of liquid wetted/filled the channel before 120 seconds. * $p \leq 0.05$, ** $p \leq 0.01$, *** $p \leq 0.001$, **** $p < 0.0001$. $n=5$ in all cases

An increase in flow rate with channel width is in partial agreement with observations from ²³⁵. This earlier work demonstrates that flow rates increase proportionally with wax-bounded paper strip width, albeit slightly reduced when compared to no wax boundary, i.e., a direct paper cut. It's noted that the effect of the wax boundary in Hong and Kim is reduced as the channel widens. This prior works also indicates that a 15 mm wide channel (without a groove) would have a flow rate that is more than 6x a 2.5 mm channel. However, in the current work, a groove is cut through the centreline of the channel. This leads to an overall faster flow rate, but one that does not increase proportionally with channel width, Figure 2, e.g., a 15 mm channel has

a flow rate less than 3x the 2.5 mm, as opposed to the predicted 6x from Hong and Kim. We attribute this to the groove, which minimizes viscous resistance, while increasing the capillary pressure along the groove. As shown in additional figures (Figure S1), the liquid fills the groove first early during flow, as wetting proceeds perpendicular to the groove. The liquid does not proceed with a uniform, flat leading edge like it does with no groove, as seen in Hong and Kim. Since the flow rate is most affected by the groove in the region local to the groove, it greatly enhances flow rates for thinner channel widths, with less of an effect on greater channel widths where boundaries are far from the centreline groove. Results demonstrate that increased channel width will increase flow rates (although not proportionally), but grooves may need to be distributed along the channel to maximize the flow rate, as has been done by others ²⁴⁵.

While liquid flows into both paper and the groove as soon as it is added to the inlet, it initially flows faster into the groove, compared to the rest of the paper, like other work²⁴⁵. This effect is distance based, with liquid travel distance being proportional to the square root of time. At the same time liquid travels down the groove, liquid imbibition occurs in the paper, albeit more slowly, additional figures (Figure S1). This appears to be contrary to what was found by Sotoudegan et al, where grooves filled completely before most of the paper was wetted. This difference could be due the difference in viscosity of blood and water or could depend on the presence of transparency layers in the current work.

3.2 Groove Width

To investigate the impact of groove width on flow rates, 15mm channels were made with a central laser cut (groove) that was varied in width. For this purpose, 1 to 15 parallel, partially overlapping laser cuts, 0.05mm apart were added. Laser passes were overlapped to minimize the amount of loose paper threads remaining after the cutting process and power was increased until the laser intensity led to a clean cut through the paper width (additional figures Figure S2). Laser power was also Measured groove widths are reported in additional figures (Figure S3). Area to time curves exhibit similar responses at all measured widths, all of which are greater than a channel with no groove, Figure 10. Flow rate also appears relatively independent of groove width for the widths considered here, indicating a singular improvement in flow rate provided by the introduction of a groove. Flow rates relative to time within the groove, itself, are also provided in additional figures (Figure S4). These follow a similar trend to Figure 3c. The volume flow rate through the groove is less than 5% of the overall flow rate. However, flow rates in paper channels with grooves are overall greater than 2x when compared to channels without grooves.

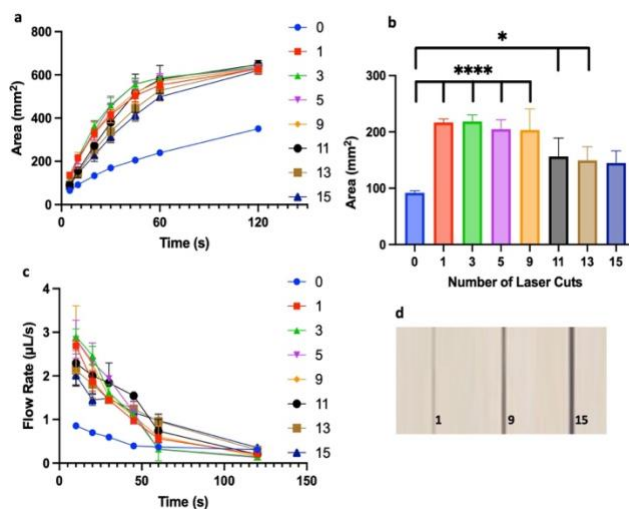


Figure 10 - (a) Wetted area at a given time for different 15mm wax-sealed paper channels with a range of laser cuts (1-15). At indicated times, the area was measured in FIJI. (b) Area changes over first 10 seconds for each channel width, representing fastest measured flow rates. (c) Flow rates at given times (a), using the given volumetric flow rate equation. (d) Example cut widths for 1, 9 and 15 laser passes, or 265.94 ± 30.83 , 785.48 ± 27.92 and $1070.42 \pm 26.90 \mu\text{m}$, respectively. * $p \leq 0.05$, **** $p < 0.0001$. $n=5$ for (a-c) and $n=9$ for (d).

Marked improvements in flow rate are seen until 9 cuts, corresponding to a groove width approaching $800 \mu\text{m}$, which is almost 4x the thickness, but does not continue to improve for larger grooves. The trend of increasing flow rate with increasing groove size is like multilayer channels consisting of a groove within a double-sided adhesive layer sandwiched between two paper layers, taller (wide) grooves led to faster flow for ²³⁰. Based on these results, we speculate that the groove helps to wet the paper along the length of liquid in the groove leading to overall faster flow rates, but that the groove, itself, provides little volume flow rate when compared to the combination of a groove with the paper channel.

3.3 Branching Grooves

Since liquid flows faster with the grooves compared to paper alone, we investigated the possibility that branching grooves could increase the speed of flow. We varied two factors: the angle at which branches join to the central groove and the spacing between branched grooves. The ideal branch angle will cause minimal interference of the flow along the central groove and will also encourage flow along additional grooves. It is noted that surface tension at the air-liquid interface at the leading edge of the liquid would need to be overcome or the paper at the bifurcation would need to be wetted for liquid to trifurcate. Two side-branching grooves were created in 15mm channels, equally spaced to either side of the central groove with which they

intersect at angles of 15-90-degrees, with 15-degree intervals. Additionally, the spacing between the branches was investigated. At certain spacings there may be higher wicking potential, as fluid can wet the paper more uniformly across and between branches.

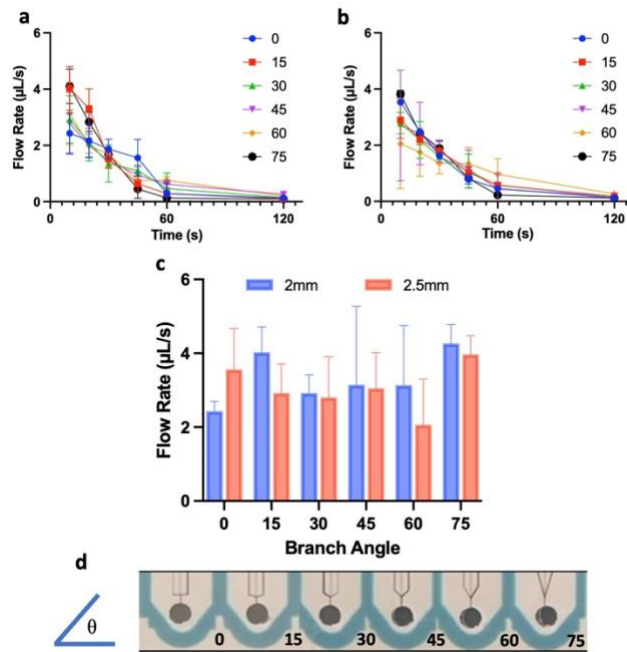


Figure 11 - (a) 75 μL dyed water was flown through the channels and recorded. Flow rates calculated using the given volumetric flow rate equation for 2mm branches. (b) The same test for branch spacing of 2.5mm. (c) Comparison of peak flow rates (10s) between 2 and 2.5mm branch channels. (d) example series 2.5mm branching cuts showing how they connect to the central groove going from 0 degrees (left) to 75 degrees (right) from horizontal. $n=5$ in all cases

The addition of trifurcating grooves led to an improvement in the area covered per second, translating to the average peak flow rate increasing from 2.70 $\mu\text{L/s}$ in the 15mm, single central groove, to 3.97 $\mu\text{L/s}$ and 4.27 $\mu\text{L/s}$ with the addition of 75 degree, 2.5mm and 2.0mm-spaced grooved branches, respectively. Note that not all branches offered an improvement, with some, such as the 0-degree branch causing a decrease in the flow rate to 2.43 $\mu\text{L/s}$. The additional groove branches could interfere with the uniformity of flow, leading to a greater variability than

with a single central groove only (Figure S1). The two 75-degree branches led to fastest flow rates with least variability. Note that while the area change between a single cut and both 75-degree cuts was not striking, the change in flow rate was found to be statistically significant (see Figure 11). The best configuration of branched cuts was then tested in 15mm channels along with an additional two 2mm-spaced grooves (bringing the total up to 5 branches).

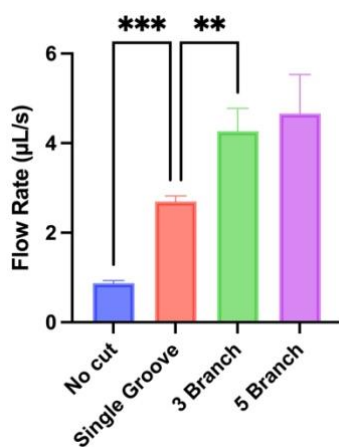


Figure 12 - Comparison of best result flow rates from for 15mm channels with no groove, compared with 1, 3, or 5 grooves. ** $p \leq 0.01$, *** $p < 0.001$

While the addition of two further grooved branches did increase the average peak flow rate to 4.66µL/s, it comes with the caveat that the flow was significantly more variable. As the number of grooves increases, the paths within which liquid can flow increases, leading to lower channel resistance and faster flow. However, the surface tension at the air-liquid interface at the leading edge of the fluid would need to be broken to split the liquid from one channel into multiple channels or paper between branches would need to be wetted to aid in splitting liquid from a single branch into multiple branches. Non-uniformities in the paper and laser cutting

could influence the timing of the split into multiple branches. This could lead to greater variability in flow profiles (Figure S1). Over the single grooved 15mm channels, the 3-branch and 5-branch channels provided a 59.23% and a 73.98% increase in the flow rate, respectively, primarily due to a flatter leading edge for the liquid when compared to a single groove. It's noted that although additional grooves increase the flow rate, Figure 12, the velocity of single grooves within the multi-groove design does not increase markedly compared to a single groove.

3.4 Flow effects

To develop further insight into how the grooves impact flow through single layer μ PADs, theoretical analyses are used. Most theory has stemmed from the Lucas-Washburn equation, commonly used to describe sample flow in μ PADs,

$$l(t) = \sqrt{\frac{\gamma \cdot r \cdot t \cdot \cos(\theta)}{2\mu}},$$

where l is the distance travelled down the channel length at time t , γ is the interfacial tension, r is the effective capillary radius, θ is the contact angle of the fluid to the surface, and μ is the viscosity. Although it was developed for flow through a capillary, it has been accurate in predicting flow through μ PADs. The equation can be extended to by considering capillary flow in bundles of parallel tubes, which approximately represents interwoven paper fibres. Iterations on this equation are also common to account for complex designs that go beyond single paper layer μ PADs. Generally, a constant in front of the equation can be adjusted to accommodate the tortuosity of flow through paper and to accommodate the additional complexities.

Flow in the presence of a wax border has been shown to be slower than when compared to paper alone and when compared to the Lucas-Washburn equation ²³⁵ due to a reduced capillary effect at the boundary caused by the $>90^\circ$ contact angle between water and the hydrophobic wax. However, for wide channels of 15 mm, the wax boundary is predicted to minimally affect flow, Figure 2,6. In this case, the Hong and Kim equation:

$$\lim_{w \rightarrow \infty} l = k \sqrt{\left(1 + \frac{\beta d \cos \theta_b}{w \phi^{\frac{1}{3}} \cos \theta}\right) \frac{\gamma}{\mu} t} = k \sqrt{\frac{\gamma}{\mu} t}$$

simplifies to the Lucas-Washburn equation for wide channels, where k is a proportional constant, ϕ is the porosity, w is the channel width, β accounts for the length of contact lines with a wax boundary, and θ_b is the contact angle with the wax boundary. Both Lucas-Washburn, and the Hong and Kim equations matched well with experiments lacking a groove, Figure 13.

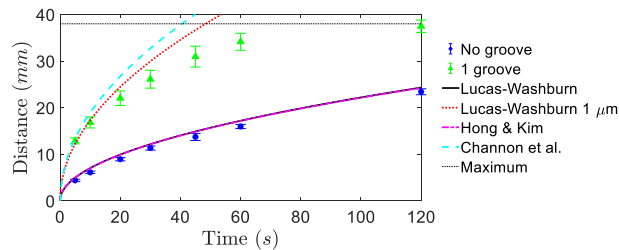


Figure 13 - Representative average distance of the leading front of dyed water in 15mm wide microfluidic devices with listed parameters. Note that the maximum distance flow can travel is denoted by the black dotted line.

With the groove, distance squared is proportional to time, which suggests a Lucas-Washburn-like behaviour. If we use a pore radius of 1 μm , results match closely, but exceed values for a single groove. A previous relationship was developed for flow through a multi-layered cut-out groove^{254,260}:

$$t \left(\frac{dl}{dt} \right)^2 + \frac{3t_h^2}{h^2} l \frac{dl}{dt} = \frac{\gamma t_h^2 \cos^2 \theta}{\mu h},$$

where t_h is the thickness of the paper and h is the half channel height for multi-layered devices. In the current work, h is taken as half of the groove width and the equation was numerically solved. This equation also over-predicts flow through the grooved single paper layer. Therefore, the groove may not be as effective as a multi-layered device. Compared to flow through the multi-layered channels, it is not expected that the leading edge of flow in the groove will have a parabolic profile. Instead, the meniscus is likely localized to area near the paper boundary. Therefore, h may be overestimated by assuming it is half of the groove width. Furthermore, laminating the device has been previously shown to reduce flow by more than half compared to open channels²³⁰. Overall, the groove in single layer devices exhibits similar flow behaviour as a groove in a multi-layered rapid flow device.

4. Conclusions

Herein, we detail a procedural method for the increasing the flow rate in small profile, single layer, microfluidic devices. Increasing the area of available paper for wicking leads to a marked improvement in flow rate. Through the addition of a single laser-cut groove down a

channel from the inlet, volumetric flow rates can be improved by 435% when compared to an equivalent channel with no groove (i.e., paper only). Flow rates reach a peak of 4.66 μ l/s, which to our knowledge is the highest in a single layer device (Table S1). Further addition of grooved branches from the central branch leads to an increase in the flow rate of 59.23% for 3 branches and 73.98% for 5 branches. It's possible that flow rate could be further improved by controlling cellulose fibre composition more completely than with commercially available papers²⁶¹, as well as by modifying channel height²³⁰, width or length^{235,262}.

The devices described here could be used as a wicking pad for other μ PAD configurations that require high flow rates such as cellular testing and point-of-care applications, slip and catch-slip bond investigation^{252,253,263} increased mixing rates^{249,264} and more.

5. Additional Figures

Figures referred to in text but added at the end for clarity.



Figure 14(S1) – Timelapse displaying how liquid flows in channels. Left- 15mm channel with single, 3-branch and 5-branch grooves. Top right – Liquid flow profile at indicated distances from the inlet with standard deviation cloud (n=4). 3mm marks the branch point. Bottom right – Variability of channels increases with additional branches.

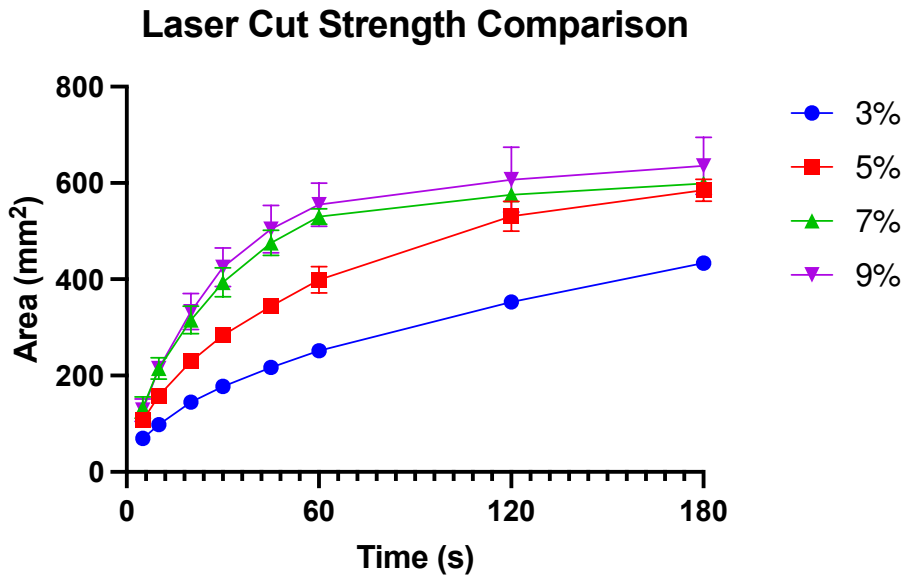


Figure 15(S2) - To compare ideal laser cut strength, identical channels were tested where groove was cut at different laser intensities. At 9% laser intensity, the paper was fully cut through.

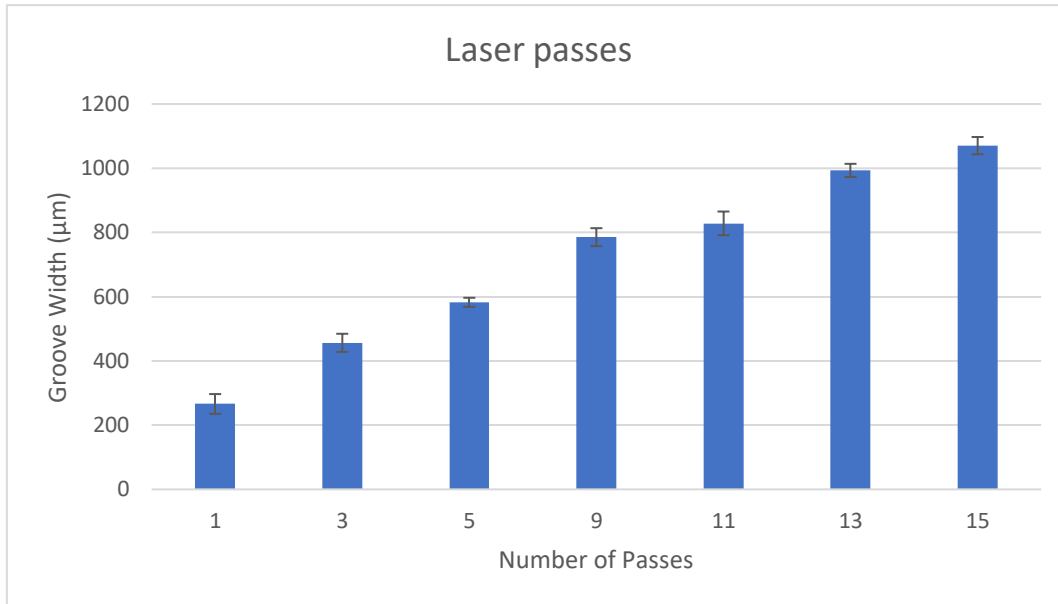


Figure 16(S3) - Width of grooves. Overlapping grooves were laser cut into channels and measured under microscope (n=5 with 3 measurements at different points per n).

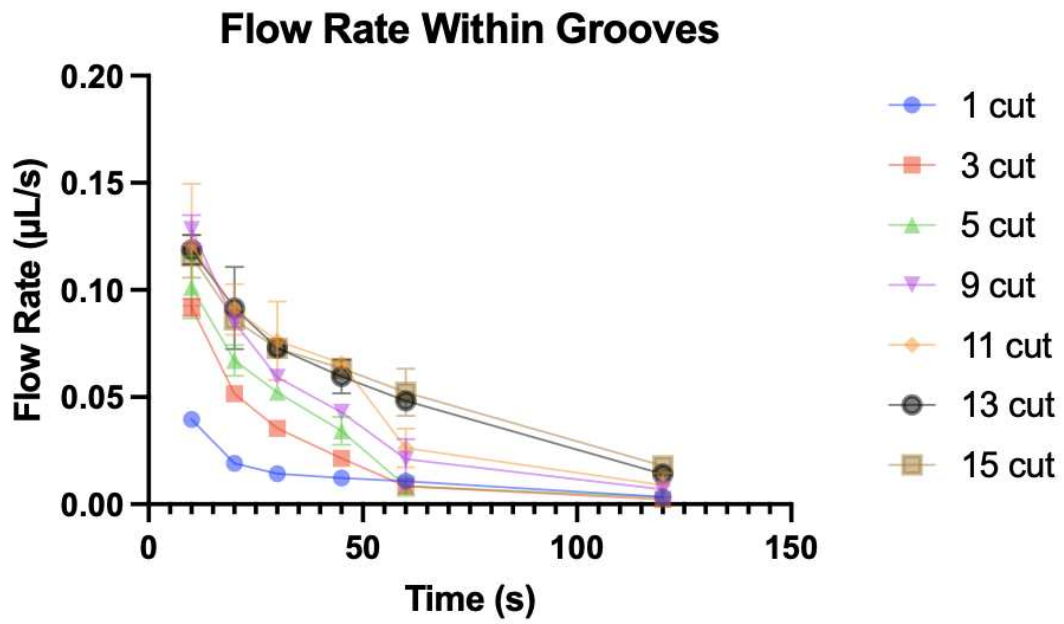


Figure 17(S4) - Flow rate within grooves of widths shown in S2. N=5

CHAPTER 4: ASSESSING THE VIABILITY OF μ PADS IN THE DIAGNOSIS OF VON WILLEBRAND DISEASE

1. Introduction

Von Willebrand Disease (VWD) is a prominent bleeding disorder that affects up to 1.3% of the global population^{265,266}. VWD is separated into categories that characterise the disease, all relating to the deficiency or dysfunction of von Willebrand Factor (VWF), a multimer in blood plasma central to platelet adhesion and aggregation in response to injury. Types 1 and 3 VWD are quantitative and display a partial and complete deficiency in VWF. Type 2, which has further subtypes, is qualitative and characterised by a range of VWF dysfunctions^{197,198,202}. While generally genetically inherited, it can also be acquired through disease, medical devices, or the use of certain medications¹⁹⁰. Depending on severity, VWD can manifest from a mild bleeding disorder that would not be recognised without medical tests, to a life-threatening condition where any bleeding is of serious risk.

Under normal conditions, VWF exists as a coiled, globular protein. Above a certain shear stress threshold, such as those found at the site of an injury or in arterial stenoses, VWF undergoes a force-induced conformational change that exposes binding sites for platelets, which in turn leads to aggregation. Diagnosis of VWD relies on a combination of lab tests that measure VWF concentration (through VWF antigen test), VWF activity (through ristocetin cofactor test) and more¹⁹⁸. While these methods are effective, they are extremely resource-intensive, requiring

specialised equipment and reagents, training, and expertise. These can make them prohibitively expensive, particularly in developing countries or resource-limited settings.

Microfluidics, the manipulation of microlitre volumes of fluids, holds potential for diagnostic application. By combining precise control of small volumes of liquid with a compact design you can increase speed and reduce the consumption of reagents. Microfluidic paper-based analytical devices (μ PADs) are an area in microfluidics with many recent developments that hold promise. These devices leverage properties inherent to certain materials, such as capillarity in paper and hydrophobicity of wax, to drive liquid motion, eliminating the need for external pumps, and therefore electricity. Being made of paper and plastics, they are also low cost and portable, making them ideal candidates for application in developing countries, resource-limited settings, and rural areas where comprehensive access to modern medicine might be more limited.

μ PADs are presently used in a range of applications. In healthcare, they are used for COVID-19 and pregnancy tests, and are in testing as simple devices for glucose monitoring for diabetics and pre-diabetics, as well as for the detection of HIV^{226,227}. They can be used for detection of heavy metals²²¹, water and air quality testing²²⁰, and the detection of pathogens²²². Through detection of nutrient levels, they are used to decide crop rotation and fertiliser choice²²⁵. μ PADs are also used for regulation of transport and reaction kinetics in some chemical and biological reaction applications^{246,247}. Assays are often slow, and high flow rates can decrease wait times, particularly between steps, where liquid can be transported to multiple reagents or reaction. High flow rates, particularly with low Reynolds numbers, can help keep cells away

from the walls and in suspension²⁴⁸, meanwhile can increase mixing rates at higher Reynolds numbers²⁴⁹. Wax, paraffin, and other hydrophobic materials can help to limit the flow rate, as can the introduction of transverse cuts in paper. This can be leveraged to control mixing, isolate components, run multiple assays on a single device, and more^{244,250}. In microfluidic systems, channel constrictions can be leveraged to induce shear. As fluid in flow transitions from a region with large cross-sectional area to a narrower one, its velocity increases, resulting in higher shear stress. In the body, these sudden changes can be produced by atherosclerosis, activating VWF and leading to clots, and result in life threatening conditions such as heart attack, stroke, or deep vein thrombosis. Thus, by mimicking these conditions in microfluidic devices, a test for the activity of VWF can be developed.

Here, we present paper microfluidic channels designed to mimic shear conditions that could trigger VWF activity, and therefore be used as a simple measure for the presence of VWD.

2. Experimental

2.1 Materials and Equipment

Whatman grade 4 qualitative filter paper (Maidstone, UK) was used as the paper component. Xerox Printer Wax (Norwalk, CT, USA) was used to print device borders. All devices were printed with a Xerox Colorqube 8870 or 8850 wax printer (Norwalk, CT, USA). 3M 468MP double-sided adhesive (DSA) sheets (Saint Paul, MN, USA) were used to construct the channel. Paper and double-sided adhesive were cut using a 30-Watt Epilog Zing Laser Cutter and Engraver (Golden, CO, USA). 3M 9984 Diagnostic Microfluidic Surfactant Free Fluid

Transport Film (Saint Paul, MN) was used as a base layer. Inlet size was standardized using a Swingline hole punch (New York, NY, USA). Green coloured dye (KTDORNS, Amazon) was flown through channels to test them. Human Whole Blood was collected into BD Vacutainer plastic blood collection tubes with no citrate (NJ, USA) and used in tests.

2.2 Device Fabrication

A general overview of the device is shown in Figure 1. Devices were designed in CorelDRAW X4 (Corel, Ottawa, Canada). Whatman grade 4 qualitative paper was printed with coloured wax, forming hydrophobic regions that surround hydrophilic channels of various widths. An inlet was cut into the printed paper channels using a ¼ inch hole punch. The printed wax was melted on an Isotemp hot plate (Fisher Scientific, Hampton, NH, USA) at 150°C for 90 seconds, allowing it to perfuse through the paper, forming a hydrophobic barrier to contain and direct fluid flow. Device grooves, branches, and inlet were designed in OnShape (Cambridge, MA, USA) which were then laser cut into the paper channels using a carbon dioxide laser engraver (Golden, CO, USA). The DSA layers were cut, aligned, and combined. Fully constricted layers were always placed on the bottom (Figure 2). Layers were laminated after each combination to remove air pockets and ensure proper adhesion. The base layer was attached to the channel and lastly the paper layer was aligned and attached. Post-fabrication, devices were excluded from the study if there were wax droplets in the channel area, if the laser cuts were not adequately centred in the channel, or if the inlet cut was not centred.

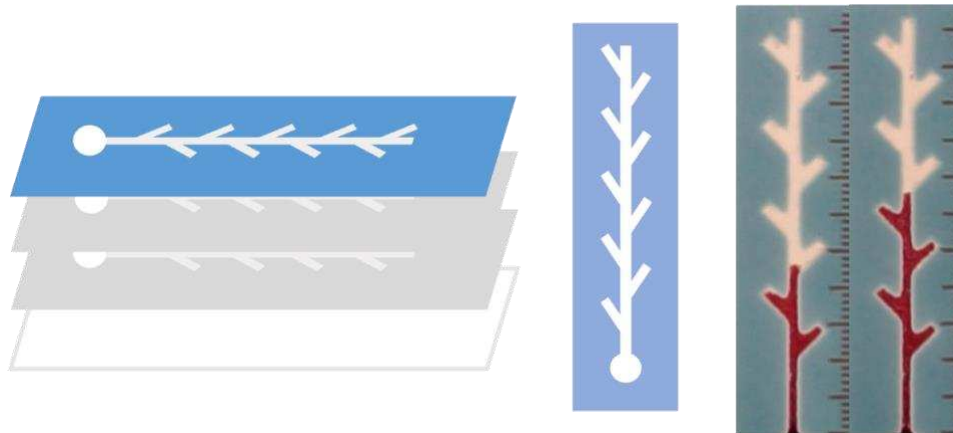


Figure 18 - An overview of the channel construction. Left: layers, top Whatman 4 cellulose filter paper, middle 3M 468MP DSA, base 3M 9984 diagnostic film. Middle: Paper layer showing inlet and channel with branches within the wax boundary. Right: An example of a physical channel showing human whole blood flowing through the channel at two different timepoints.

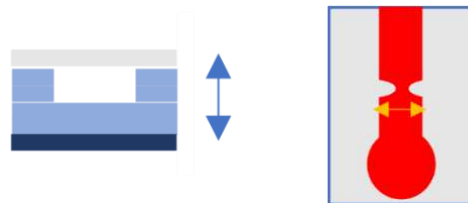


Figure 19 - An overview of the channel constrictions. Left: microfluidic device layers, top Whatman 4 cellulose filter paper, middle 3M 468MP DSA, base 3M 9984 diagnostic film. Of the four middle layers, 1, 2 or 3 were not cut through only at the constriction site. The inlet and channel were always cut through. 1, 2, and 3 not cut through layers correspond to 25%, 50% and 75% height constrictions, respectively. Right: Top view showing DSA layer. Constricted region varied with laser cutter to 0% (no constriction/straight channel), 50%, 75% and 90% (almost complete constriction).

2.3 Blood Collection

Whole blood was collected from human volunteers (with prior consent and following IRB guidelines) using a butterfly needle attached to a vacutainer. 75 μ l of blood was perfused through the devices. To avoid dependency on pipetting speed, blood was gently pipetted to form a droplet at the tip and then placed on the channel inlet. Haematocrit was controlled by centrifugation of human whole blood and resuspension of the erythrocytes only in Tyrode's solution (Sigma Aldrich, MO, USA). This was repeated three times to ensure red blood cells (RBCs) were isolated from plasma proteins and platelets. RBCs were resuspended at desired haematocrit in Tyrode's solution. Channels in which fluid the pre-occlusion region did not fully wet were excluded, as this was indicative of improper alignment between the DSA and other DSA layers or the paper layer in the fabrication process.

2.4 Image Analysis and Data Processing

All images were captured using a Song Alpha 7 II camera at 24 fps. There were three techniques used in analysis. In the dyed water channels, area and flow rate were calculated manually. For the blood channels, to find areas, a MATLAB script was written that used edge detection to detect the leading edge of the liquid. Area was smoothed. To find the peak flow rate, the number of frames taken to flow 2mm and 5mm past the constriction was measured in FIJI ImageJ, and flow rate was calculated. Flow rate was calculated using the standard equation for volumetric flow:

$$Q = \frac{\Delta A}{\Delta t} h$$

, where Q is the volumetric flow rate, A is the total area, h is the channel height, and t is the time. Graphs were generated in Graphpad Prism (San Diego, CA, USA) and MATLAB.

Statistical analyses (one- and two-way ANOVAs with multiple comparisons) were generated in Graphpad Prism. Shear Stress data was found using ANSYS Fluent (Canonsburg, PA, USA)

3. Results and Discussion

Based on prior work^{230,267}, where flow velocity can be increased and kept above Lucas-Washburn predictions, we investigated the possibility that multi-layered μ PADs with a hollow channel can be combined with a constriction (or stenosis) in the channel could create a region of sufficiently high shear stress to induce VWF elongation. For whole blood, shear rates reaching 1800 s⁻¹ are sufficient to create VWF-dependent thrombi. We made channels as described, with 3 different vertical constrictions each paired with 4 different horizontal constrictions and ran dyed water through them. Outside the constriction, channels were 1mm wide and 0.52mm tall, and the constriction was 1mm long. Within the constriction, channels were either 1mm (0%), 0.5mm (50%), 0.25mm (75%) or 0.1mm (90%) wide. Channels were first tested with water.

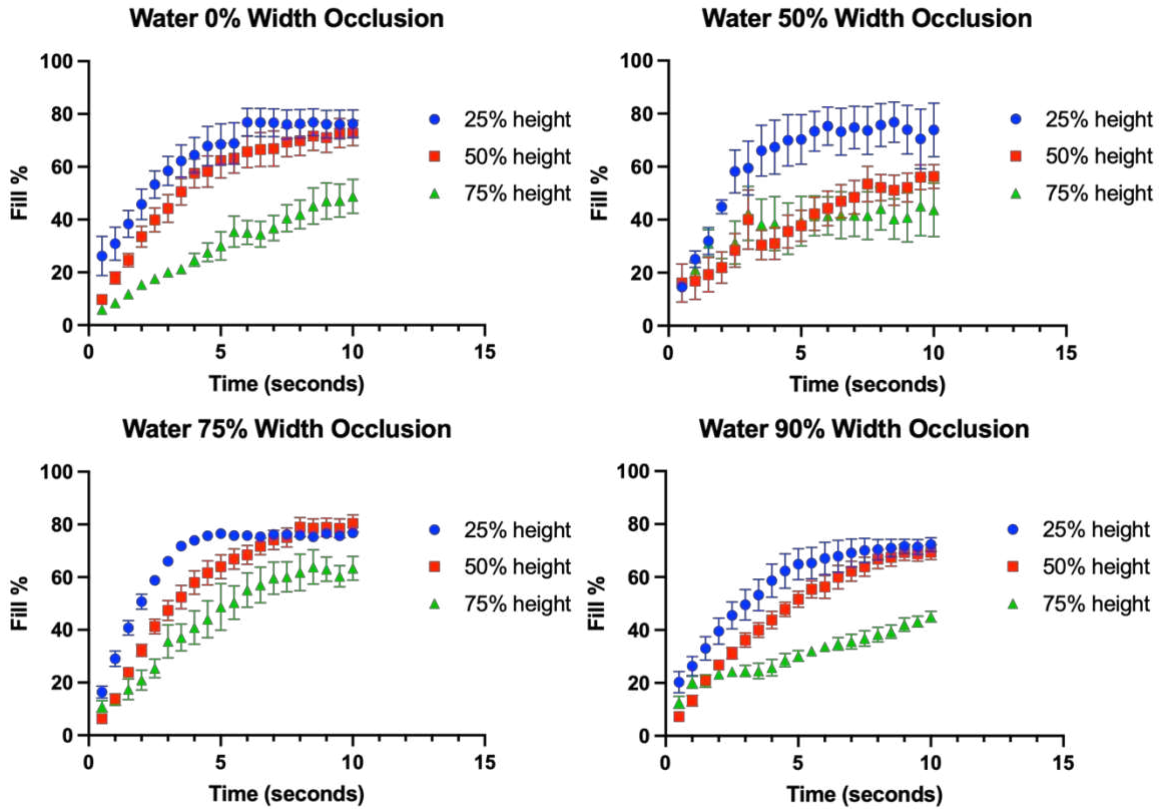


Figure 20 - Dyed water was flowed through channels with different height and width occlusions. Channel fill percentage, a proxy for surface area was found per 0.5s. Here comparing the same width occlusion at different height occlusions (n=5) with SEM.

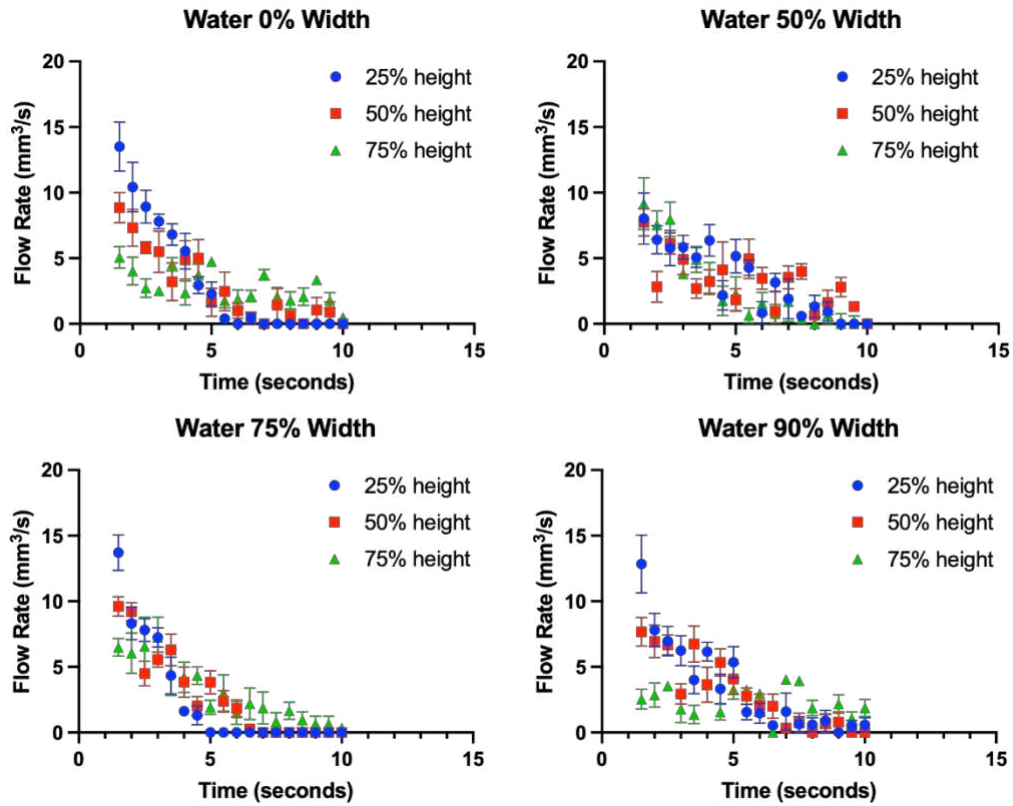


Figure 21 - Volumetric flow rates for water filled microfluidic channels (n=5) with SEM comparing the same width occlusion at different height occlusions, from the same channels in figure 3.

As can be seen in figure 20, smaller height stenoses filled faster than the larger height stenosis, indicative of a difference in flow rates, meaning that greater constrictions reduced filling rates. However, flow rates at a given point in time (figure 21) were not so clearly differentiated. Flow differences were established initially and statistically significant (figure 22) but decrease over time. This is likely due to the Lucas-Washburn equation, which states that as liquid flows further through a channel, speed decreases. Therefore, there is a notable initial difference where liquid flows more quickly through the less constricted channels, likely due to a

greater pressure drop across the stenosis. However, as it has flowed further, the flow rate will decrease faster than that of the more constricted channels, which will have flowed a smaller distance at the equivalent timepoint. It is of note that for peak flow rates, there is a strong relationship between the flow rate and the height of the stenosis at a given width of a stenosis, but the same effect is not seen between the flow rate and the width of the stenosis at a given height (figure 22). There are two possible reasons for this difference. It is possible that the vertical occlusion has a more significant effect as it provides a barrier that must be passed over, much like a river dam. While the paper layer above will provide some flow, the fluid front still is still partially impeded, and cohesion between water molecules could then slow flow further. Comparatively, the horizontal occlusions always allow liquid to pass through. It is also possible that there is too much variability in using a laser cutter to be able to accurately predict flow at this scale, whereas standardised materials (i.e., uncut DSA) are less variable and therefore provide more precision and granularity.

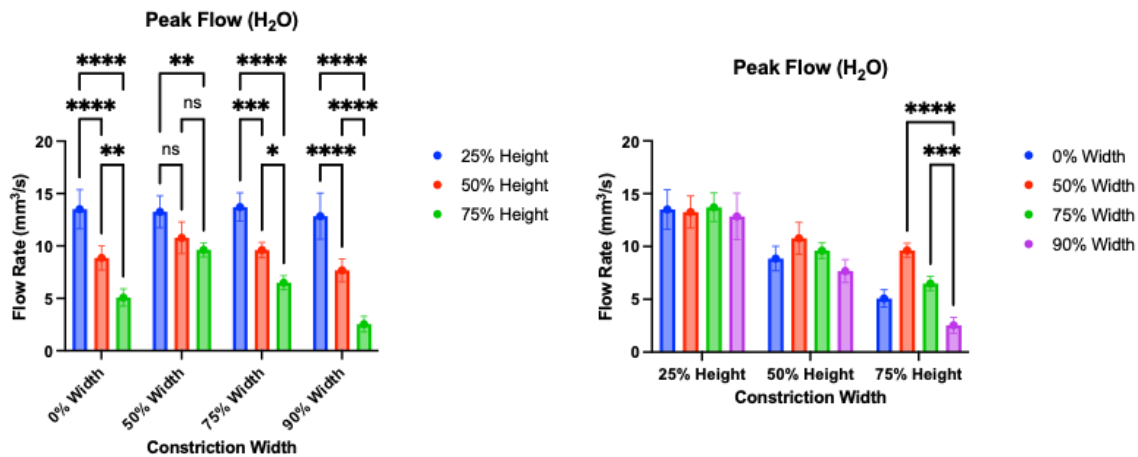


Figure 22: Peak flow rates after the constriction for water (n=5) with SEM. Left: Peak flow rate comparing stenosis height at a given width. Right: Peak flow rates comparing stenosis width at a given height. * $p \leq 0.05$, ** $p \leq 0.01$, *** $p \leq 0.001$, **** $p < 0.0001$.

With ANSYS Fluent, taking the peak flow rate and channel dimensions for 90% width and 75% height stenosis, we find a shear stress of $\sim 17,700 \text{ s}^{-1}$, well above the threshold for VWF elongation.

With validation in water channels, we repeated the tests using washed RBCs. As it is possible that when whole blood is used, blockages could be not due to VWF but also due to cells blocking the constriction, we tested RBCs without platelets and VWF at all dimensions and at different haematocrits. As haematocrit is directly proportional to viscosity^{268,269}, we expect higher haematocrits to flow more slowly.

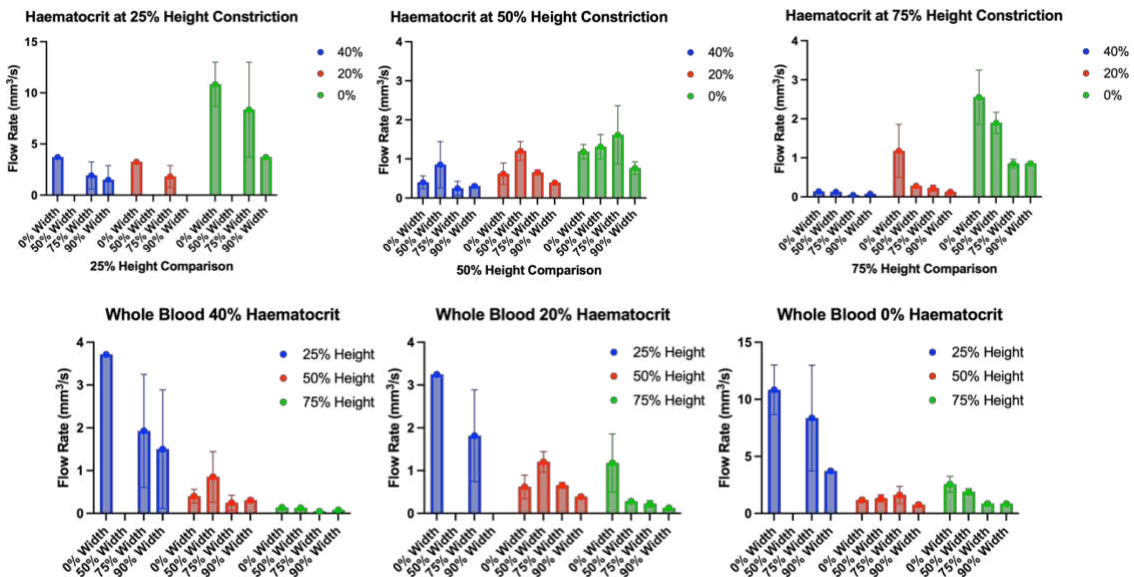


Figure 23 - Erythrocytes were flowed through these microfluidic channels. Time taken for fluid to flow the first 2mm after constriction was calculated, from which flow rate was found. Top: Peak flow rates after the constriction for different haematocrits of erythrocytes (n=2) with Std Dev. Bottom: Comparison of the effect of constriction height on flow rate for given haematocrit.

As can be seen in figure 23, results suggest that for a given constriction height there is minimal difference between 40% and 20% haematocrit, but a larger difference with the 0% haematocrit, approximately equivalent to what is found in the dyed water channels. Note the different scale in top left and bottom right, indicating much higher flow rates at the smallest height constriction as well as the 0% haematocrit. It is worth noting that for both 40% and 20% haematocrit, there is a differential response in the flow rate based on the height of the constriction. As RBCs were washed to remove platelets and plasma proteins, it is unlikely that this is because of the formation of aggregates, and most likely a consequence of viscosity and/or blockage by RBCs. Note that missing data for the 50% width was due to channels failing exclusion criteria listed earlier. ANSYS Fluent analysis shows that shear stresses drop to 450-1300s⁻¹, which is well below the threshold for significant VWF activation.

To further investigate, we ran whole blood with ristocetin at 1 mg/ml, which induces platelet aggregation by activating VWF. If the channel constrictions are appropriately sized, then we would expect ristocetin treatment to further decrease the flow through these channels, if not completely block it.

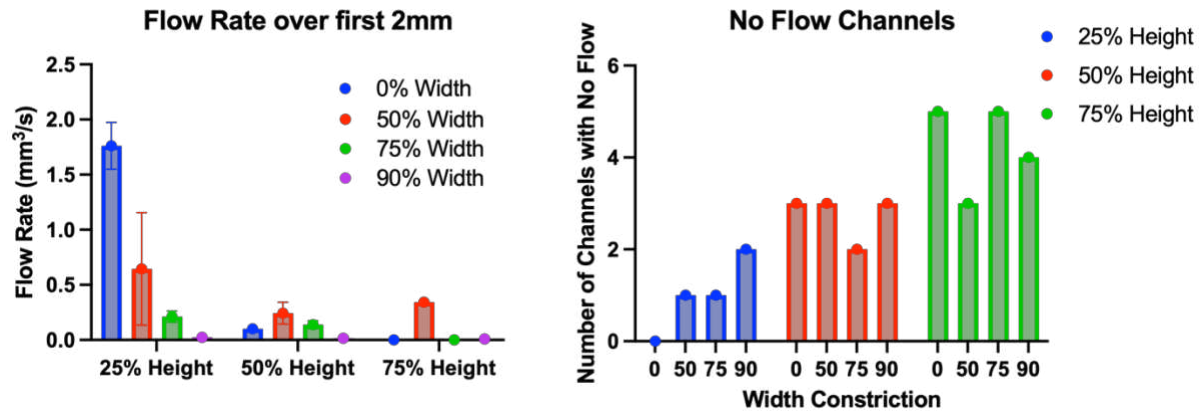


Figure 24: Whole blood with ristocetin was flowed through these microfluidic channels. Time taken for fluid to flow the first 2mm after constriction was calculated, from which flow rate was found. Left: Peak flow rates after the constriction for different haematocrits of whole blood (n=varied, due to right figure). Right: Number of channels at each height and width constriction in which blood did not flow past the constriction.

Figure 24 shows both a decrease in the flow rate in channels that did flow past the constriction, and a marked decrease in the number of channels that showed any flow, which also correlated with constriction size (more constriction = fewer channels). In all cases, blood flowed up to the occlusion, indicating that this was the site of aggregation and blockage. When compared to the RBC test, where only one channel (75% height, 90% width, 40% haematocrit) was blocked, this is a strong indication that the change is driven by aggregation.

Shear stresses reached a range of $\sim 17,700\text{-}26,000\text{-}1$ in water across the different constrictions, and for blood peaked in the 25% height, 75% width stenosis at a haematocrit of 20% (figure 25) at $\sim 9700\text{s}^{-1}$. The lack of a differential response suggests that while we are achieving required shear stresses, they are not being reached for sufficiently long for a significant thrombus to form.

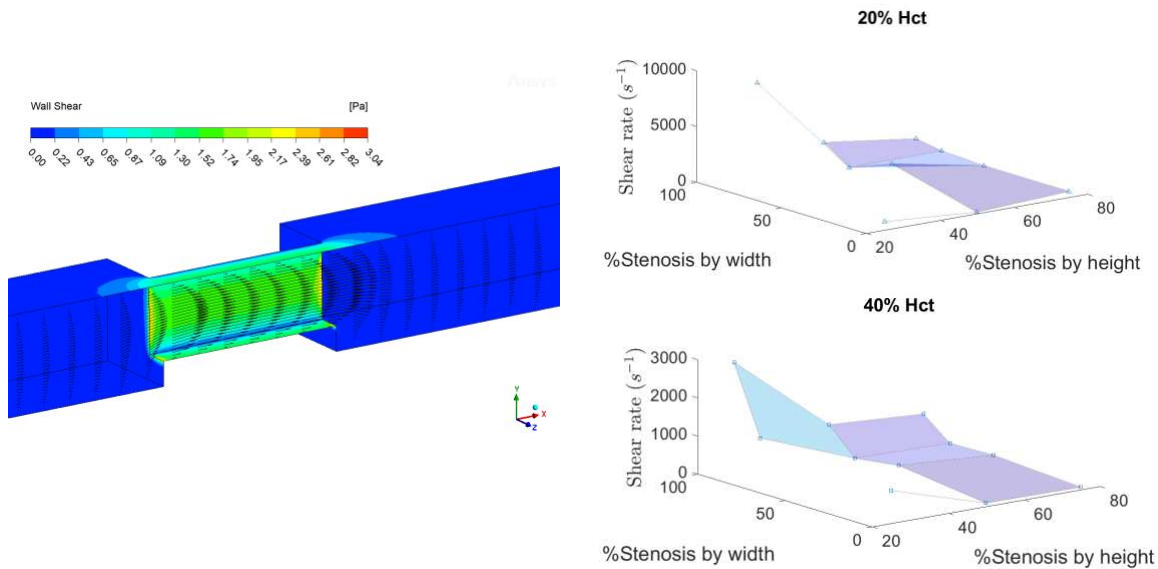


Figure 25: Shear stresses in stenoses for red blood cells in Tyrodes (haematocrit test). Left, shear stresses for 25% height, 75% width at 20% haematocrit. Right, top, shear stress for each stenosis at 20% haematocrit. Right, bottom, shear stress for each stenosis at 40% haematocrit.

4. Conclusion

Herein, we provide initial evidence supporting the possibility that μ PADs could be used as a potential diagnostic tool for type 1 and 3 VWD. By carefully designing a stenosis through which fluid flows, shear rate can be maximised. This can be applied to whole blood, with the aim of triggering VWF to cause aggregation. While certain channels did achieve required shear rates for VWF elongation and therefore VWF-led thrombosis to occur, the lack of a differential response suggests that they were not achieved for long enough. Ristocetin testing confirmed that pre-activated VWF further decreases the flow rate in the channels, or completely stops it. However, a few further tests are required to confirm if VWF is the only cause for this blockage,

as it is possible that a physical blockage is also occurring. Future designs might benefit from leveraging laser-cut hard plastic with double sided adhesive added on top and below. A single piece of hard plastic could be cut more uniformly and would minimise the complications that arise from having to align pieces manually when fabricating. Further, certain plastic types could be washed and reused. Collagen coatings are durable, and therefore if the hard plastic design were used, a thin layer just past the stenosis could also be added to initiate a VWF response.

CHAPTER 5: INVESTIGATING PLATELET RESPONSE TO SURFACE STIFFNESS

1. Introduction

Platelets are central to haemostasis. Upon vascular injury, von Willebrand Factor (VWF) and collagen can interact with and be bound to platelets^{2,3}. This adhesion triggers intracellular cascades that lead to platelet activation, followed by aggregation thereby forming a thrombus or clot. Activated platelets mechanosense through focal adhesions and respond to cues in their microenvironment through morphological changes, extension of filopodia and lamellipodia, and release of granule contents, which further amplify haemostasis^{110,111}. The biomechanical properties of platelets, and how they interact with their environment, is of significant clinical interest, as it can help understand one of the major aspects of the haemostatic process, and in turn developing therapeutic methods to fight excess bleeding, and excess clotting, which is one of the leading drivers of death globally^{270,271}. The stiffness of surfaces, cells, and other components to which cell bind can influence their behaviour. This is particularly important in medical device design, such that devices with controlled stiffness can also control platelet responses.

Given the heterogeneous nature of the cardiovascular system, platelets can encounter vessels, arteries, arterioles, venules, veins, and capillaries, all of which have distinct surface stiffnesses²⁷². Platelets at different layers in clots may also experience different stiffnesses²⁷³. Therefore, understanding how substrate stiffness influences platelets can provide insight into how they act under different conditions. Substrate stiffness mediates platelet adhesion and spreading. When platelets were allowed to spread on polyacrylamide gels with different

stiffnesses (ranging from 0.25-100kPa), it was found that as stiffness increases, so does both the number of platelets attaching to the surface and the average spread area of the platelets.

However, this study jumped from 5kPa to 50kPa surfaces, within which is a range of biological relevance to platelets that needs more information and will be studied here (4, 8, 16, and 34kPa).

Precise values vary due to different measurement techniques²⁷⁴, but can range from 30-80+kPa for aorta^{275,276}, 3-50kPa for veins²⁷⁷, and the endothelial matrix 2.5-10 kPa²⁷⁸. This effect was independent of ligand density, as fibrinogen concentration was kept constant¹⁴⁹.

Advanced biomechanical techniques such as traction force microscopy (TFM) allow for more detailed understanding of how platelets are interacting with substrates. Early studies suggest that platelets exert force on their substrate in geometric patterns such as circles, triangles, and lines, that line up with actin localisation in stained platelets, supporting the central role of actin in force generation. One study suggest that platelets do not generate more force as substrate stiffness increased¹⁵⁷. However, it contradicts experiments using atomic force microscope cantilevers to measure contractile strength in platelets, where they found that a 2.5fold increase in cantilever stiffness resulted in a twofold increase in platelet force generation¹⁶⁸. It is worth noting that the former study was on a 2D surface, while the latter was 3D when considering the surface and the cantilever, therefore these results are not necessarily mutually exclusive.

Furthermore, TFM output is dependent on the sensitivity of bead tracking. As stiffness increases, beads will move less when the same force is applied to a surface and movement can become so small that is not detectable despite the force production potentially being very high. Another study shows a difference in force generation and actomyosin localisation based on surface ligand – fibrinogen or VWF. VWF bound platelets generated more force, and f-actin was shown to

radiate from the centre to the edges. Meanwhile, fibrinogen bound platelets generated less force and generally had a “hollow” actin structure (although morphology was more varied than in VWF), with actin localising around the platelet edge and not in the centre¹⁶⁹. Another recent work somewhat contradicts this, where they directly show on fibrinogen substrates that actomyosin is the driver of force generation through a combination of TFM and super resolution STED microscopy. Platelets in this paper did not display the “hollow” pattern to the same degree. Force generation was measured across time, and after 30 minutes, the same platelets were labelled for actin and vinculin. Vinculin is a focal adhesion protein responsible for linking integrins to actin¹⁷⁰.

Due to the uncertainties and contradicting results in the field, it is important to validate results and tip the research scales one way or another. Herein, we investigate the effect of surface stiffness on platelet force generation. We also investigate the platelet response at the moment of death to understand how surface stiffness might contribute.

2. Experimental

2.1 Gel Fabrication

Polyacrylamide gels were made by modification of Tse 2010¹²⁴. Coverslips were coated with 0.1M NaOH (Honeywell, USA) at ~80°C and washed, followed by a coating of APTES (Thermo Scientific, MA, USA). These were rinsed and submerged in 0.5% glutaraldehyde (Thermo Scientific, MA, USA) in PBS (Thermo Scientific, MA, USA). This was aspirated and

coverslips airdried. A separate slide was coated with DMDCS (Sigma-Aldrich, MO, USA) for 5 minutes then rinsed in distilled water.

For the gel segment, Acrylamide (Thermo Scientific, MA, USA) and bis-acrylamide (Fisher BioReagents, MA, USA) were mixed to appropriate concentrations for 4, 8, 16, and 34 kPa gels¹²⁴ in PBS and mixed with APS (MP Biomedicals, CA, USA). After degassing, carboxylated, fluorescent nanobeads (Thermo Scientific, MA, USA) were added with TEMED (Thermo Scientific, MA, USA), mixed, and pipetted onto the coverslip, onto which was placed the slide. Once polymerisation was complete, fibrinogen (Invitrogen, MA, USA) was crosslinked onto the surface.

2.2 Blood Collection and Platelet Isolation

Whole blood was collected from human volunteers (with prior consent and following IRB guidelines) into a vacutainer containing 6/1 blood/ACD (BD, NJ, USA), and transferred into a tube Clexane at 20 U/ml (Sigma Aldrich, MO, USA) , and 0.005U/ml apyrase (Thermo Fisher, MA, USA) and incubate at 37oC for 15 minutes. Blood was centrifuged at 300xg, and platelet rich plasma (PRP) was transferred to a fresh tube and rested for 10 minutes with Clexane and apyrase at the same concentrations. PRP was centrifuged again at 1700 x g for 7 minutes. Platelet poor plasma was aspirated, and the platelet pellet was resuspended in platelet wash buffer, Clexane (20 U/ml final) and apyrase (0.01U/ml) to a volume equal to the original volume of PRP. Platelet count was adjusted to $\sim 3 \times 10^8$ /ml. Platelets were rested at 37°C for 10 minutes, then centrifuge at 1500 x g for 7 minutes. Pellet was resuspended Tyrode's buffer (pH 7.3)

containing 5mg/ml bovine serum albumin (BSA) (Thermo Scientific, MA, USA), 1mM Calcium (Thermo Scientific Chemicals, MA, USA) and Apyrase (0.02 U/ml).

2.3 Experimental

Gels were precoated in BSA to minimise non-specific binding. Isolated platelets were allowed to spread on a range of surface stiffnesses (4, 8, 16 and 34kPa) and imaged alternating between a fluorescent image and a brightfield image, totalling one image per second.

2.4 Image Analysis and Data Processing

Platelets that displayed full attachment, spreading, and death cycle were isolated from larger images, and the images capturing the moment of platelet release upon death, and the moment of full gel relaxation (as measured by the end of bead motion) were used. Images were aligned based on stationary regions using template matching and slice alignment plugins²⁷⁹ for FIJI ImageJ²⁵⁹. Bead positions and movement were found using the Trackmate plugin for FIJI ImageJ^{280,281}. Bead displacement was calculated and mapped using an in-lab MATLAB script (Bark 2023). Displacement maps were converted to force maps using a Traction Force Microscopy plugin for FIJI ImageJ²⁸². Traction Force maps and bead displacement were processed in MATLAB and Excel for data analysis, and figures were made in MATLAB in and PRISM, where statistical analysis was conducted using one ordinary one-way ANOVAS with multiple comparisons. See figure 26 for visual workflow.

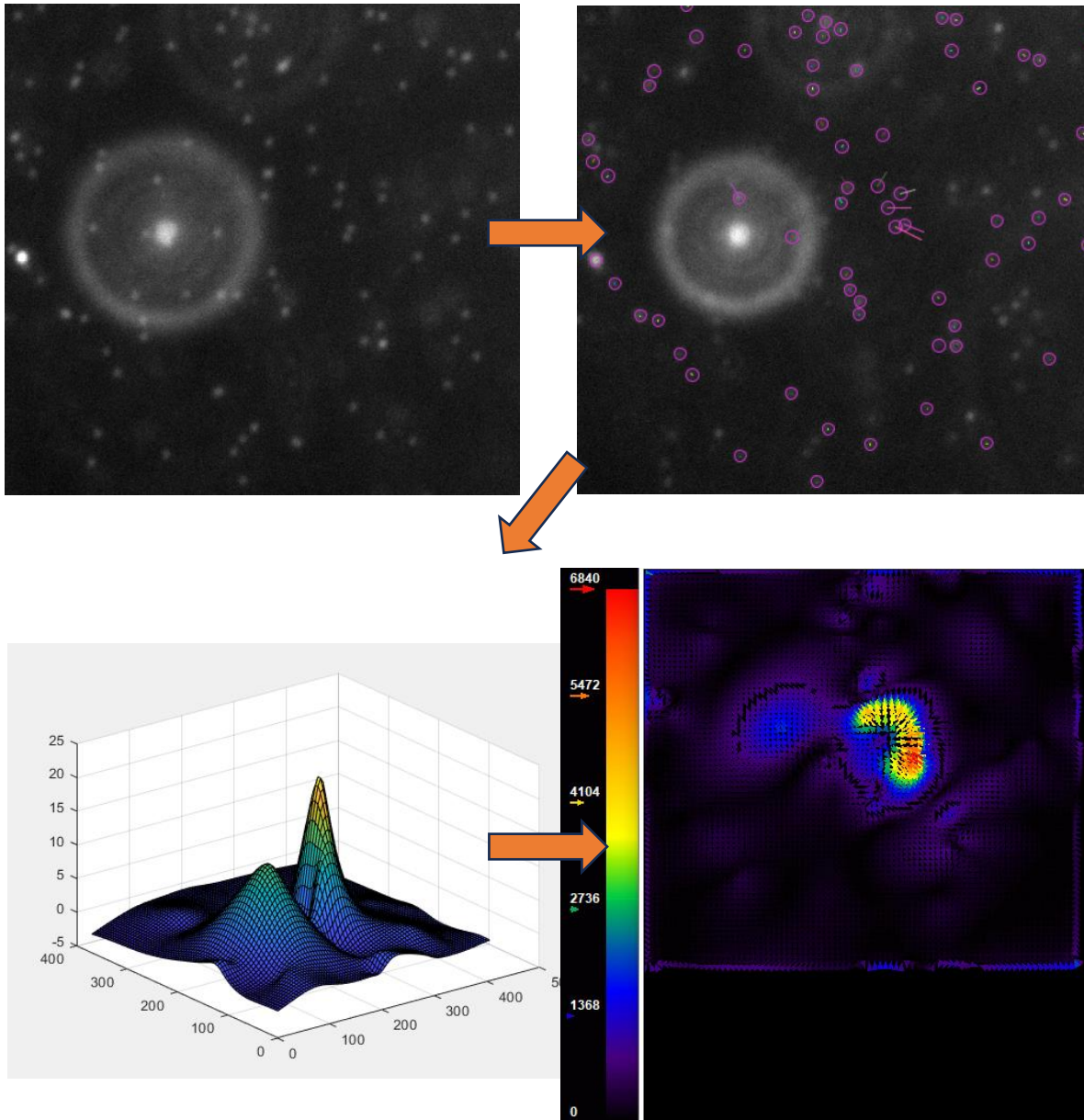
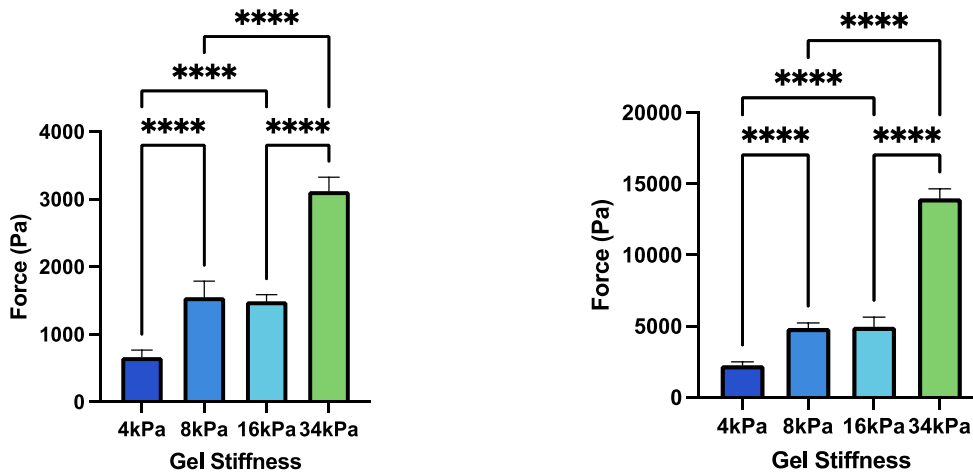


Figure 26 – TFM Image processing workflow (top left to bottom right. Top Left: Platelets isolated from larger image, and drift corrected. Top Right: Trackmate recognises beads and change in position over time. Bottom Left: Displacement is mapped onto a grid equivalent to platelet area. Bottom Right: Displacement converted to traction force and direction map (Pa).

3. Results and Discussion

There is a discrepancy in results regarding measurements of force exertion by platelets in response to surface stiffness. To investigate and reconcile these results, we suspended washed platelets over surfaces of varying stiffnesses (4, 8 , 16 and 34 kPa) to see if there was a differential response in spreading and contractile behaviour. As other cells display a differential result on different surface stiffnesses^{283,284}, and platelets generally have the same internal machinery in terms of immediate, short-term response (they do not have a nucleus²⁸⁵, but carry within the cytoskeleton all the other machinery, proteins, etc²⁸⁶), it would conclude that platelets also have this differential response.

Average Force Generated by Surface Stiffness Maximum Force Generated by Surface Stiffness



Average Bead Displacement by Surface Stiffness

Maximum Bead Displacement by Surface Stiffness

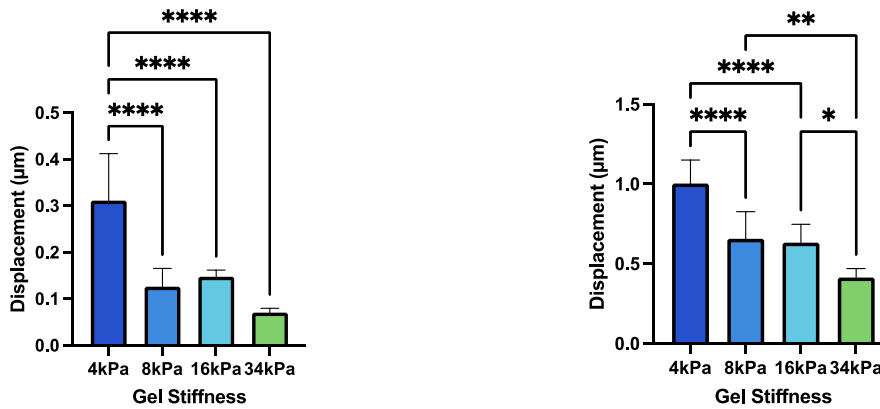


Figure 27 – An overview of the force generation and bead displacement. Isolated platelets allowed to spread on polyacrylamide gels with different surface stiffnesses n=9-11 with SEM and * $p \leq 0.05$, ** $p \leq 0.01$, *** $p \leq 0.001$, **** $p < 0.0001$ in all subfigures. Top Left: Average force generation by platelets. Top Right: Maximum force generation by platelets. Bottom Left: Average bead displacement by platelets. Bottom Right: Maximum bead displacement by platelets.

As seen in figure 27, both average and maximum force generation increase with surface stiffness. Note that 8kPa and 16kPa are not statistically significant in difference. From a biomolecular perspective, the mediators of cellular force generation are integrins that form a

connection between the extracellular matrix (ECM) and the intracellular actin cytoskeleton. When cells encounter stiffer substrates, platelets spread more and integrins form more focal adhesions (the collection of proteins involved in mechanotransduction). This feedback might trigger intracellular signalling to also increase myosin activity¹⁴⁹, leading to greater contractility and generation of more force. Notably, this is not a linear relationship, likely a combination of energy cost, cytoskeletal limitations (in terms of how quickly it can reorganise and how many stress fibres can form), as well as how sensitive cells are to specific differences in substrate stiffness. Bead displacement was higher on average and at its maximum on gels of lower stiffnesses. Displacement is proportional to the amount of force applied (based on Hooke's law)²⁸⁷, so given an equivalent applied force, softer gels will allow for greater displacement. This is also not linear, likely due to the biological complexities mentioned earlier. Note that in this study we did not consider the position of the bead relative to the centre of the platelet nor the focal centre of the platelet (i.e., the specific location in the platelet to which the actin cytoskeleton is pulling).

As discussed earlier, platelet area and force generation are positively correlated with surface stiffness, however it is unclear if the same can be said for platelet area and bead displacement (figure 28).

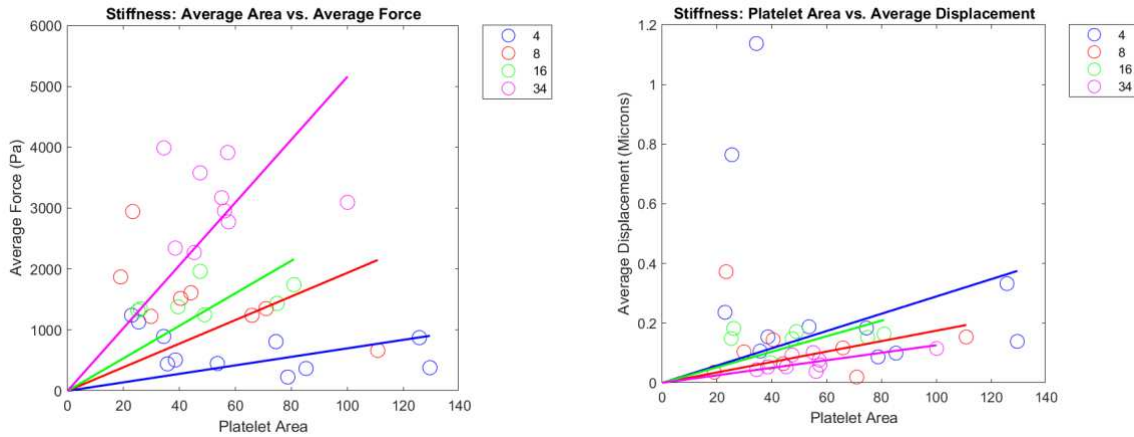


Figure 28: Isolated platelets allowed to spread on polyacrylamide gels with different surface stiffnesses n=9-11 Left: The relationship between platelet area and the force they generate at different substrate stiffnesses. Right: The relationship between platelet area and the displacement they cause at different substrate stiffnesses

There was a trend for platelet area to be an indicator of force generation across all surface stiffnesses. The slope of the lines through the origin, representing a force to area ratio for each substrate stiffness supports the idea that as platelets spread more, they also generate more force. Note that there was not a large difference between the 8kPa and 16 kPa groups, maybe indicative of a platelet inability to distinguish those stiffnesses. This supports results from Qui et al¹⁴⁹, within a force range that they had not investigated but that is of biological relevance to platelets, as well as other studies in other cells^{150,158}. While average displacement was positively correlated with area for all surface stiffnesses, there was not a significant difference between these, particularly when factoring out two leveraged outliers for the 4kPa results. Recent studies

suggest that platelets form groups of focal adhesions (“hotspots”) that account for large amounts of the force generated¹⁶⁵, therefore if beads do not lie close to those groups, they will not displace significantly. Higher resolution would be required to fully understand this relationship. To further investigate this, it would also be necessary to label integrins or focal adhesion proteins.

An area that is not well studied is how surface stiffness might affect the speed at which platelets attach, spread, and die. As they die, they become procoagulant and can support secondary haemostasis. To investigate this, platelets were allowed to spread on gels of different surface stiffnesses for 45 minutes. Platelet death was evaluated by the moment of release of the gel surface. On each surface, a minimum of 12 platelets that went through their full attachment and activation lifecycle were tracked and the time it took to attach, to spread, and to die was found. To assess the relative number of platelets that complete this lifecycle, a 1000x1000 pixel area was assessed to see the number of platelets that attached but did not spread, that spread but did not die, and that spread and died over the course of the image series. The amount of time it took from attachment to death, plus one standard deviation, was used as a time limit for this measurement, to exclude platelets that attached later in the video but could not be tracked for their full lifecycle. Finally, the amount of time it took for platelets to fully release their substrate upon death was found. It is of clinical interest to understand if platelets attach and die faster on stiffer or softer substrates, as it could lead into better understanding of atherosclerosis, wound healing, and blood-contacting implant development.

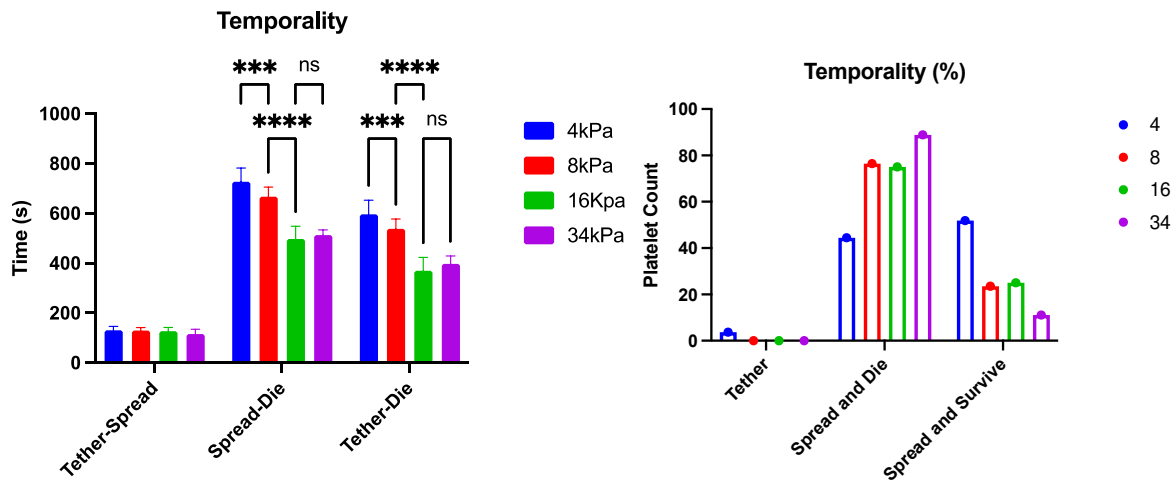


Figure 29: Platelets were tracked at different points in their interaction with the surface. Left: Time taken for platelets that went through full lifecycle within 45 minutes to tether (bind to the surface), spread on the surface and die (release the surface) measured at each surface stiffness (n=11-16 with SEM, * p≤0.05, ** p≤0.01, *** p≤0.001, **** p<0.0001). Right: For a representative region, number of platelets that attached but didn't spread; attached and ultimately died; and attached and didn't die (n= 8-16, dictated by number of platelets within representative region).

As can be seen in figure 29, there is not a difference in the amount of time it takes for platelets to bind and initiate spreading on different surface stiffnesses. It is possible that once activated, the initiation of spreading is uniform across all surfaces. Substrate stiffness does, however, appear to dictate the time from spreading to death. As surface stiffness increases, so does the speed at which platelets die. When cells die, either through apoptosis, damage, or other, they expose intracellular molecules recognised by immune cells, which are involved in collecting and clearing dead cells, fighting pathogens, and contributing to wound healing^{288,289}. Hence, in situations where platelets are binding to stiffer surfaces, such as those found in an atherosclerosis or in a clot, it is possible that there is a mechanotransductive drive to die faster to induce a faster

immune response, which will contribute to the resolution of the issue. The area of the platelet did not appear to affect the amount of time it took for platelets to release upon death (Figure 30).

This suggests that release is a relatively uniform process independent cell size.

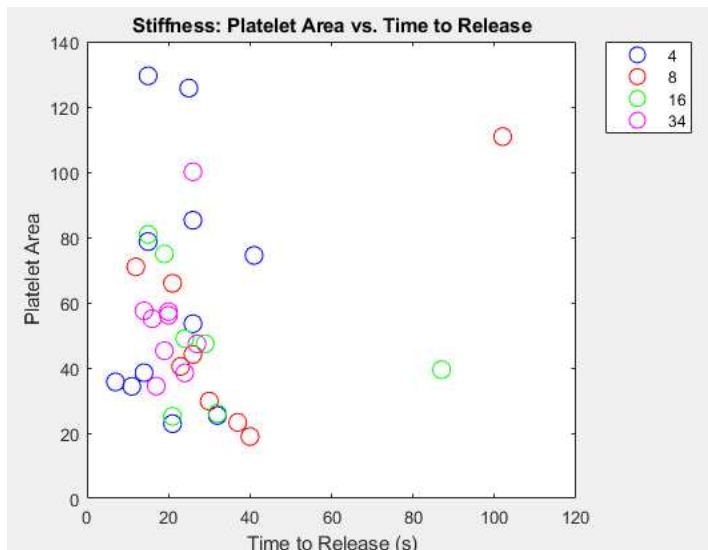


Figure 30: Isolated platelets allowed to spread on polyacrylamide gels with different surface stiffnesses $n=9-11$. The time taken for platelets to fully release upon death was plotted.

4. Conclusion

This study examined the response of platelets to various surface stiffnesses. We found a clear differential response to force generation and bead displacement, contradicting previous TFM work but supporting other work using AFM cantilevers. The exception was in the 8-16kPa range, where there was no difference, possibly indicating a limit to the granularity of the mechanosensory response. Platelet area showed a positive trend, but there was not statistical significance across all stiffnesses, possibly due to resolution limitations. There is other work that supports (but does not test) the idea that the more a cell spreads, the more force it produces – likely due to an increase in the area within which focal adhesions can form and therefore

generate force¹⁴⁹. In terms of the dynamics of a platelet's lifecycle, the initial, attachment to spreading phase did not vary across surface stiffnesses. However, the spreading to death did vary, with platelets dying more quickly on stiffer surfaces.

To validate and add to these results, higher resolution work should be conducted to understand the full scope of force dynamics. Focal adhesions should be measured to see if they are larger or there are more of them under larger area platelets. Given the non-linear relationship between surface stiffness and force generation, testing a broader range, specifically in the 34-100kPa range would be of interest. Understanding the limits of force generation would also be of interest, so possibly going past the 100kPa range as well, with the appropriate experimental setup and resolution.

CHAPTER 6 – CONCLUSION AND FUTURE DIRECTIONS

1. Conclusion

This dissertation explored two topics - the viability of developing a paper microfluidic device for the diagnosis of von Willebrand Disease, and an investigation into force generation by platelets on deformable substrates. We found that through careful use of laser cuts, the flow rate in simple paper microfluidic devices could be increased by 435% over paper alone, and by 59.23-73.98% over a single cut, depending on configuration. Insights from specific design aspects, such as herringbone branches were used in the development of a microfluidic device with a stenosis. Flow rates decreased with increasing vertical occlusion, however, were not significantly affected by horizontal occlusion. Testing with water showed that the device could theoretically achieve a threshold of over $10,000\text{s}^{-1}$, which was also supported in isolated RBC tests at 20% haematocrit. However, thrombus formation did not occur, or was not significant enough to give differential results, suggesting a need for higher shear stresses, longer flow times, or less variability in construction. Ristocetin was used to assess the channels when von Willebrand Factor was activated, which led to an almost complete blockage of all channels tested, increasing with the size of the constriction. Therefore, the channels could work to assess von Willebrand Factor activity with the help of a reagent, limiting its viability as a WHO ASSURED device.

In the TFM work, platelets were found to generate more force with increasing surface stiffness, which supported AFM¹⁶⁸ work and contradicted previous TFM¹⁷¹ work. Once spread, platelets survived longer on lower stiffnesses than on higher ones, suggesting a temporal relationship between platelet survival and surface stiffness.

2. Future Directions

In microfluidics, future attempts should focus on a change in materials. By using hard plastics coated in DSA, instead of simply DSA, devices can be made more precisely, potentially reusable, and with regions that could be coated in either durable protein coatings, or with altered geometry (such as micro serrations) that could increase the surface area for aggregation and/or increase turbulence to encourage interaction, while also keeping the occlusion small.

In TFM, results would benefit from significantly higher resolution, which will help explain the full platelet response. This can be achieved with multiple nanobead fluorophores, which when alternately imaged, can increase resolution artificially beyond the resolution limit. It would also provide many more beads for which more accurate displacement data could be collected and calculated as a function of distance from both the platelet centre, and locations of focal adhesions – when paired with cytoskeletal/focal adhesion fluorophores. As the relationship between force generation and surface stiffness was non-linear, increasing the testing range to above 34kPa would be informative, and would also inform as to how platelets act on the stiffer surfaces in the vasculature.

BIBLIOGRAPHY

1. LBPI. Overview of Haemostasis. *n/a* (2014).
2. Ordinas, A. *et al.* The role of subendothelial laminin and platelet laminin receptors in haemostasis. *Nouv Rev Fr Hematol* **34**, 61–65 (1992).
3. Houdijk, W. P., de Groot, P. G., Nievelstein, P. F., Sakariassen, K. S. & Sixma, J. J. Subendothelial proteins and platelet adhesion. von Willebrand factor and fibronectin, not thrombospondin, are involved in platelet adhesion to extracellular matrix of human vascular endothelial cells. *Arteriosclerosis: An Official Journal of the American Heart Association, Inc.* **6**, 24–33 (1986).
4. CRAWLEY, J. T. B., DE GROOT, R. & LUKEN, B. M. Circulating ADAMTS-13–von Willebrand factor complexes: an enzyme on demand. *Journal of Thrombosis and Haemostasis* **7**, 2085–2087 (2009).
5. Weibel, E. R. & Palade, G. E. NEW CYTOPLASMIC COMPONENTS IN ARTERIAL ENDOTHELIA. *J Cell Biol* **23**, 101–112 (1964).
6. MORALES, L. D., MARTIN, C. & CRUZ, M. A. The interaction of von Willebrand factor-A1 domain with collagen: mutation G1324S (type 2M von Willebrand disease) impairs the conformational change in A1 domain induced by collagen. *Journal of Thrombosis and Haemostasis* **4**, 417–425 (2006).
7. Fu, H. *et al.* Flow-induced elongation of von Willebrand factor precedes tension-dependent activation. *Nat Commun* **8**, 324 (2017).
8. Kroll, M. H., Harris, T. S., Moake, J. L., Handin, R. I. & Schafer, A. I. von Willebrand factor binding to platelet Gplb initiates signals for platelet activation. *Journal of Clinical Investigation* **88**, 1568–1573 (1991).
9. Modderman, P. W., Admiraal, L. G., Sonnenberg, A. & von dem Borne, A. E. Glycoproteins V and Ib-IX form a noncovalent complex in the platelet membrane. *J Biol Chem* **267**, 364–9 (1992).
10. Savage, B., Sixma, J. J. & Ruggeri, Z. M. Functional self-association of von Willebrand factor during platelet adhesion under flow. *Proceedings of the National Academy of Sciences* **99**, 425–430 (2002).
11. Savage, B., Saldívar, E. & Ruggeri, Z. M. Initiation of Platelet Adhesion by Arrest onto Fibrinogen or Translocation on von Willebrand Factor. *Cell* **84**, 289–297 (1996).
12. Kroll, M. H., Harris, T. S., Moake, J. L., Handin, R. I. & Schafer, A. I. von Willebrand factor binding to platelet Gplb initiates signals for platelet activation. *Journal of Clinical Investigation* **88**, 1568–1573 (1991).
13. Huang, J. *et al.* Platelet integrin $\alpha\text{IIb}\beta\text{3}$: signal transduction, regulation, and its therapeutic targeting. *J Hematol Oncol* **12**, 26 (2019).
14. Tomaiuolo, M., Brass, L. F. & Stalker, T. J. Regulation of Platelet Activation and Coagulation and Its Role in Vascular Injury and Arterial Thrombosis. *Interv Cardiol Clin* **6**, 1–12 (2017).

15. Kahn, M. L., Nakanishi-Matsui, M., Shapiro, M. J., Ishihara, H. & Coughlin, S. R. Protease-activated receptors 1 and 4 mediate activation of human platelets by thrombin. *Journal of Clinical Investigation* **103**, 879–887 (1999).
16. Moore, S. F. *et al.* Dual Regulation of Glycogen Synthase Kinase 3 (GSK3) α/β by Protein Kinase C (PKC) α and Akt Promotes Thrombin-mediated Integrin $\alpha\text{IIb}\beta\text{3}$ Activation and Granule Secretion in Platelets. *Journal of Biological Chemistry* **288**, 3918–3928 (2013).
17. Lee, C. J. & Ansell, J. E. Direct thrombin inhibitors. *Br J Clin Pharmacol* **72**, 581–592 (2011).
18. Nieswandt, B. & Watson, S. P. Platelet-collagen interaction: is GPVI the central receptor? *Blood* **102**, 449–461 (2003).
19. Quinton, T. M., Ozdener, F., Dangelmaier, C., Daniel, J. L. & Kunapuli, S. P. Glycoprotein VI-mediated platelet fibrinogen receptor activation occurs through calcium-sensitive and PKC-sensitive pathways without a requirement for secreted ADP. *Blood* **99**, 3228–3234 (2002).
20. Gachet, C. Identification, Characterization, and Inhibition of the Platelet ADP Receptors. *Int J Hematol* **74**, 375–381 (2001).
21. Jin, J., Quinton, T. M., Zhang, J., Rittenhouse, S. E. & Kunapuli, S. P. Adenosine diphosphate (ADP)-induced thromboxane A₂ generation in human platelets requires coordinated signaling through integrin $\alpha\text{IIb}\beta\text{3}$ and ADP receptors. *Blood* **99**, 193–198 (2002).
22. Caldwell, A. T. & Watkins, E. B. Recent Advances in the Development of P2Y₁₂ Receptor Antagonists as Antiplatelet Agents. in 87–99 (2014). doi:10.1016/B978-0-12-800167-7.00007-9.
23. Devillier, P. & Bessard, G. Thromboxane A₂ and related prostaglandins in airways. *Fundam Clin Pharmacol* **11**, 2–18 (1997).
24. Fontana, P., Zufferey, A., Daali, Y. & Reny, J.-L. Antiplatelet Therapy: Targeting the TxA₂ Pathway. *J Cardiovasc Transl Res* **7**, 29–38 (2014).
25. HOFFMAN, B. B., MICHEL, T., BRENNEMAN, T. B. & LEFKOWITZ, R. J. Interactions of Agonists with Platelet α_2 -Adrenergic Receptors. *Endocrinology* **110**, 926–932 (1982).
26. Spalding, A. *et al.* Mechanism of Epinephrine-Induced Platelet Aggregation. *Hypertension* **31**, 603–607 (1998).
27. Saitoh, M., Salzman, E. W., Smith, M. & Ware, J. A. Activation of protein kinase C in platelets by epinephrine and A23187: correlation with fibrinogen binding. *Blood* **74**, 2001–6 (1989).
28. Peerschke, E. I. B. Effect of epinephrine on fibrinogen receptor exposure by aspirin-treated platelets and platelets from concentrates in response to ADP and thrombin. *Am J Hematol* **16**, 335–345 (1984).
29. Jiménez-Orozco, F. A. *et al.* Monosubstituted Coumarins Inhibit Epinephrine-induced Platelet Aggregation. *Cardiovasc Hematol Agents Med Chem* **20**, 43–51 (2022).
30. Habib, G. B. Hypertension. in *Cardiology Secrets* 369–376 (Elsevier, 2018). doi:10.1016/B978-0-323-47870-0.00041-6.
31. Ishii, S., Nagase, T. & Shimizu, T. Platelet-activating factor receptor. *Prostaglandins Other Lipid Mediat* **68–69**, 599–609 (2002).

32. Chesney, C., Pifer, D., Byers, L. & Muirhead, E. Effect of platelet-activating factor (PAF) on human platelets. *Blood* **59**, 582–585 (1982).
33. Ashraf, M. A. & Nookala, V. *Biochemistry of Platelet Activating Factor*. (2023).
34. De Clerck, F. F. & Herman, A. G. 5-hydroxytryptamine and platelet aggregation. *Fed Proc* **42**, 228–32 (1983).
35. Li, X. *et al.* Decreased platelet 5-hydroxytryptamin (5-HT) levels: a response to antidepressants. *J Affect Disord* **187**, 84–90 (2015).
36. Gilbert, J. C. *et al.* First-in-Human Evaluation of Anti–von Willebrand Factor Therapeutic Aptamer ARC1779 in Healthy Volunteers. *Circulation* **116**, 2678–2686 (2007).
37. Hollifield, A. L., Arnall, J. R. & Moore, D. C. Caplacizumab: an anti–von Willebrand factor antibody for the treatment of thrombotic thrombocytopenic purpura. *American Journal of Health-System Pharmacy* **77**, 1201–1207 (2020).
38. Quinn, M. J., Plow, E. F. & Topol, E. J. Platelet Glycoprotein IIb/IIIa Inhibitors. *Circulation* **106**, 379–385 (2002).
39. Deng, W. *et al.* Platelet clearance via shear-induced unfolding of a membrane mechanoreceptor. *Nat Commun* **7**, 12863 (2016).
40. Holme, P. A. *et al.* Shear-Induced Platelet Activation and Platelet Microparticle Formation at Blood Flow Conditions as in Arteries With a Severe Stenosis. *Arterioscler Thromb Vasc Biol* **17**, 646–653 (1997).
41. Zucker, M. B. & Nachmias, V. T. Platelet activation. *Arteriosclerosis: An Official Journal of the American Heart Association, Inc.* **5**, 2–18 (1985).
42. NIESWANDT, B., VARGA-SZABO, D. & ELVERS, M. Integrins in platelet activation. *Journal of Thrombosis and Haemostasis* **7**, 206–209 (2009).
43. Kee, M. F., Myers, D. R., Sakurai, Y., Lam, W. A. & Qiu, Y. Platelet Mechanosensing of Collagen Matrices. *PLoS One* **10**, e0126624 (2015).
44. VARGA-SZABO, D., BRAUN, A. & NIESWANDT, B. Calcium signaling in platelets. *Journal of Thrombosis and Haemostasis* **7**, 1057–1066 (2009).
45. Harrison, P. & Martin Cramer, E. Platelet α -granules. *Blood Rev* **7**, 52–62 (1993).
46. ITALIANO JR., J. E. & BATTINELLI, E. M. Selective sorting of alpha-granule proteins. *Journal of Thrombosis and Haemostasis* **7**, 173–176 (2009).
47. Smith, C. W. Release of α -granule contents during platelet activation. *Platelets* **33**, 491–502 (2022).
48. Meyers, K. M., Holmsen, H. & Seachord, C. L. Comparative study of platelet dense granule constituents. *American Journal of Physiology-Regulatory, Integrative and Comparative Physiology* **243**, R454–R461 (1982).
49. McNicol, A. & Israels, S. J. Platelet Dense Granules. *Thromb Res* **95**, 1–18 (1999).
50. Wall, J. E. *et al.* A flow cytometric assay using mepacrine for study of uptake and release of platelet dense granule contents. *Br J Haematol* **89**, 380–385 (1995).
51. Thon, J. N. *et al.* T granules in human platelets function in TLR9 organization and signaling. *Journal of Cell Biology* **198**, 561–574 (2012).
52. King, S. M. & Reed, G. L. Development of platelet secretory granules. *Semin Cell Dev Biol* **13**, 293–302 (2002).
53. Li, J. *et al.* SPECIAL ARTICLE. *Journal of Surgical Research* **61**, 543–548 (1996).

54. Du, X. *et al.* Ligands “activate” integrin $\alpha\text{IIb}\beta\text{3}$ (platelet GPIIb-IIIa). *Cell* **65**, 409–416 (1991).
55. Kent Gartner, T. *et al.* Characterization of adhesion of “resting” and stimulated platelets to fibrinogen and its fragments. *Thromb Res* **71**, 47–60 (1993).
56. Niewiarowski, S., Kordecki, E., Budzynski, A. Z., Morinelli, T. A. & Tuszynski, G. P. FIBRINOGEN INTERACTION WITH PLATELET RECEPTORS? *Ann N Y Acad Sci* **408**, 536–555 (1983).
57. Moake, J., Turner, N., Stathopoulos, N., Nolasco, L. & Hellums, J. Shear-induced platelet aggregation can be mediated by vWF released from platelets, as well as by exogenous large or unusually large vWF multimers, requires adenosine diphosphate, and is resistant to aspirin. *Blood* **71**, 1366–1374 (1988).
58. Andrews, R. K. & Berndt, M. C. Platelet physiology and thrombosis. *Thromb Res* **114**, 447–453 (2004).
59. Ruggeri, Z. M. Structure of von Willebrand factor and its function in platelet adhesion and thrombus formation. *Best Pract Res Clin Haematol* **14**, 257–279 (2001).
60. LearnHaem. Revised Coagulation Cascade. *learnhaem.com* (2020).
61. Gailani, D. & Renné, T. Intrinsic Pathway of Coagulation and Arterial Thrombosis. *Arterioscler Thromb Vasc Biol* **27**, 2507–2513 (2007).
62. Mackman, N., Tilley, R. E. & Key, N. S. Role of the Extrinsic Pathway of Blood Coagulation in Hemostasis and Thrombosis. *Arterioscler Thromb Vasc Biol* **27**, 1687–1693 (2007).
63. Swieringa, F., Kuijpers, M. J. E., Lamers, M. M. E., van der Meijden, P. E. J. & Heemskerk, J. W. M. Rate-limiting roles of the tenase complex of factors VIII and IX in platelet procoagulant activity and formation of platelet-fibrin thrombi under flow. *Haematologica* **100**, 748–756 (2015).
64. Núñez-Navarro, N. E., Santana, F. M., Parra, L. P. & Zacconi, F. C. Surfing the Blood Coagulation Cascade: Insight into the Vital Factor Xa. *Curr Med Chem* **26**, 3175–3200 (2019).
65. GREEN, D. Coagulation cascade. *Hemodialysis International* **10**, S2–S4 (2006).
66. Riddel, J. P., Auizerat, B. E., Miaskowski, C. & Lillicrap, D. P. Theories of Blood Coagulation. *Journal of Pediatric Oncology Nursing* **24**, 123–131 (2007).
67. Kushner, A., West, W. P., Khan Suheb, M. Z. & Pillarisetty, L. S. *Virchow Triad*. (2023).
68. Rudolf Hellmuth. *Virchow’s triad*. *Wikipedia* (2012).
69. NIESWANDT, B., PLEINES, I. & BENDER, M. Platelet adhesion and activation mechanisms in arterial thrombosis and ischaemic stroke. *Journal of Thrombosis and Haemostasis* **9**, 92–104 (2011).
70. Blann, A. D. & Draper, Z. Platelet activation as a marker of heart attack. *Clinica Chimica Acta* **412**, 841–842 (2011).
71. Stubbs, M. J., Mouyis, M. & Thomas, M. Deep vein thrombosis. *BMJ* k351 (2018) doi:10.1136/bmj.k351.
72. Chen, Y., Ju, L., Rushdi, M., Ge, C. & Zhu, C. Receptor-mediated cell mechanosensing. *Mol Biol Cell* **28**, 3134–3155 (2017).
73. Qiu, Y., Ciciliano, J., Myers, D. R., Tran, R. & Lam, W. A. Platelets and physics: How platelets “feel” and respond to their mechanical microenvironment. *Blood Rev* **29**, 377–386 (2015).

74. Zhang, Y. *et al.* Platelet integrins exhibit anisotropic mechanosensing and harness piconewton forces to mediate platelet aggregation. *Proceedings of the National Academy of Sciences* **115**, 325–330 (2018).
75. Qiu, Y. *et al.* Platelet mechanosensing of substrate stiffness during clot formation mediates adhesion, spreading, and activation. *Proceedings of the National Academy of Sciences* **111**, 14430–14435 (2014).
76. Zhu, C., Chen, W., Lou, J., Rittase, W. & Li, K. Mechanosensing through immunoreceptors. *Nat Immunol* **20**, 1269–1278 (2019).
77. Biomeca. Overview of mechanotransduction. <https://www.bio-meca.com/en/beyond-biomechanics-there-is-mechanotransduction/>.
78. Farge, E. Mechanotransduction in Development. in 243–265 (2011). doi:10.1016/B978-0-12-385065-2.00008-6.
79. Duchemin, A.-L., Vignes, H., Vermot, J. & Chow, R. Mechanotransduction in cardiovascular morphogenesis and tissue engineering. *Curr Opin Genet Dev* **57**, 106–116 (2019).
80. Haack, T. & Abdelilah-Seyfried, S. The force within: endocardial development, mechanotransduction and signalling during cardiac morphogenesis. *Development* **143**, 373–386 (2016).
81. Bewick, G. S. & Banks, R. W. Mechanotransduction in the muscle spindle. *Pflugers Arch* **467**, 175–190 (2015).
82. Ó Maoiléidigh, D. & Ricci, A. J. A Bundle of Mechanisms: Inner-Ear Hair-Cell Mechanotransduction. *Trends Neurosci* **42**, 221–236 (2019).
83. Nakatani, M., Maksimovic, S., Baba, Y. & Lumpkin, E. A. Mechanotransduction in epidermal Merkel cells. *Pflugers Arch* **467**, 101–108 (2015).
84. Roman, B. L. & Pekkan, K. Mechanotransduction in embryonic vascular development. *Biomech Model Mechanobiol* **11**, 1149–1168 (2012).
85. Broders-Bondon, F., Nguyen Ho-Boulidoires, T. H., Fernandez-Sanchez, M.-E. & Farge, E. Mechanotransduction in tumor progression: The dark side of the force. *Journal of Cell Biology* **217**, 1571–1587 (2018).
86. Chin, L., Xia, Y., Discher, D. E. & Janmey, P. A. Mechanotransduction in cancer. *Curr Opin Chem Eng* **11**, 77–84 (2016).
87. Engler, A. *et al.* Substrate Compliance versus Ligand Density in Cell on Gel Responses. *Biophys J* **86**, 617–628 (2004).
88. Hanks, S. K. & Polte, T. R. Signaling through focal adhesion kinase. *BioEssays* **19**, 137–145 (1997).
89. Parsons, J. T. Focal adhesion kinase: the first ten years. *J Cell Sci* **116**, 1409–1416 (2003).
90. Yi, B., Xu, Q. & Liu, W. An overview of substrate stiffness guided cellular response and its applications in tissue regeneration. *Bioact Mater* **15**, 82–102 (2022).
91. Janmey, P. A., Fletcher, D. A. & Reinhart-King, C. A. Stiffness Sensing by Cells. *Physiol Rev* **100**, 695–724 (2020).
92. Yeoman, B. *et al.* Adhesion strength and contractility enable metastatic cells to become adurotactic. *Cell Rep* **34**, 108816 (2021).
93. Kim, D.-H. & Wirtz, D. Focal adhesion size uniquely predicts cell migration. *FASEB J* **27**, 1351–61 (2013).
94. Ridley, A. J. Life at the Leading Edge. *Cell* **145**, 1012–1022 (2011).

95. Cramer, L. P. Mechanism of cell rear retraction in migrating cells. *Curr Opin Cell Biol* **25**, 591–599 (2013).
96. Huang, B. *et al.* The three-way switch operation of Rac1/RhoA GTPase-based circuit controlling amoeboid-hybrid-mesenchymal transition. *Sci Rep* **4**, 6449 (2014).
97. Vargas, D. A. *et al.* Modeling of Mechanosensing Mechanisms Reveals Distinct Cell Migration Modes to Emerge From Combinations of Substrate Stiffness and Adhesion Receptor–Ligand Affinity. *Front Bioeng Biotechnol* **8**, (2020).
98. Bangasser, B. L., Rosenfeld, S. S. & Odde, D. J. Determinants of maximal force transmission in a motor-clutch model of cell traction in a compliant microenvironment. *Biophys J* **105**, 581–92 (2013).
99. Shi, L., Lim, J. Y. & Kam, L. C. Substrate stiffness enhances human regulatory T cell induction and metabolism. *Biomaterials* **292**, 121928 (2023).
100. Scott, K. E., Fraley, S. I. & Rangamani, P. A spatial model of YAP/TAZ signaling reveals how stiffness, dimensionality, and shape contribute to emergent outcomes. *Proceedings of the National Academy of Sciences* **118**, (2021).
101. Qin, R. *et al.* Tumor Suppressor DAPK1 Catalyzes Adhesion Assembly on Rigid but Anoikis on Soft Matrices. *Front Cell Dev Biol* **10**, (2022).
102. Witkowska-Zimny, M. *et al.* Effect of substrate stiffness on the osteogenic differentiation of bone marrow stem cells and bone-derived cells. *Cell Biol Int* **37**, 608–616 (2013).
103. Keung, A. J., Asuri, P., Kumar, S. & Schaffer, D. V. Soft microenvironments promote the early neurogenic differentiation but not self-renewal of human pluripotent stem cells. *Integrative Biology* **4**, 1049–1058 (2012).
104. Han, S., Kim, J., Lee, G. & Kim, D. Mechanical Properties of Materials for Stem Cell Differentiation. *Adv Biosyst* **4**, 2000247 (2020).
105. Ng, M. R., Besser, A., Danuser, G. & Brugge, J. S. Substrate stiffness regulates cadherin-dependent collective migration through myosin-II contractility. *Journal of Cell Biology* **199**, 545–563 (2012).
106. Haeger, A., Wolf, K., Zegers, M. M. & Friedl, P. Collective cell migration: guidance principles and hierarchies. *Trends Cell Biol* **25**, 556–566 (2015).
107. Case, L. B. & Waterman, C. M. Integration of actin dynamics and cell adhesion by a three-dimensional, mechanosensitive molecular clutch. *Nat Cell Biol* **17**, 955–963 (2015).
108. Swaminathan, V. & Waterman, C. M. The molecular clutch model for mechanotransduction evolves. *Nat Cell Biol* **18**, 459–461 (2016).
109. Cooper GM. *The Cell: A Molecular Approach. 2nd edition; Actin, Myosin, and Cell Movement.* (2000).
110. Petrie, R. J. & Yamada, K. M. At the leading edge of three-dimensional cell migration. *J Cell Sci* **125**, 5917–5926 (2012).
111. Svitkina, T. The Actin Cytoskeleton and Actin-Based Motility. *Cold Spring Harb Perspect Biol* **10**, a018267 (2018).
112. Han, S. J. *et al.* Pre-complexation of talin and vinculin without tension is required for efficient nascent adhesion maturation. *Elife* **10**, (2021).
113. Yamaguchi, N. & Knaut, H. Focal adhesion-mediated cell anchoring and migration: from *in vitro* to *in vivo*. *Development* **149**, (2022).

114. Wittmann, T., Bokoch, G. M. & Waterman-Storer, C. M. Regulation of leading edge microtubule and actin dynamics downstream of Rac1. *J Cell Biol* **161**, 845–851 (2003).
115. Gomez, T. M. & Letourneau, P. C. Actin dynamics in growth cone motility and navigation. *J Neurochem* **129**, 221–234 (2014).
116. Swaminathan, V. & Waterman, C. M. The molecular clutch model for mechanotransduction evolves. *Nat Cell Biol* **18**, 459–461 (2016).
117. Bennett, M. *et al.* Molecular clutch drives cell response to surface viscosity. *Proceedings of the National Academy of Sciences* **115**, 1192–1197 (2018).
118. Gaertner, F. *et al.* Migrating Platelets Are Mechano-scavengers that Collect and Bundle Bacteria. *Cell* **171**, 1368-1382.e23 (2017).
119. Seifert, J., Rheinlaender, J., von Eysmond, H. & Schäffer, T. E. Mechanics of migrating platelets investigated with scanning ion conductance microscopy. *Nanoscale* **14**, 8192–8199 (2022).
120. Nicolai, L. *et al.* Vascular surveillance by haptotactic blood platelets in inflammation and infection. *Nat Commun* **11**, 5778 (2020).
121. KAHNER, B. N., SHANKAR, H., MURUGAPPAN, S., PRASAD, G. L. & KUNAPULI, S. P. Nucleotide receptor signaling in platelets. *Journal of Thrombosis and Haemostasis* **4**, 2317–2326 (2006).
122. Lekka, M., Gnanachandran, K., Kubiak, A., Zieliński, T. & Zemła, J. Traction force microscopy – Measuring the forces exerted by cells. *Micron* **150**, 103138 (2021).
123. Lekka, M., Gnanachandran, K., Kubiak, A., Zieliński, T. & Zemła, J. Traction force microscopy – Measuring the forces exerted by cells. *Micron* **150**, 103138 (2021).
124. Tse, J. R. & Engler, A. J. Preparation of Hydrogel Substrates with Tunable Mechanical Properties. *Curr Protoc Cell Biol* **47**, (2010).
125. Teo, J. L., Lim, C. T., Yap, A. S. & Saw, T. B. A Biologist’s Guide to Traction Force Microscopy Using Polydimethylsiloxane Substrate for Two-Dimensional Cell Cultures. *STAR Protoc* **1**, 100098 (2020).
126. Holenstein, C. N., Silvan, U. & Snedeker, J. G. High-resolution traction force microscopy on small focal adhesions - improved accuracy through optimal marker distribution and optical flow tracking. *Sci Rep* **7**, 41633 (2017).
127. Sabass, B., Gardel, M. L., Waterman, C. M. & Schwarz, U. S. High Resolution Traction Force Microscopy Based on Experimental and Computational Advances. *Biophys J* **94**, 207–220 (2008).
128. Plotnikov, S. V., Pasapera, A. M., Sabass, B. & Waterman, C. M. Force Fluctuations within Focal Adhesions Mediate ECM-Rigidity Sensing to Guide Directed Cell Migration. *Cell* **151**, 1513–1527 (2012).
129. Korobchevskaya, K., Colin-York, H., Barbieri, L. & Fritzsche, M. Extended mechanical force measurements using structured illumination microscopy. *Philosophical Transactions of the Royal Society A: Mathematical, Physical and Engineering Sciences* **379**, 20200151 (2021).
130. Dembo, M. & Wang, Y.-L. Stresses at the Cell-to-Substrate Interface during Locomotion of Fibroblasts. *Biophys J* **76**, 2307–2316 (1999).
131. Yang, Z., Lin, J.-S., Chen, J. & Wang, J. H.-C. Determining substrate displacement and cell traction fields—a new approach. *J Theor Biol* **242**, 607–616 (2006).

132. Han, S. J., Oak, Y., Groisman, A. & Danuser, G. Traction microscopy to identify force modulation in subresolution adhesions. *Nat Methods* **12**, 653–656 (2015).
133. Legant, W. R. *et al.* Multidimensional traction force microscopy reveals out-of-plane rotational moments about focal adhesions. *Proceedings of the National Academy of Sciences* **110**, 881–886 (2013).
134. Blumberg, J. W. & Schwarz, U. S. Comparison of direct and inverse methods for 2.5D traction force microscopy. *PLoS One* **17**, e0262773 (2022).
135. Franck, C., Maskarinec, S. A., Tirrell, D. A. & Ravichandran, G. Three-Dimensional Traction Force Microscopy: A New Tool for Quantifying Cell-Matrix Interactions. *PLoS One* **6**, e17833 (2011).
136. Córdor, M., Steinwachs, J., Mark, C., García-Aznar, J. M. & Fabry, B. Traction Force Microscopy in 3-Dimensional Extracellular Matrix Networks. *Curr Protoc Cell Biol* **75**, (2017).
137. Banda, O. A., Sabanayagam, C. R. & Slater, J. H. Reference-Free Traction Force Microscopy Platform Fabricated via Two-Photon Laser Scanning Lithography Enables Facile Measurement of Cell-Generated Forces. *ACS Appl Mater Interfaces* **11**, 18233–18241 (2019).
138. Beussman, K. M. *et al.* Black dots: High-yield traction force microscopy reveals structural factors contributing to platelet forces. *Acta Biomater* **163**, 302–311 (2023).
139. Plotnikov, S. V., Sabass, B., Schwarz, U. S. & Waterman, C. M. High-Resolution Traction Force Microscopy. in 367–394 (2014). doi:10.1016/B978-0-12-420138-5.00020-3.
140. Huse, M. Mechanical forces in the immune system. *Nat Rev Immunol* **17**, 679–690 (2017).
141. Trepap, X. *et al.* Physical forces during collective cell migration. *Nat Phys* **5**, 426–430 (2009).
142. Mollica, M. Y. *et al.* Distinct platelet F-actin patterns and traction forces on von Willebrand factor versus fibrinogen. *Biophys J* (2023) doi:10.1016/j.bpj.2023.07.006.
143. Bajpai, A., Tong, J., Qian, W., Peng, Y. & Chen, W. The Interplay Between Cell-Cell and Cell-Matrix Forces Regulates Cell Migration Dynamics. *Biophys J* **117**, 1795–1804 (2019).
144. Wang, N. Review of cellular mechanotransduction. *J Phys D Appl Phys* **50**, 233002 (2017).
145. Xie, J. & Minc, N. Cytoskeleton Force Exertion in Bulk Cytoplasm. *Front Cell Dev Biol* **8**, (2020).
146. Wang, X. & Ha, T. Defining Single Molecular Forces Required to Activate Integrin and Notch Signaling. *Science (1979)* **340**, 991–994 (2013).
147. Jaalouk, D. E. & Lammerding, J. Mechanotransduction gone awry. *Nat Rev Mol Cell Biol* **10**, 63–73 (2009).
148. Kalaskar, D. M. & Alshomer, F. Micro- and Nanotopographical Cues Guiding Biomaterial Host Response. in *In Situ Tissue Regeneration* 137–163 (Elsevier, 2016). doi:10.1016/B978-0-12-802225-2.00008-8.
149. Qiu, Y. *et al.* Platelet mechanosensing of substrate stiffness during clot formation mediates adhesion, spreading, and activation. *Proceedings of the National Academy of Sciences* **111**, 14430–14435 (2014).
150. Han, S. J., Bielawski, K. S., Ting, L. H., Rodriguez, M. L. & Sniadecki, N. J. Decoupling Substrate Stiffness, Spread Area, and Micropost Density: A Close Spatial Relationship between Traction Forces and Focal Adhesions. *Biophys J* **103**, 640–648 (2012).

151. Bangasser, B. L. *et al.* Shifting the optimal stiffness for cell migration. *Nat Commun* **8**, 15313 (2017).
152. Park, J. S. *et al.* The effect of matrix stiffness on the differentiation of mesenchymal stem cells in response to TGF- β . *Biomaterials* **32**, 3921–3930 (2011).
153. Petzold, J. & Gentleman, E. Intrinsic Mechanical Cues and Their Impact on Stem Cells and Embryogenesis. *Front Cell Dev Biol* **9**, (2021).
154. Gaudet, C. *et al.* Influence of Type I Collagen Surface Density on Fibroblast Spreading, Motility, and Contractility. *Biophys J* **85**, 3329–3335 (2003).
155. McCarty, O. J. T. *et al.* Rac1 Is Essential for Platelet Lamellipodia Formation and Aggregate Stability under Flow. *Journal of Biological Chemistry* **280**, 39474–39484 (2005).
156. Kee, M. F., Myers, D. R., Sakurai, Y., Lam, W. A. & Qiu, Y. Platelet Mechanosensing of Collagen Matrices. *PLoS One* **10**, e0126624 (2015).
157. Hanke, J., Probst, D., Zemel, A., Schwarz, U. S. & Köster, S. Dynamics of force generation by spreading platelets. *Soft Matter* **14**, 6571–6581 (2018).
158. Califano, J. P. & Reinhart-King, C. A. Substrate Stiffness and Cell Area Predict Cellular Traction Stresses in Single Cells and Cells in Contact. *Cell Mol Bioeng* **3**, 68–75 (2010).
159. Han, S. J., Bielawski, K. S., Ting, L. H., Rodriguez, M. L. & Sniadecki, N. J. Decoupling Substrate Stiffness, Spread Area, and Micropost Density: A Close Spatial Relationship between Traction Forces and Focal Adhesions. *Biophys J* **103**, 640–648 (2012).
160. Savage, B., Saldívar, E. & Ruggeri, Z. M. Initiation of Platelet Adhesion by Arrest onto Fibrinogen or Translocation on von Willebrand Factor. *Cell* **84**, 289–297 (1996).
161. Reininger, A. J. Mechanism of platelet adhesion to von Willebrand factor and microparticle formation under high shear stress. *Blood* **107**, 3537–3545 (2006).
162. Mody, N. A. & King, M. R. Platelet Adhesive Dynamics. Part II: High Shear-Induced Transient Aggregation via GPIIb α -vWF-GPIIb α Bridging. *Biophys J* **95**, 2556–2574 (2008).
163. Fu, H. *et al.* Flow-induced elongation of von Willebrand factor precedes tension-dependent activation. *Nat Commun* **8**, 324 (2017).
164. Hantgan, R. R., Stahle, M. C. & Lord, S. T. Dynamic Regulation of Fibrinogen: Integrin α IIb β 3 Binding. *Biochemistry* **49**, 9217–9225 (2010).
165. Zelená, A. *et al.* Force generation in human blood platelets by filamentous actomyosin structures. *Biophys J* (2023) doi:10.1016/j.bpj.2023.07.010.
166. Myers, D. R. *et al.* Single-platelet nanomechanics measured by high-throughput cytometry. *Nat Mater* **16**, 230–235 (2017).
167. Paknikar, A. K., Eltzner, B. & Köster, S. Direct characterization of cytoskeletal reorganization during blood platelet spreading. *Prog Biophys Mol Biol* **144**, 166–176 (2019).
168. Lam, W. A. *et al.* Mechanics and contraction dynamics of single platelets and implications for clot stiffening. *Nat Mater* **10**, 61–66 (2011).
169. Mollica, M. Y. *et al.* Distinct platelet F-actin patterns and traction forces on von Willebrand factor versus fibrinogen. *Biophys J* (2023) doi:10.1016/j.bpj.2023.07.006.
170. Grashoff, C. *et al.* Measuring mechanical tension across vinculin reveals regulation of focal adhesion dynamics. *Nature* **466**, 263–266 (2010).
171. Henriques, S. S., Sandmann, R., Strate, A. & Köster, S. Force field evolution during human blood platelet activation. *J Cell Sci* (2012) doi:10.1242/jcs.108126.

172. Hartwig, J. H. The Platelet: Form and Function. *Semin Hematol* **43**, S94–S100 (2006).
173. Linde, T., Clauser, J., Meuris, B. & Steinseifer, U. Assessing the Thrombogenic Potential of Heart Valve Prostheses: An Approach for a Standardized In-Vitro Method. *Cardiovasc Eng Technol* **10**, 216–224 (2019).
174. Eppihimer, M. J. *et al.* Impact of Stent Surface on Thrombogenicity and Vascular Healing. *Circ Cardiovasc Interv* **6**, 370–377 (2013).
175. Federici, A. B. The factor VIII/von Willebrand factor complex: basic and clinical issues. *Haematologica* **88**, EREP02 (2003).
176. Hassan, M. I., Saxena, A. & Ahmad, F. Structure and function of von Willebrand factor. *Blood Coagul Fibrinolysis* **23**, 11–22 (2012).
177. Yin, J. *et al.* Mutations in the D1 domain of von Willebrand factor impair their propeptide-dependent multimerization, intracellular trafficking and secretion. *J Hematol Oncol* **8**, 73 (2015).
178. Przeradzka, M. A. *et al.* The D' domain of von Willebrand factor requires the presence of the D3 domain for optimal factor VIII binding. *Biochemical Journal* **475**, 2819–2830 (2018).
179. Ju, L. *et al.* Von Willebrand factor-A1 domain binds platelet glycoprotein Iba in multiple states with distinctive force-dependent dissociation kinetics. *Thromb Res* **136**, 606–12 (2015).
180. Posch, S. *et al.* Interaction of von Willebrand factor domains with collagen investigated by single molecule force spectroscopy. *J Chem Phys* **148**, (2018).
181. Ma, Z. *et al.* The co-influence of VWD type 2B/2M mutations in the A1 domain and platelet GPIba on the rate of cleavage to VWF by ADAMTS13. *Thromb Res* **136**, 987–95 (2015).
182. Lynch, C. J., Lane, D. A. & Luken, B. M. Control of VWF A2 domain stability and ADAMTS13 access to the scissile bond of full-length VWF. *Blood* **123**, 2585–2592 (2014).
183. Hassenpflug, W. A. *et al.* The Impact of Mutations in the A2 Domain of Von Willebrand Factor on its Cleavage by ADAMTS13. *Blood* **104**, 3666–3666 (2004).
184. Lankhof, H. *et al.* A3 domain is essential for interaction of von Willebrand factor with collagen type III. *Thromb Haemost* **75**, 950–8 (1996).
185. Flood, V. H. *et al.* Absent collagen binding in a VWF A3 domain mutant: utility of the VWF:CB in diagnosis of VWD. *J Thromb Haemost* **8**, 1431–3 (2010).
186. Keuren, J. F. W. *et al.* Von Willebrand factor C1C2 domain is involved in platelet adhesion to polymerized fibrin at high shear rate. *Blood* **103**, 1741–1746 (2004).
187. Zhou, Y.-F. & Springer, T. A. Highly reinforced structure of a C-terminal dimerization domain in von Willebrand factor. *Blood* **123**, 1785–93 (2014).
188. Mody, N. A. & King, M. R. Platelet Adhesive Dynamics. Part II: High Shear-Induced Transient Aggregation via GPIba-vWF-GPIba Bridging. *Biophys J* **95**, 2556–2574 (2008).
189. BUDDE, U. Diagnosis of von Willebrand disease subtypes: implications for treatment. *Haemophilia* **14**, 27–38 (2008).
190. Kumar, S., Pruthi, R. K. & Nichols, W. L. Acquired von Willebrand Disease. *Mayo Clin Proc* **77**, 181–187 (2002).
191. Shetty, S., Kasatkar, P. & Ghosh, K. Pathophysiology of acquired von Willebrand disease: a concise review. *Eur J Haematol* **87**, 99–106 (2011).

192. Ingerslev, J. A sensitive ELISA for von Willebrand factor (vWf:Ag). *Scand J Clin Lab Invest* **47**, 143–149 (1987).
193. Mohammed, S. & Favalaro, E. J. Laboratory Testing for von Willebrand Factor Ristocetin Cofactor (VWF:RCo). in 435–451 (2017). doi:10.1007/978-1-4939-7196-1_32.
194. Favalaro, E. J. *et al.* Desmopressin therapy to assist the functional identification and characterisation of von Willebrand disease: Differential utility from combining two (VWF:CB and VWF:RCo) von Willebrand factor activity assays? *Thromb Res* **123**, 862–868 (2009).
195. VERBRUGGEN, B., MEIJER, P., NOVÁKOVA, I. & VAN HEERDE, W. Diagnosis of factor VIII deficiency. *Haemophilia* **14**, 76–82 (2008).
196. Favalaro, E. J. Rethinking the diagnosis of von Willebrand disease. *Thromb Res* **127**, S17–S21 (2011).
197. James, P. D. & Goodeve, A. C. von Willebrand disease. *Genetics in Medicine* **13**, 365–376 (2011).
198. Sadler, J. E. *et al.* Impact, Diagnosis and Treatment of von Willebrand Disease. *Thromb Haemost* **84**, 160–174 (2000).
199. Favalaro, E. J. & Lippi, G. Preanalytical issues that may cause misdiagnosis in haemophilia and von Willebrand disease. *Haemophilia* **24**, 198–210 (2018).
200. Othman, M. Platelet-Type Von Willebrand Disease: A Rare, Often Misdiagnosed and Underdiagnosed Bleeding Disorder. *Semin Thromb Hemost* **37**, 464–469 (2011).
201. Franchini, M. & Mannucci, P. M. Von Willebrand factor (Vonvendi®): the first recombinant product licensed for the treatment of von Willebrand disease. *Expert Rev Hematol* **9**, 825–830 (2016).
202. Favalaro, E. J., Franchini, M. & Lippi, G. Biological therapies for von Willebrand disease. *Expert Opin Biol Ther* **12**, 551–564 (2012).
203. Erickson, D. & Li, D. Integrated microfluidic devices. *Anal Chim Acta* **507**, 11–26 (2004).
204. Wang, G. R., Yang, F. & Zhao, W. There can be turbulence in microfluidics at low Reynolds number. *Lab Chip* **14**, 1452–1458 (2014).
205. Pandey, C. M. *et al.* Microfluidics Based Point-of-Care Diagnostics. *Biotechnol J* **13**, 1700047 (2018).
206. Wang, G., Yang, F. & Zhao, W. Microelectrokinetic turbulence in microfluidics at low Reynolds number. *Phys Rev E* **93**, 013106 (2016).
207. Yin, J. *et al.* Integrated microfluidic systems with sample preparation and nucleic acid amplification. *Lab Chip* **19**, 2769–2785 (2019).
208. Singh, R., Lee, H.-J., Singh, A. K. & Kim, D.-P. Recent advances for serial processes of hazardous chemicals in fully integrated microfluidic systems. *Korean Journal of Chemical Engineering* **33**, 2253–2267 (2016).
209. Khater, A., Abdelrehim, O., Mohammadi, M., Mohamad, A. & Sanati-Nezhad, A. Thermal droplet microfluidics: From biology to cooling technology. *TrAC Trends in Analytical Chemistry* **138**, 116234 (2021).
210. Fan, X. & White, I. M. Optofluidic microsystems for chemical and biological analysis. *Nat Photonics* **5**, 591–597 (2011).
211. Zhang, P., Bachman, H., Ozcelik, A. & Huang, T. J. Acoustic Microfluidics. *Annual Review of Analytical Chemistry* **13**, 17–43 (2020).

212. Gorkin, R. *et al.* Centrifugal microfluidics for biomedical applications. *Lab Chip* **10**, 1758 (2010).
213. Gong, M. M. & Sinton, D. Turning the Page: Advancing Paper-Based Microfluidics for Broad Diagnostic Application. *Chem Rev* **117**, 8447–8480 (2017).
214. Shang, L., Cheng, Y. & Zhao, Y. Emerging Droplet Microfluidics. *Chem Rev* **117**, 7964–8040 (2017).
215. Pamme, N. Continuous flow separations in microfluidic devices. *Lab Chip* **7**, 1644 (2007).
216. Zhang, C., Kelkar, A. & Neelamegham, S. von Willebrand factor self-association is regulated by the shear-dependent unfolding of the A2 domain. *Blood Adv* **3**, 957–968 (2019).
217. Sing, C. E. & Alexander-Katz, A. Elongational Flow Induces the Unfolding of von Willebrand Factor at Physiological Flow Rates. *Biophys J* **98**, L35–L37 (2010).
218. Nishat, S., Jafry, A. T., Martinez, A. W. & Awan, F. R. Paper-based microfluidics: Simplified fabrication and assay methods. *Sens Actuators B Chem* **336**, 129681 (2021).
219. Bhardwaj, T., Ramana, L. N. & Sharma, T. K. Current Advancements and Future Road Map to Develop ASSURED Microfluidic Biosensors for Infectious and Non-Infectious Diseases. *Biosensors* vol. 12 Preprint at <https://doi.org/10.3390/bios12050357> (2022).
220. Jaywant, S. A. & Arif, K. M. A Comprehensive Review of Microfluidic Water Quality Monitoring Sensors. *Sensors* **19**, 4781 (2019).
221. Aryal, P., Brack, E., Alexander, T. & Henry, C. S. Capillary Flow-Driven Microfluidics Combined with a Paper Device for Fast User-Friendly Detection of Heavy Metals in Water. *Anal Chem* **95**, 5820–5827 (2023).
222. Campbell, J. *et al.* Microfluidic and Paper-Based Devices for Disease Detection and Diagnostic Research. *Int J Mol Sci* **19**, 2731 (2018).
223. Qin, X. *et al.* Microfluidic paper-based chips in rapid detection: Current status, challenges, and perspectives. *TrAC Trends in Analytical Chemistry* **143**, 116371 (2021).
224. Beshana, S., Hussien, A., Leta, S. & Kaneta, T. Microfluidic Paper Based Analytical Devices for the Detection of Carbamate Pesticides. *Bull Environ Contam Toxicol* **109**, 344–351 (2022).
225. Kung, C.-T., Hou, C.-Y., Wang, Y.-N. & Fu, L.-M. Microfluidic paper-based analytical devices for environmental analysis of soil, air, ecology and river water. *Sens Actuators B Chem* **301**, 126855 (2019).
226. Tay, A., Pavesi, A., Yazdi, S. R., Lim, C. T. & Warkiani, M. E. Advances in microfluidics in combating infectious diseases. *Biotechnol Adv* **34**, 404–421 (2016).
227. Burklund, A., Tadimety, A., Nie, Y., Hao, N. & Zhang, J. X. J. Advances in diagnostic microfluidics. in 1–72 (2020). doi:10.1016/bs.acc.2019.08.001.
228. Martinez, A. W., Phillips, S. T., Whitesides, G. M. & Carrilho, E. Diagnostics for the Developing World: Microfluidic Paper-Based Analytical Devices. *Anal Chem* **82**, 3–10 (2010).
229. Berry, S. B., Fernandes, S. C., Rajaratnam, A., DeChiara, N. S. & Mace, C. R. Measurement of the hematocrit using paper-based microfluidic devices. *Lab Chip* **16**, 3689–3694 (2016).
230. Channon, R. B. *et al.* Rapid flow in multilayer microfluidic paper-based analytical devices. *Lab Chip* **18**, 793–802 (2018).

231. Elizalde, E., Urteaga, R. & Berli, C. L. A. Rational design of capillary-driven flows for paper-based microfluidics. *Lab Chip* **15**, 2173–2180 (2015).
232. Yang, Y. *et al.* Paper-Based Microfluidic Devices: Emerging Themes and Applications. *Anal Chem* **89**, 71–91 (2017).
233. Carrilho, E., Martinez, A. W. & Whitesides, G. M. Understanding Wax Printing: A Simple Micropatterning Process for Paper-Based Microfluidics. *Anal Chem* **81**, 7091–7095 (2009).
234. Berthier, E. & Beebe, D. J. Flow rate analysis of a surface tension driven passive micropump. *Lab Chip* **7**, 1475–1478 (2007).
235. Hong, S. & Kim, W. Dynamics of water imbibition through paper channels with wax boundaries. *Microfluid Nanofluidics* **19**, 845–853 (2015).
236. Martinez, A. W., Phillips, S. T., Butte, M. J. & Whitesides, G. M. Patterned paper as a platform for inexpensive, low-volume, portable bioassays. *Angew Chem Int Ed Engl* **46**, 1318–1320 (2007).
237. Hamedpour, V., Leardi, R., Suzuki, K. & Citterio, D. Fabrication of paper-based analytical devices optimized by central composite design. *Analyst* **143**, 2102–2108 (2018).
238. Soum, V., Park, S., Brilian, A. I., Kwon, O.-S. & Shin, K. Programmable Paper-Based Microfluidic Devices for Biomarker Detections. *Micromachines (Basel)* **10**, 516 (2019).
239. Charbaji, A., Heidari-Bafroui, H., Anagnostopoulos, C. & Faghri, M. A New Paper-Based Microfluidic Device for Improved Detection of Nitrate in Water. *Sensors* **21**, (2021).
240. Guan, Y. & Sun, B. Detection and extraction of heavy metal ions using paper-based analytical devices fabricated via atom stamp printing. *Microsyst Nanoeng* **6**, 14 (2020).
241. Nilghaz, A. *et al.* Paper-based microfluidics for food safety and quality analysis. *Trends Food Sci Technol* **118**, 273–284 (2021).
242. Renault, C., Li, X., Fosdick, S. E. & Crooks, R. M. Hollow-Channel Paper Analytical Devices. *Anal Chem* **85**, 7976–7979 (2013).
243. Ren, Y., Ray, S. & Liu, Y. Reconfigurable Acrylic-tape Hybrid Microfluidics. *Sci Rep* **9**, 4824 (2019).
244. Giokas, D. L., Tsogas, G. Z. & Vlessidis, A. G. Programming Fluid Transport in Paper-Based Microfluidic Devices Using Razor-Crafted Open Channels. *Anal Chem* **86**, 6202–6207 (2014).
245. Sotoudegan, M. S., Mohd, O., Ligler, F. S. & Walker, G. M. Paper-based passive pumps to generate controllable whole blood flow through microfluidic devices. *Lab Chip* **19**, 3787–3795 (2019).
246. Roder, H., Maki, K., Cheng, H. & Ramachandra Shastry, M. C. Rapid mixing methods for exploring the kinetics of protein folding. *Methods* **34**, 15–27 (2004).
247. Chatterjee, M. S., Denney, W. S., Jing, H. & Diamond, S. L. Systems Biology of Coagulation Initiation: Kinetics of Thrombin Generation in Resting and Activated Human Blood. *PLoS Comput Biol* **6**, e1000950- (2010).
248. Campos Marín, A., Brunelli, M. & Lacroix, D. Flow perfusion rate modulates cell deposition onto scaffold substrate during cell seeding. *Biomech Model Mechanobiol* **17**, 675–687 (2018).
249. Tan, J. N. & Neild, A. Microfluidic mixing in a Y-junction open channel. *AIP Adv* **2**, 032160 (2012).

250. Noh, H. & Phillips, S. T. Metering the Capillary-Driven Flow of Fluids in Paper-Based Microfluidic Devices. *Anal Chem* **82**, 4181–4187 (2010).
251. Pierres, A., Benoliel, A.-M. & Bongrand, P. Studying Molecular Interactions at the Single Bond Level with a Laminar Flow Chamber. *Cell Mol Bioeng* **1**, 247–262 (2008).
252. Zhou, F. *et al.* The kinetics of E-selectin- and P-selectin-induced intermediate activation of integrin $\alpha\text{L}\beta\text{2}$ on neutrophils. *J Cell Sci* **134**, jcs258046 (2021).
253. Marshall, B. T. *et al.* Direct observation of catch bonds involving cell-adhesion molecules. *Nature* **423**, 190–193 (2003).
254. Channon, R. B., Nguyen, M. P., Henry, C. S. & Dandy, D. S. Multilayered Microfluidic Paper-Based Devices: Characterization, Modeling, and Perspectives. *Anal Chem* **91**, 8966–8972 (2019).
255. Park, J., Shin, J. H. & Park, J.-K. Experimental Analysis of Porosity and Permeability in Pressed Paper. *Micromachines (Basel)* **7**, 48 (2016).
256. Ward, T., Faivre, M., Abkarian, M. & Stone, H. A. Microfluidic flow focusing: Drop size and scaling in pressure versus flow-rate-driven pumping. *Electrophoresis* **26**, 3716–3724 (2005).
257. Jang, I., Berg, K. E. & Henry, C. S. Viscosity measurements utilizing a fast-flow microfluidic paper-based device. *Sens Actuators B Chem* **319**, 128240 (2020).
258. Nesbitt, W. S. *et al.* A shear gradient-dependent platelet aggregation mechanism drives thrombus formation. *Nat Med* **15**, 665–673 (2009).
259. Schindelin, J. *et al.* Fiji: an open-source platform for biological-image analysis. *Nat Methods* **9**, 676–682 (2012).
260. Camplisson, C. K., Schilling, K. M., Pedrotti, W. L., Stone, H. A. & Martinez, A. W. Two-ply channels for faster wicking in paper-based microfluidic devices. *Lab Chip* **15**, 4461–4466 (2015).
261. Böhm, A., Carstens, F., Trieb, C., Schabel, S. & Biesalski, M. Engineering microfluidic papers: effect of fiber source and paper sheet properties on capillary-driven fluid flow. *Microfluid Nanofluidics* **16**, 789–799 (2014).
262. Songok, J. & Toivakka, M. Controlling capillary-driven surface flow on a paper-based microfluidic channel. *Microfluid Nanofluidics* **20**, 63 (2016).
263. Christophis, C. *et al.* Shear stress regulates adhesion and rolling of CD44+ leukemic and hematopoietic progenitor cells on hyaluronan. *Biophys J* **101**, 585–593 (2011).
264. Ward, K. & Fan, Z. H. Mixing in microfluidic devices and enhancement methods. *J Micromech Microeng* **25**, 094001 (2015).
265. Werner, E. J. *et al.* Prevalence of von Willebrand disease in children: A multiethnic study. *J Pediatr* **123**, 893–898 (1993).
266. Rodeghiero, F., Castaman, G. & Dini, E. Epidemiological investigation of the prevalence of von Willebrand's disease. *Blood* **69**, 454–459 (1987).
267. Macleod Briongos, I., Call, Z. D., Henry, C. S. & Bark, D. L. Maximizing flow rate in single paper layer, rapid flow microfluidic paper-based analytical devices. *Microfluid Nanofluidics* **27**, 70 (2023).
268. Trejo-Soto, C. & Hernández-Machado, A. Normalization of Blood Viscosity According to the Hematocrit and the Shear Rate. *Micromachines (Basel)* **13**, 357 (2022).

269. Eckmann, D. M., Bowers, S., Stecker, M. & Cheung, A. T. Hematocrit, Volume Expander, Temperature, and Shear Rate Effects on Blood Viscosity. *Anesth Analg* **91**, 539–545 (2000).
270. Mensah, G. A., Roth, G. A. & Fuster, V. The Global Burden of Cardiovascular Diseases and Risk Factors. *J Am Coll Cardiol* **74**, 2529–2532 (2019).
271. Barquera, S. *et al.* Global Overview of the Epidemiology of Atherosclerotic Cardiovascular Disease. *Arch Med Res* **46**, 328–338 (2015).
272. Yuan-Cheng Fung. *Biomechanics: Mechanical Properties of Living Tissues*. (Springer, 1993).
273. Stalker, T. J. *et al.* Hierarchical organization in the hemostatic response and its relationship to the platelet-signaling network. *Blood* **121**, 1875–1885 (2013).
274. Spronck, B. & Humphrey, J. D. Arterial Stiffness: Different Metrics, Different Meanings. *J Biomech Eng* **141**, 0910041–09100412 (2019).
275. Segers, P., Rietzschel, E. R. & Chirinos, J. A. How to Measure Arterial Stiffness in Humans. *Arterioscler Thromb Vasc Biol* **40**, 1034–1043 (2020).
276. Couade, M. *et al.* Quantitative Assessment of Arterial Wall Biomechanical Properties Using Shear Wave Imaging. *Ultrasound Med Biol* **36**, 1662–1676 (2010).
277. Xue, C. *et al.* Substrate stiffness regulates arterial-venous differentiation of endothelial progenitor cells via the Ras/Mek pathway. *Biochimica et Biophysica Acta (BBA) - Molecular Cell Research* **1864**, 1799–1808 (2017).
278. Kohn, J. C. *et al.* Cooperative Effects of Matrix Stiffness and Fluid Shear Stress on Endothelial Cell Behavior. *Biophys J* **108**, 471–478 (2015).
279. Tseng, Q. *et al.* A new micropatterning method of soft substrates reveals that different tumorigenic signals can promote or reduce cell contraction levels. *Lab Chip* **11**, 2231 (2011).
280. Ershov, D. *et al.* TrackMate 7: integrating state-of-the-art segmentation algorithms into tracking pipelines. *Nat Methods* **19**, 829–832 (2022).
281. Tinevez, J.-Y. *et al.* TrackMate: An open and extensible platform for single-particle tracking. *Methods* **115**, 80–90 (2017).
282. Tseng, Q. *et al.* Spatial organization of the extracellular matrix regulates cell–cell junction positioning. *Proceedings of the National Academy of Sciences* **109**, 1506–1511 (2012).
283. Zemel, A. & Safran, S. A. Active self-polarization of contractile cells in asymmetrically shaped domains. *Phys Rev E* **76**, 021905 (2007).
284. Lo, C.-M., Wang, H.-B., Dembo, M. & Wang, Y. Cell Movement Is Guided by the Rigidity of the Substrate. *Biophys J* **79**, 144–152 (2000).
285. Leytin, V. Apoptosis in the anucleate platelet. *Blood Rev* **26**, 51–63 (2012).
286. Hartwig, J. H. The Platelet: Form and Function. *Semin Hematol* **43**, S94–S100 (2006).
287. Zancla, A., Mozetic, P., Orsini, M., Forte, G. & Rainer, A. A primer to traction force microscopy. *Journal of Biological Chemistry* **298**, 101867 (2022).
288. Guido Majno & Isabelle Joris. *Cells, Tissues, and Disease: Principles of General Pathology*. (Oxford University Press, 2004).
289. Matzinger, P. Tolerance, Danger, and the Extended Family. *Annu Rev Immunol* **12**, 991–1045 (1994).